Stepped-Frequency Pulse Train Waveforms for Improved Radar Range Resolution

by

Chung-Hsiu Ma

Submitted to the Department of Electrical Engineering and Computer Science
in partial fulfillment of the requirements for the degrees of

Master of Engineering in Electrical Science and Engineering

and

Bachelor of Science in Electrical Engineering and Computer Science

at the

MASSACHUSETTS INSTITUTE OF TECHNOLOGY

June 1996

Signature of Author .. ..
Department of Electrical Engineering and Computer Science

Certified by .....
Herbert M. Aumann
Senior Staff, MIT Lincoln Laboratory
Thesis Supervisor

Certified by ....
Prof. James K. Roberge
Engineering, MIT
Thesis Supervisor

Accepted by..... .....
Morgenthaler
Chairperson, Department Committee on Graduate Students

Stepped-Frequency Pulse Train Waveforms for Improved Radar Range Resolution

by

Chung-Hsiu Ma

Submitted to the Department of Electrical Engineering and Computer Science
on May 20, 1996, in partial fulfillment of the
requirements for the degrees of
Master of Engineering in Electrical Science and Engineering
and
Bachelor of Science in Electrical Engineering and Computer Science

Abstract

The traditional approach of improving radar range resolution using a linear frequency modulated chirp signal requires the full width of the frequency spectrum, which is not feasible in the UHF band due to interference or frequency allocation for other purposes. In this study a linear frequency modulated chirp signal is approximated using two stepped-frequency pulse train waveforms, a continuous wave pulse train and a linear frequency modulated pulse train. The continuous wave pulse train consists of a series of single frequency pulses, each at a different frequency. It is found to be susceptible to corruption due to target motion. The linear frequency modulated pulse train consists of linear frequency modulation within pulses, each at a different center frequency. Simulations are used to demonstrate that both approaches approximate a linear frequency modulated chirp signal, and performance is degraded when there is a gap in the frequency band or if there is phase distortion due to target motion. However, it is shown that a linear frequency modulated pulse train with frequency overlaps between pulses can be used to reduce or eliminate phase distortions resulting from target motion provided the target is moving with constant velocity.

The validity of the technique is demonstrated by non-coherently processing radar data from an internal moving target simulator and data from actual planes to resolve targets from their reflected image in order to estimate target height.

Thesis Supervisor: Herbert M. Aumann
Title: Senior Staff, MIT Lincoln Laboratory

Thesis Supervisor: Prof. James K. Roberge
Title: Professor of Electrical Engineering, MIT

[1]This work was sponsored by the United States Department of the Navy under Air Force contract F19628-95-C0002. Opinions, interpretations, conclusions, and recommendations are those of the author and are not necessarily endorsed by the United States Air Force.

Acknowledgments

First and foremost, I would like to thank my supervisor at Lincoln Lab Dr. H. Aumann. Thank you so much for your guidance, patience, and understanding.

Secondly, I want to thank my MIT thesis supervisor and VI-A advisor Prof. J. Roberge. Thank you for taking time out of your busy schedule to help me with my thesis.

My utmost gratitude for my family, my Father, my Mother, my sisters Linda and Lenore.

My thanks to the professors at MIT who have taught me and inspired me so much.

Thank you very much, L. Upton, J. Austin, G. Titi, and E. Evans for giving me the opportunity to work in the Radar Systems group. Thank you D. Fitzgerald, M. Mullins, E. Marin, and R. LeBlanc for collecting data for my thesis and being there to answer my questions. I would also like to thank some members of Group 103. Thank you R. Gabel, L. Goodman, B. Carlson, P. Haddad, A. Kackelmyer, R. McSheehy, P. Phu, S. Smith, J. Ward, F. Willwerth, I. Zabel, H. Maguire, R. Aucoin, J. Li, E. Baszkiewicz, R. LaPat, and J. Scalsi.

For those of you who made my stay at the Lab more enjoyable, I thank you. Thank you D. Giordano, G. Hackett, G. Milkowski, T. Emberley, K. Favreau, L. Larosa, C. Wilson, and B. Pesaturo. To the organizers of M. Eng. and VI-A programs at MIT, thank you very much. Thank you A. Hunter, M. Zahn, J. Lee, and L. Wereminski.

Last, but most definitely not least, I want to thank some of my very close friends at MIT. Thank you so much Yee Chuan, Joyce, Dawn, Jessica, and Janet for standing by me and always for being there for me.

Contents

List of Figures

Chapter 1

Introduction

The mission of an Airborne Early Warning (AEW) radar is to seek information about targets in a background of clutter and possible jammers. Existing airborne radar systems must be continuously upgraded to meet future challenges. Since developing new techniques in an airborne radar testbed is extremely expensive, a ground based radar system is built. This system, known as Radar Technology Experimental Radar (RSTER), is shown in Figure 1-1. It is located on a high cliff overlooking the ocean, thus simulating the conditions of an AEW radar. The radar transmits in the UHF band, which ranges from 400 MHz to 500 MHz and has an instantaneous bandwidth of 250 kHz, which means it can maintain a linear frequency characteristic in both the transmitter and the receiver over a frequency range of at most 250 kHz.

The purpose of this thesis is to study methods for enhancing the instantaneous bandwidth of the RSTER radar system to allow target length estimation and target height finding. Chapter 1 explains the applications of the increased bandwidth for target length estimation and target height finding, as well as provides an overview of what the rest of the thesis will cover.

Length measurement is an important target classification parameter. The range resolution δR of a radar is given by Equation 1.1.

$$\delta R = \frac{c}{BW} \tag{1.1}$$

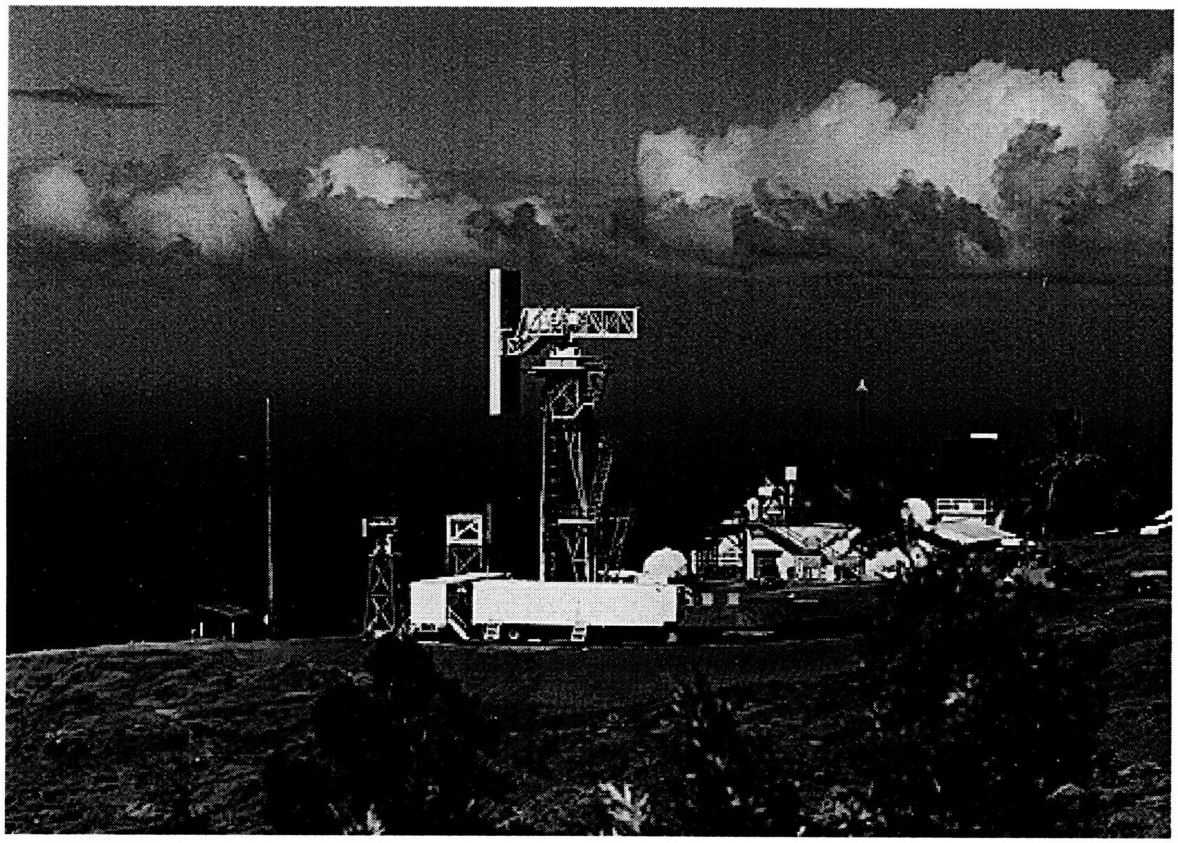

Figure 1-1: Picture of the Radar Technology Experimental Radar (RSTER) at Makaha Ridge, Kauai.

where c is the speed of light, and BW is the bandwidth of the radar [24]. Figure 1-2 is a plot of the instantaneous bandwidth required to resolve the lengths of a variety of targets. The curve separates the resolvable region from the non-resolvable region. Some typical

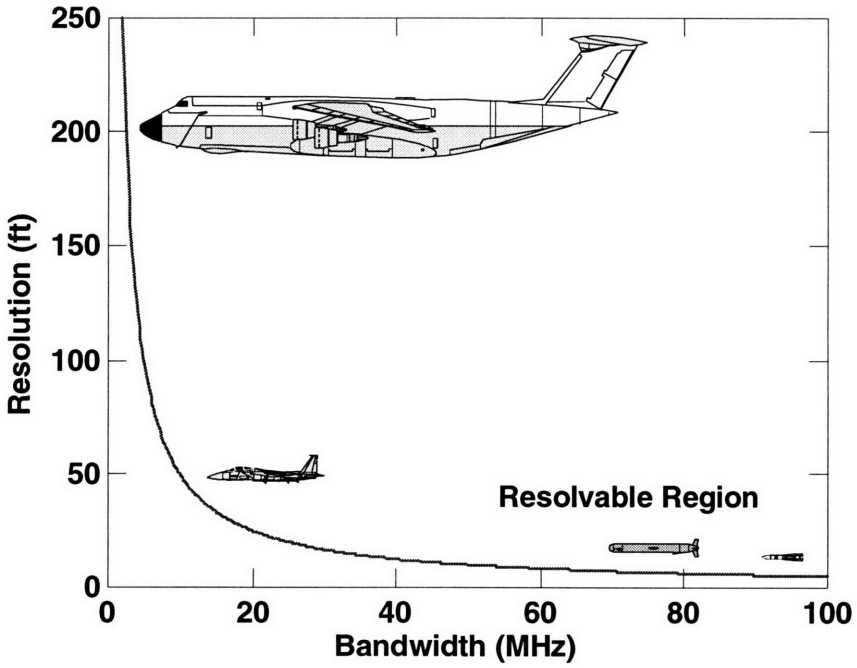

Figure 1-2: Plot of Bandwidth Requirement versus Resolvable Lengths for a Variety of Targets.

targets are drawn next to their respective lengths. The targets of particular interest are usually missiles, given by the two targets in the lower right hand corner of the plot, and it would require a bandwidth of at least 60 MHz to resolve the lengths of those targets. In general, target length identification requires an extremely wide bandwidth in order for it to be effective. The instantaneous bandwidth of the present radar system is only 250 kHz. Increasing the bandwidth to 60 MHz would require major, unrealistically expensive modifications to the hardware of the radar system. It will be shown subsequently that increasing the bandwidth to 60 MHz by stepped-frequency pulse train waveform approximations may also be very difficult as a result of phase distortions due to target motion. Therefore, it is more practical to focus on improving the present radar system for target height finding,

which is considerably less demanding on bandwidth.

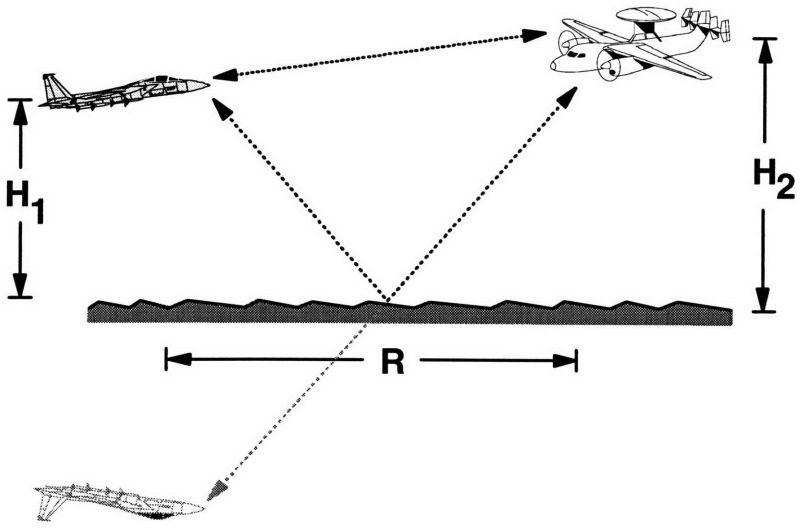

Figure 1-3: Illustration of Target Height Finding

The concept of target height finding using a radar that has wide bandwidth is illustrated in Figure 1-3[1]. This technique works only above water or highly reflective ground. Suppose that an airborne radar system is at height H_2 above the water observing a target at height H_1 above the water and a distance R from the radar. The transmission to and the reflection off the target can follow one of two paths. They can either follow a direct path, or they can bounce off the surface of the water. There are four possible combinations of paths that the transmission and the reflection can follow.

1. Both the transmission and the reflection can follow a direct path.

2. The transmission can follow the direct path and the reflection can bounce off of the water surface.

3. The transmission can bounce off of the water surface and the reflection can follow the

[1]The R shown in figure refers to the actual distance from the radar to the target and *not* the horizontal distance.

direct path.

4. Both the transmission and the reflection can bounce off of the water surface.

As a result, if the radar has sufficient range resolution, the target will appear at a range that corresponds to the actual range, and there will be a multipath image at a distance which corresponds to the difference in path length ΔR between the actual range and the length of the double bounce multipath described in situation 4. Given the height of the radar system, the range R of target, and the delay for the multipath – which can then be used to calculate ΔR, the height of the target is given by Equation 1.2 [14].

$$H_1 = \frac{2\,H_2}{R\,\Delta R} \tag{1.2}$$

This relationship is plotted in Figure 1-4 for some typical airborne radar operating parameters.

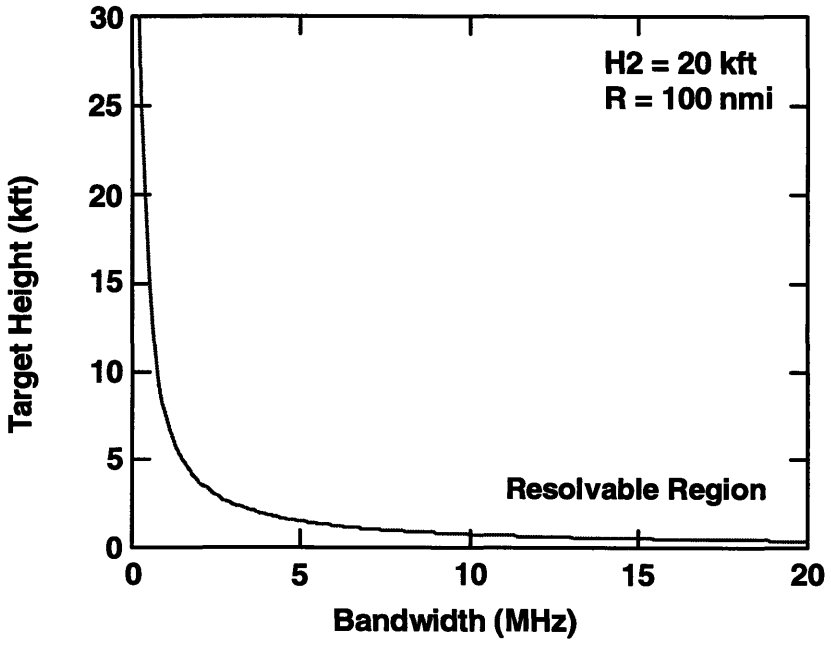

Figure 1-4: Plot of Bandwidth Requirement versus Resolvable Target Height for a Set of Typical Radar Operating Parameters.

The plot shows the bandwidth required to resolve target height when the airborne radar is at an altitude of 20 kft and a distance of 100 nmi from the target. The curve separates the resolvable region from the region where the target return and the image of return would overlap. If the present radar bandwidth can be increased from 250 kHz to about 5 MHz, which is possible using stepped-frequency pulse train waveform approximations, the system can resolve target heights above 2 kft, which would be very practical and highly desirable. In either the target length measurement application or the target height finding application, the ultimate goal is to increase the bandwidth of the present radar system.

The thesis is organized as follows: Chapter 2 investigates a linear frequency modulated chirp signal, which would be the most desirable signal to use in order to achieve a wide bandwidth. The mathematics governing the chirp signal as well as the concept of matched filtering the chirp signal is presented. There are also certain implementation issues involved that are addressed. Chapter 3 presents one stepped-frequency pulse train waveform approximation of the chirp signal, namely the continuous wave pulse train. The mathematics governing the processing of the continuous wave pulse train and Matlab simulations of the processing algorithm are presented. Simulations are done for the ideal case as well as for cases when there are non-uniform frequency steps, gaps in the frequency band, and phase distortions due to target motion. The linear frequency modulated pulse train, which is an enhancement of the continuous wave pulse train and more effective in some cases, is studied in Chapter 4. The mathematics and Matlab simulations behind the linear frequency modulated pulse train are shown, and an overlapping linear frequency modulated pulse train is introduced in order to reduce phase distortions due to target motion for constant moving targets. In Chapter 5, some practical applications of the algorithm as well as some non-coherent processing methods are used for multipath height finding on radar data collected using the RSTER system for various targets, including an internal moving target simulator and actual planes. Chapter 6 gives a summary of the findings and proposals for work to be done in the future.

Chapter 2

Chirp Signal

2.1 Mathematics of Pulse Compression

The advantages of using a chirp signal to increase radar range resolution, usually referred to as pulse compression, have long been recognized and exploited. A detailed analysis of the linear frequency modulated chirp signal is given in order to derive some stepped-frequency pulse train waveform approximations later on. A linear frequency modulated chirp signal, which is the only type of chirp signal that can be transmitted and received by the present radar system, is a signal whose frequency increases *linearly* with time. Although there may be other types of chirp signals, only the linear frequency modulated chirp will be studied and referred to from this point on. The following analysis and further detailed analyses can be found in Reference [9].

After a chirp signal is transmitted, the signal reflected by the target and received by the radar receiver is similar to the transmitted signal but delayed by the target range. It is then convolved with a signal whose frequency characteristic is the opposite to that of the chirp signal. The process of convolution is commonly referred to as pulse compression. The phase characteristic of the transmitter as well as the receiver is given in Figure 2-1.

The output of this convolution process, commonly known as the matched filter response, is a pulse compressed waveform in the time domain. It will be shown that there is a pulse width reduction factor of $T\Delta$ between the width of the transmitted pulse and the width of the compressed pulse, where T is the duration of the transmitted pulse and Δ is the

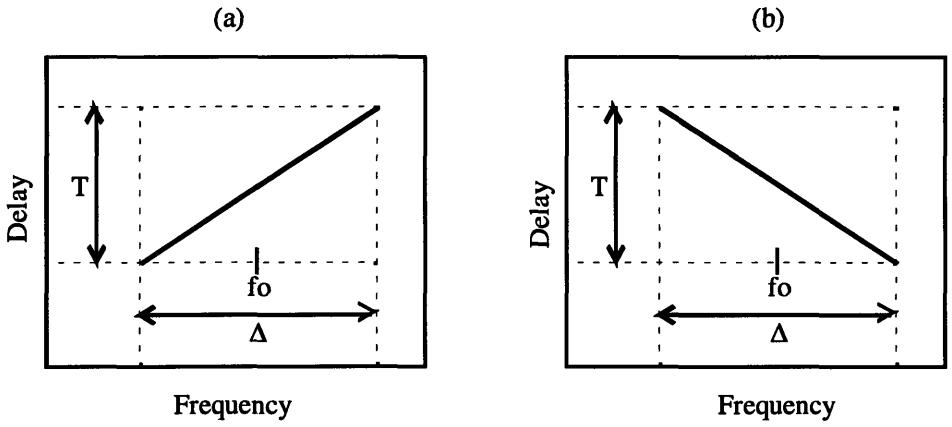

Figure 2-1: (a) Transmitted Pulse Characteristic and (b) Receiver Characteristic for Pulse Compressing a Linear Frequency Modulated Chirp Signal.

bandwidth of the transmitted pulse. The compressed signal will result in better range resolution, which can then be used for target height finding.

The transmitted pulse $s(t)$ can be expressed as a product of the envelope wave $e(t)$ and the carrier wave $c(t)$, where $e(t)$ is a rectangular envelope and $c(t)$ is an exponential with a linear frequency characteristic about a center frequency f_o.

$$\begin{aligned} s(t) &= e(t) \cdot c(t) \\ e(t) &= rect\left(\frac{t}{T}\right) \\ c(t) &= e^{2\pi i(f_o t + kt^2/2)} \end{aligned} \tag{2.1}$$

The function $rect(\frac{t}{T})$ is commonly known as the rectangular function and is expressed as:

$$\begin{aligned} rect(z) &= 1, |z| < 1/2 \\ &= 0, |z| > 1/2 \end{aligned} \tag{2.2}$$

It is clear from the expression of the envelope $e(t)$ that the domain of the signal is

$(-T/2, T/2)$, and the signal has a duration of T. Throughout the duration of the signal, the instantaneous frequency of the carrier waveform ranges from $f_o - kT/2$ to $f_o + KT/2$. The total change in frequency, Δ is the difference between the highest frequency and the lowest frequency and is equal to kT. The term Δ is known as the bandwidth of the signal. The mathematical analysis can be made easier if a simple change of variables is performed.

$$\begin{aligned} y &= t\Delta \\ x &= \frac{f}{\Delta} \\ D &\equiv T\Delta \end{aligned} \tag{2.3}$$

The product $T\Delta$ is a dimensionless product, commonly known as the "time-bandwidth product" and is a characteristic parameter of radar performance. The new signal $w(t)$ is expressed in terms of the new variables.

$$w(t) = rect\left(\frac{y}{D}\right) e^{2\pi i(x_o y + y^2/2D)} \tag{2.4}$$

where $x_o \equiv f_o/\Delta$ and $k = \Delta/T$. The duration of the signal is now D.

The signal $w(t)$ can be expressed in terms of its Fourier Transform $W(f)$, which is given by:

$$W(f) = \int_{-\infty}^{\infty} w(t) \cdot e^{-2\pi i f t} dt \tag{2.5}$$

The Continuous Time (CT) Fourier Transform for the chirp signal can be expressed in terms of the Fresnel integral. The Fourier Transform that is used throughout the thesis is the Discrete Fourier Transform (DFT) found using the Fast Fourier Transform (FFT) algorithm in Matlab, [3] and [20]. The FFT of the chirp signal and the matched filtered chirp signal are generated in Matlab using the procedure `chirp.m`, which can be found in Appendix A, along with other Matlab simulation routines. Figure 2-2 shows the plot of a portion of a chirp signal whose time-bandwidth product is 100. The plot shows only a portion of the signal rather than the entire signal because it becomes very cluttered otherwise, and the linear frequency characteristic of the signal will no longer be evident.

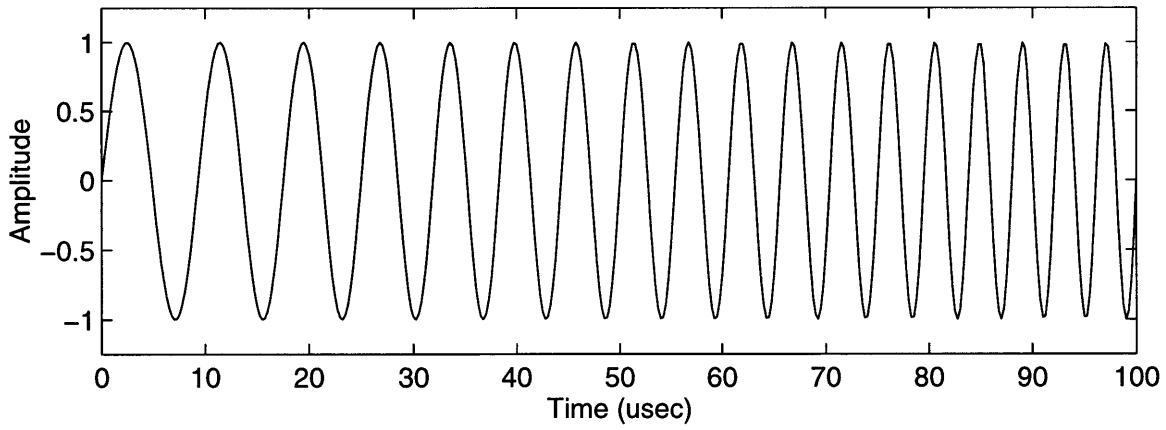

Figure 2-2: Plot of Portion of Chirp Signal (TB = 100).

It can be seen from the plot that the frequency of the signal is increasing with time. The frequency spectrum of the signal is given in Figure 2-3. It is evident that the signal has a wide bandwidth. There are ripples along the top of the chirp signal as a result of the FFT routine in Matlab.

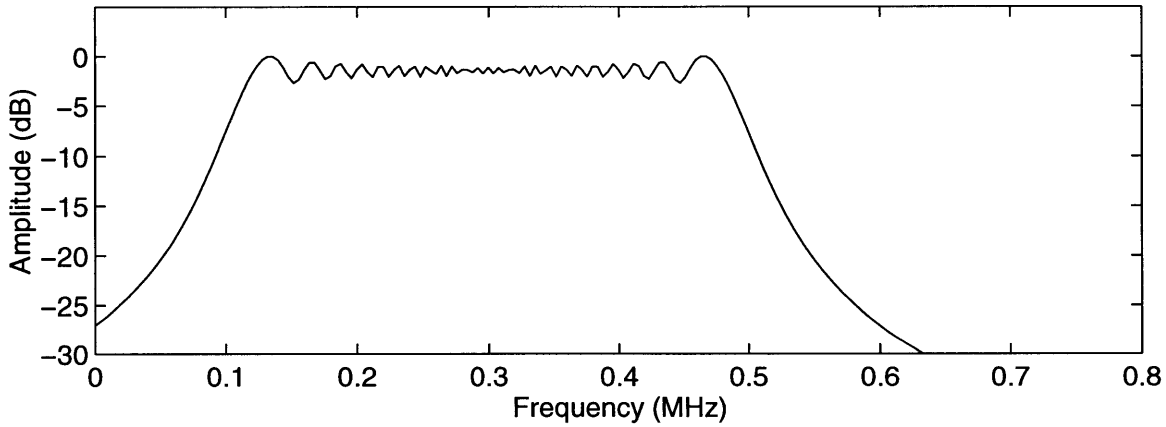

Figure 2-3: Plot of Frequency Spectrum of Chirp Signal (TB = 100).

The optimum method of processing a chirp signal is to pass it through a filter whose delay versus frequency characteristic is opposite to that of the signal, as shown in Figure

2-1(b). The frequency characteristic of the filter is given by:

$$H(f) = e^{i\pi(f-f_o)^2/k} \tag{2.6}$$

The frequency spectrum of the output of the matched filter, $Z(f)$ is given by the product of the Fourier Transform of the chirp signal and the Fourier Transform of the matched filter response. The output of the matched filter in the time domain, $z(t)$ is by Fourier analysis, the convolution of the chirp signal and the inverse Fourier Transform of the matched filter response $h(t)$. The mathematical analysis is given below:

$$\begin{aligned} Z(f) &= W(f) \cdot H(f) \\ z(t) &= w(t) \otimes h(t) \\ &= \int_{-\infty}^{\infty} w(t-v) \cdot h(v)\ dv \\ &= \int_{-\infty}^{\infty} w(l) \cdot h(t-l)\ dl \\ h(t) &= \int_{-\infty}^{\infty} H(f) \cdot e^{2\pi i f t}\ df \\ &= \int_{-\infty}^{\infty} e^{2\pi i[ft+(f-f_o)^2/2k]}\ df \end{aligned} \tag{2.7}$$

The inverse Fourier Transform integral evaluates to:

$$h(t) = \sqrt{\frac{i\Delta}{T}} e^{2\pi i(f_o t - kt^2/2)} \tag{2.8}$$

The output of the matched filter can then be found by convolution:

$$\begin{aligned} z(t) &= \sqrt{\frac{i\Delta}{T}} \int_{-T/2}^{T/2} e^{2\pi i[f_o t + k\tau^2/2 - k(t-\tau)^2/2]}\ d\tau \\ &= \sqrt{\frac{i\Delta}{T}} e^{2\pi i(f_o t - kt^2/2)} \int_{-T/2}^{T/2} e^{2\pi i k\tau}\ d\tau \end{aligned} \tag{2.9}$$

The integral can then be evaluated, simplified, and regrouped as follows:

$$z(t) = \frac{1}{\pi kt}\sqrt{\frac{i\Delta}{T}}\sin(\pi ktT)e^{2\pi i(f_o t - kt^2/2)} \quad (2.10)$$
$$= \sqrt{Di}\frac{\sin(\pi\Delta t)}{\pi\Delta t}e^{2\pi i(f_o t - kt^2/2)}$$

The matched filter output can also be expressed in terms of the new variable $y = \Delta t$.

$$z(y) = \sqrt{D}\frac{\sin(\pi y)}{\pi y}e^{2\pi i(x_o y - y^2/2D) + i\pi/4} \quad (2.11)$$

In order to simplify the notation for $z(y)$ further, the sinc function is defined.

$$\text{sinc}(x) = \frac{\sin(\pi x)}{\pi x} \quad (2.12)$$

The output of the matched filter can then be expressed as:

$$z(y) = \sqrt{D}\text{sinc}(y)e^{2\pi i(x_o y - y^2/2D) + i\pi/4} \quad (2.13)$$

The magnitude of the matched filter output is:

$$|z(y)| = \sqrt{D}\,|\text{sinc}(y)| \quad (2.14)$$

Figure 2-4 is the plot of the magnitude of the output of the matched filter. The sinc function is the Fourier Transform of the rectangular envelope of the transmitted signal, [18] and [19]. The linear magnitude of the output of the matched filter has zero crossings at integer multiples of $1/\Delta$, which in this case is equal to 2.5μs. It is evident from the plot that the time index where the first sidelobe begins in $2.5\mu s$. There is a net pulse width reduction of approximately $T\Delta$. The original pulse duration T is equal to $250\mu s$, and the bandwidth Δ is 0.4 MHz The compressed pulse duration, determined from the - 3dB points from the peak amplitude, is approximately $2\mu s$, and there is a net pulse width reduction by about two orders of magnitude.

A sinc function has unacceptably high near in sidelobes at approximately -12.5 dB from the peak, as seen in the plot. Therefore, a weighting function can be applied to the signal

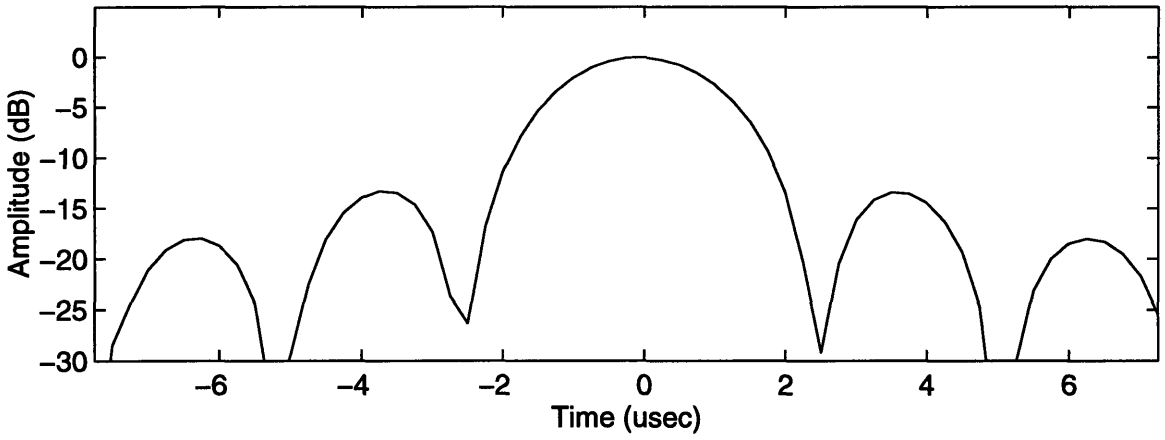

Figure 2-4: Plot of Matched Filter Output for Chirp Signal (TB = 100).

to reduce the signal sidelobes. A Chebychev weighting function with peak sidelobes at -40 dB below the peak is applied to the signal in Figure 2-2, and the results are shown in Figure 2-5 and Figure 2-6. The Chebychev weighting function used is the one in the Signal Processing Toolbox of Matlab and is specified by the total number of points (which in this case is 1,001) and the sidelobe level (which in this case is -40 dB below the peak). Figure 2-5 shows the magnitude of a portion of the chirp signal after it has been weighted by the Chebychev filter. The plot again only shows a portion of the chirp signal for clarity. The entire weighted chirp signal is symmetric and tapered at both ends. Figure 2-6 is the plot of the result after the matched filter is applied to the weighted signal in solid and the result after the matched filter is applied to the unweighted signal in dashed. The sidelobe is about -30 dB below the peak amplitude, which is a significant improvement over the unweighted case. The sidelobe is not -40 dB below the peak because only the chirp signal is weighted and not the matched filter response. There is also an increase in the width of the peak amplitude, although not by much. The width of the envelope of the compressed pulse is still reduced by approximately two orders of magnitude, and given the decrease in sidelobe level, it is clear that time weighting the transmitted signals will result in better resolution.

Since weighting the signal results in lower sidelobes, the Chebychev weighting function with the -40 dB sidelobe level will be applied to all subsequent simulations. The Chebychev weighting functions will only differ by the number of points in the weighting sequence.

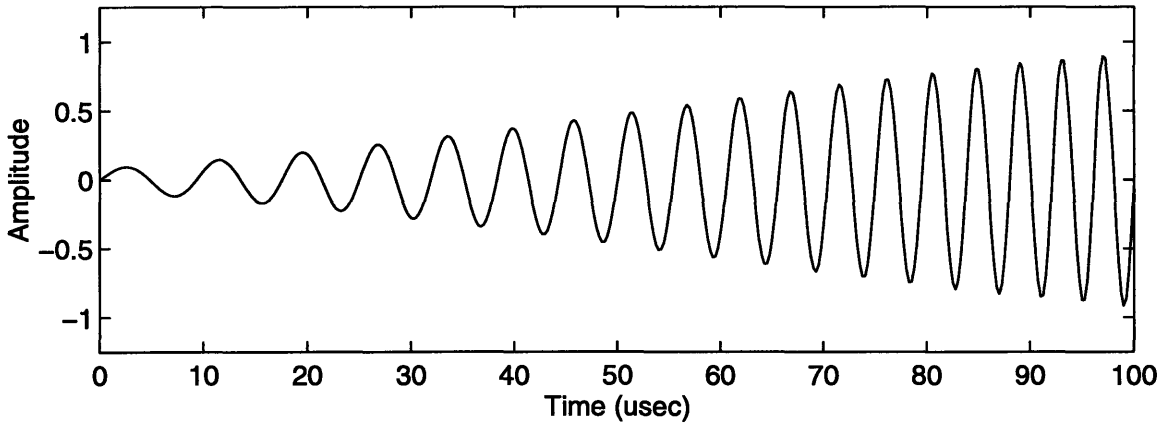

Figure 2-5: Plot of Portion of Chirp Signal (TB = 100) Weighted by Chebychev Weighting Function (1,001 pts, -40 dB sidelobe level).

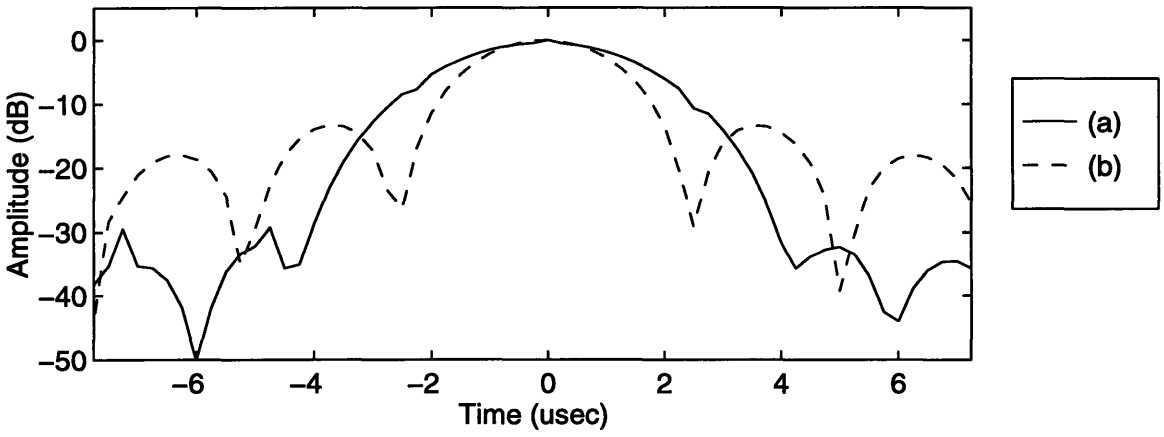

Figure 2-6: Plot of (a) Matched Filter Output of Weighted Chirp Signal and (b) Matched Filter Output of Unweighted Chirp Signal (TB = 100).

2.2 Implementation Issues

From the preceding analysis, it is obvious that transmitting and receiving chirp signals result in narrow pulses in the time domain, thus increasing the resolution of the system. Ideally, the radar system would transmit a chirp signal with a large bandwidth Δ. This is not practical to implement in the present radar system for several reasons.

The chirp signal is usually very expensive to implement, and since the present radar system has an instantaneous bandwidth of 250 kHz, it is not capable of matched filtering signals with a bandwidth greater than 250 kHz. Furthermore, the radar system operates in the UHF band, which ranges from 400 MHz to 500 MHz, as illustrated in Figure 2-7. It

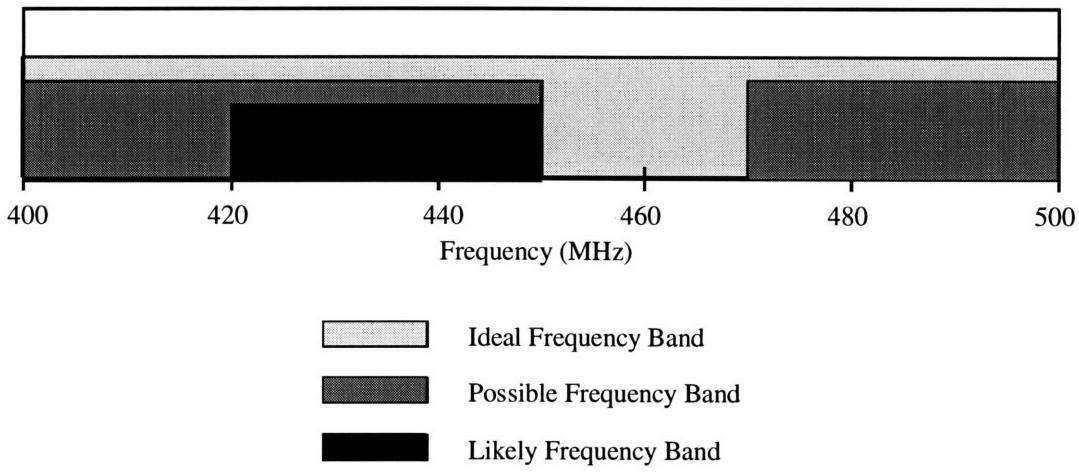

Figure 2-7: Plot of UHF Transmission Band.

would be ideal for the radar to transmit over the entire UHF band, as would have to be the case if a chirp signal were used. Realistically, the UHF band contains certain frequencies that are reserved for land mobile communications and television. As a result, there are gaps in the frequency band over which the radar is not permitted to transmit. Sometimes, the possible transmission frequency ranges are between 400 MHz - 450 MHz and 470 MHz - 500 MHz. Most of the time, the radar system can only transmit in a very narrow frequency

range, between 420 MHz - 450 MHz. At times, the available frequency band may even be as narrow as 5 to 10 MHz. In addition to gaps in the frequency band, there are often non-uniformities in frequency steps as a result of radar hardware. If the chirp signal were matched filtered over a frequency band with interference and noise due to hardware, the pulse compression would fail. It is therefore imperative in this case to look into certain approximations of the chirp signal that are more accommodating and less susceptible to interference and noise due to hardware.

2.3 Approximations of the Chirp Signal

Keeping in mind these implementation issues, several approximations of the chirp signal that require minimal changes to the present radar system are explored. These approximations are classes of Stepped-Frequency Pulse Train (SPT) waveforms. The SPT waveforms that are investigated include the continuous wave pulse train and the linear frequency modulated pulse train. The continuous wave pulse train consists of pulses at a single frequency, increasing linearly with each pulse. The linear frequency modulated pulse train consists of pulses that are themselves chirp signals but with a smaller bandwidth, one that the radar system is capable of transmitting and receiving. The center frequency of the smaller chirp signal increases linearly with each pulse.

Each approximation waveform is studied in detail. Due to the nature of the SPT waveforms implemented using the present radar system, there is additional phase distortion introduced as a result of target motion. Because the target is moving and there is delay between consecutive pulse transmissions in the waveform approximations, the target range will change between consecutive pulse transmissions. If significant, it will result in certain distortions in the processed waveforms of the continuous wave and the linear frequency modulated pulse train. This phenomenon is referred to as range walk. Range walk has not been a problem in the traditional implementation of SPT waveforms because the traditional implementation usually involves a burst of pulses transmitted very rapidly one after another, so the target motion during pulse transmissions is insignificant. This is not the case for the RSTER system. Due to certain hardware constraints, there is significant delay

between consecutive pulse transmissions. Rather than transmitting a burst of pulses and processing the burst of returns, a single pulse is transmitted and the return processed before the next pulse is transmitted. Consequently, the phase distortion due to target motion is present and has to be addressed. It will be shown that it can be reduced by overlapping frequencies between consecutive pulses in the linear frequency modulated pulse train.

In order to better understand the effect of implementation issues on the outcome of SPT waveform approximations, the following cases will be simulated for both the continuous wave pulse train and linear frequency modulated pulse train in Chapter 3 and Chapter 4.

1. Ideal pulse train.
2. Pulse train with non-uniform frequency steps between consecutive pulses.
3. Pulse train with gaps in frequency steps.
4. Pulse train with phase distortion due to target motion.

Chapter 3

CW Pulse Train

3.1 Background

The approximation of a chirp signal by a Continuous Wave (CW) pulse train is given in Figure 3-1. The term CW refers to sinusoids at a single frequency. The linear frequency

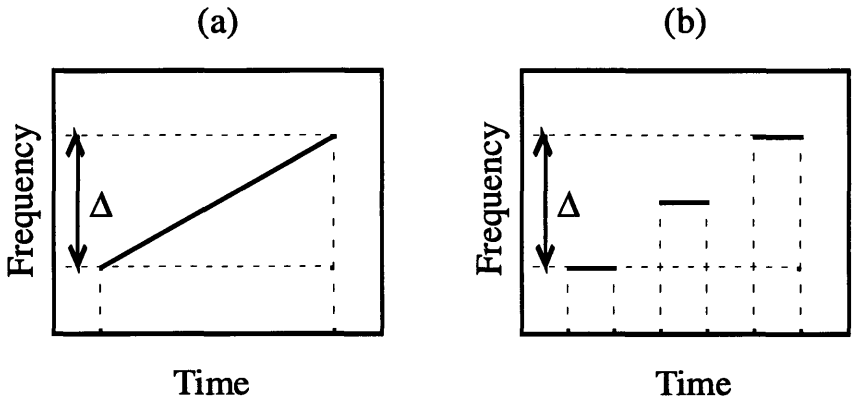

Figure 3-1: (a) Frequency Characteristic of Chirp Signal and (b) Frequency Characteristic of CW Pulse Train Implementation.

characteristic of a chirp signal is approximated by a series of discrete steps, each at a constant frequency and increasing linearly with every step. The overall bandwidth in both cases would be the same. The hardware implementation of the waveform is outlined in the block diagram in Figure 3-2. The modulator determines the frequency that will be

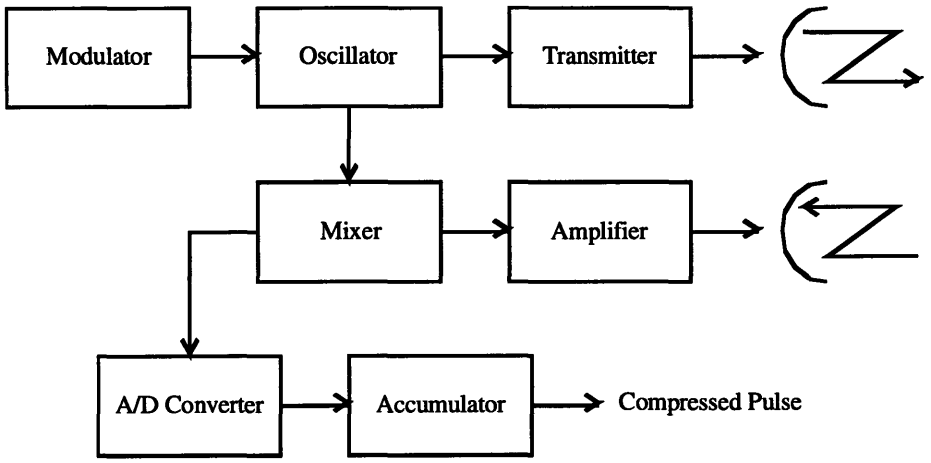

Figure 3-2: Block Diagram of Hardware Implementation of CW Pulse Train.

transmitted for a particular pulse. The local oscillator produces the discrete frequencies (f_k) of the transmitted signal and is also used to bring the frequency of the received and amplified signal down to baseband in the mixer. Because the same oscillator is used in the transmitter and receiver, the detection is coherent. After the signal is brought down to baseband, it can then be digitized, and the resulting pulse is weighted and summed with previous pulses to produce a compressed pulse.

The mathematical model of transmission and detection is given as follows: the transmitted signal is given by $r(t)$, which is the product of the pulse envelope multiplied by an exponential at a single frequency.

$$r(t) = p(t) \cdot e^{2\pi i f_k t} \tag{3.1}$$

The received signal is the transmitted signal shifted by the phase offset x, found in terms of the range of target R from the radar and the speed of light c.

$$\begin{aligned} x &= \frac{2R}{c} \\ y(t) &= r(t-x) \end{aligned} \tag{3.2}$$

$$= \quad p(t-x) \cdot e^{2\pi i f_k (t-x)}$$

In order to bring the signal down to baseband, i.e. a band that can accommodate the A/D converter, the coherent mixing operation is performed. The operation effectively multiplies the received pulse $y(t)$ by the complex conjugate of the transmitted pulse $r(t)$, and the resulting signal $v(t)$ has, upon filtering out the high carrier frequency component, only a low frequency component containing the phase offset due to range.

$$\begin{aligned} v(t) &= y(t) \cdot r^*(t) \\ &= p(t-x) \cdot e^{2\pi i f_k (t-x)} \cdot e^{-2\pi i f_k t} \\ &= p(t-x) \cdot e^{-2\pi i f_k x} \end{aligned} \tag{3.3}$$

After the signal is brought down to baseband, the complex envelope at each discrete frequency $V(f_k, t)$, is shifted and combined to form the compressed pulse $q(x, t)$ governed by the pulse compression equation in Equation 3.4,

$$q(x,t) = \sum_{k=0}^{N-1} V(f_k, t) \cdot e^{2\pi i f_k x} \cdot \Delta f \tag{3.4}$$

where Δf is the frequency spacing between each pulse. It can be seen from this equation that each complex envelope is "phase weighted" by the appropriate frequency and then summed. This equation can also be seen as the N-point DFT of the complex envelopes.

The CW pulse train approximations of a chirp signal will be simulated in subsequent sections for the four cases specified at the end of Chapter 2.

3.2 Simulations

3.2.1 Ideal CW Pulse Train

The condition for an ideal CW pulse train requires that CW pulses of duration T be transmitted at various frequencies, each a uniform frequency step Δf higher than the previous frequency. The different transmission frequencies comprise a frequency train. For the purpose of detection and better jammer suppression, the frequency train does not have to be

transmitted in order but can be randomized instead. However, the simulated frequency train will be in increasing order in the simulations for better characterization and understanding of the issues addressed.

The case when there are "large" frequency steps is considered first. The term "large" refers to frequency steps that violate the Nyquist criterion, which will be explained further subsequently. Figure 3-3 shows the plot of the frequency characteristic of a linear CW frequency train as a function of pulse number. The size of frequency steps in this case is 14 kHz, and the total bandwidth of the CW pulse train is 28 kHz. There is a frequency offset of approximately 0.11 MHz, which is introduced for better presentation of the frequency spectrum. It is the overall bandwidth of the pulse train that is most important to the width of the compressed pulse, so the offset is basically irrelevant in the analysis.

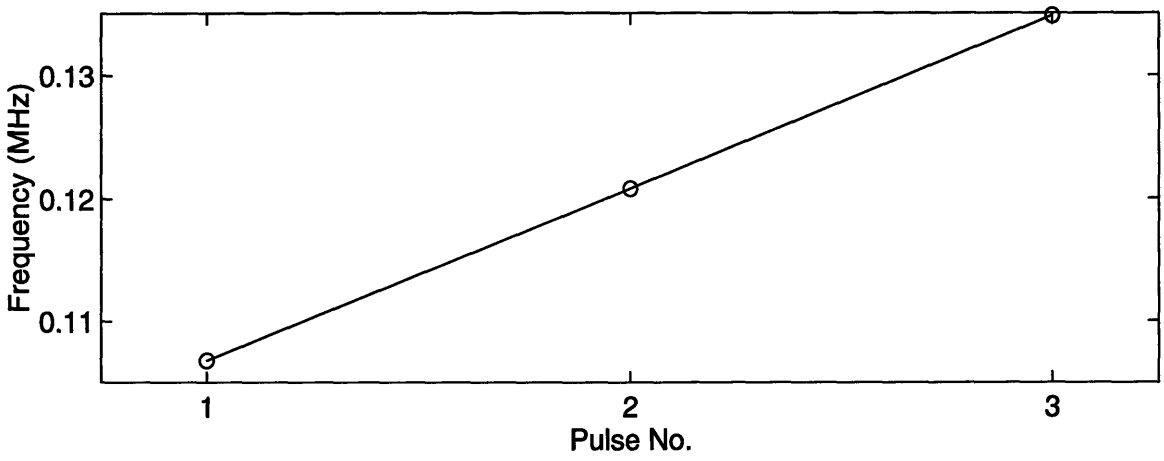

Figure 3-3: Plot of Frequency Characteristic of CW Pulse Train Violating Nyquist Criterion ($\Delta f = 14$ kHz, $\Delta = 28$ kHz).

A Matlab program was written which simulates the processing and pulse compression procedures for a CW pulse train. The name of the program is `simuspt.m` and can be found in Appendix A, along with many other Matlab procedures used to simulate both the CW and the LFM pulse train. The procedure simulates the process of transmission, pulse compression and pulse summation based on equation for $q(x,t)$ for an ideal CW pulse train. The time signal is weighted by the Chebychev weighting function used in Chapter 2, with a

-40 dB sidelobe reduction. The procedure used to generated the plots using the simulation program is `vncspt1.m`.

There is a restriction imposed on the frequency step sizes in order to prevent aliasing in the time domain, which is effectively the dual of the Nyquist criterion for the frequency domain. The requirement on Δf is expressed in terms of the pulse duration T.

$$\Delta f < \frac{1}{2T} \tag{3.5}$$

When the condition for frequency step size is not satisfied, there is aliasing in the time domain and ripples in the frequency spectrum of the compressed waveform. The case when the frequency steps do not satisfy the Nyquist criterion is simulated using `simuspt.m` and is plotted in Figure 3-4 for the time domain and Figure 3-5 for the frequency domain. The original signal has a pulse duration of 52 μs, which clearly violates the Nyquist criterion.

$$14,000 > \frac{1}{2(52 \times 10^{-6})} \approx 9,615$$

Figure 3-4 shows the compressed pulse in the time domain in solid. It is apparent that

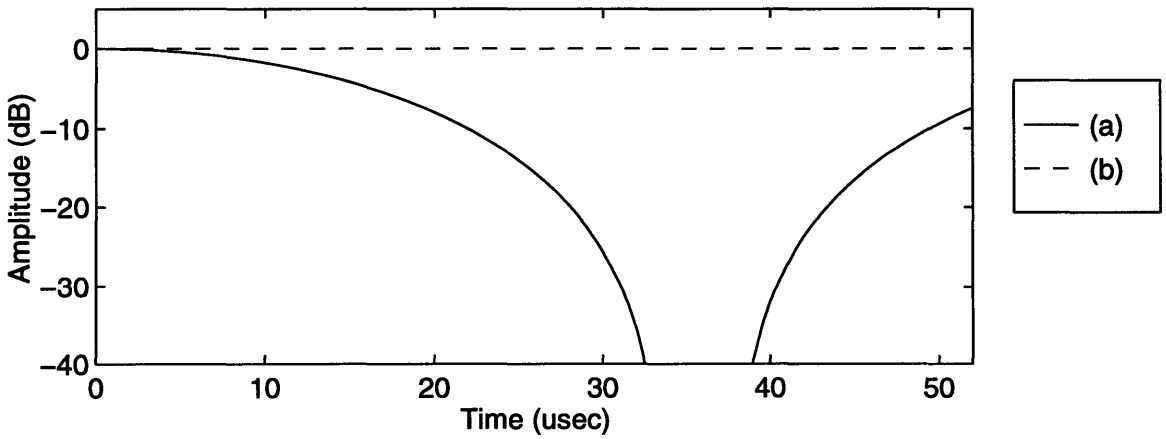

Figure 3-4: Plot of (a) Compressed Pulse of CW Pulse Train Violating Nyquist Criterion and (b) Envelope of a Single Pulse of CW Pulse Train.

there is severe distortion of the compressed pulse, and that it does not have the shape of the pulse compressed waveform given in Chapter 2. The dashed line shows the shape of

the envelope of a single pulse. It is clear that there is no significant reduction of the width of the compressed pulse when using a CW pulse train that violates the Nyquist criterion as compared to an envelope for a single carrier frequency. The frequency spectrum of the compressed pulse is shown in Figure 3-5.

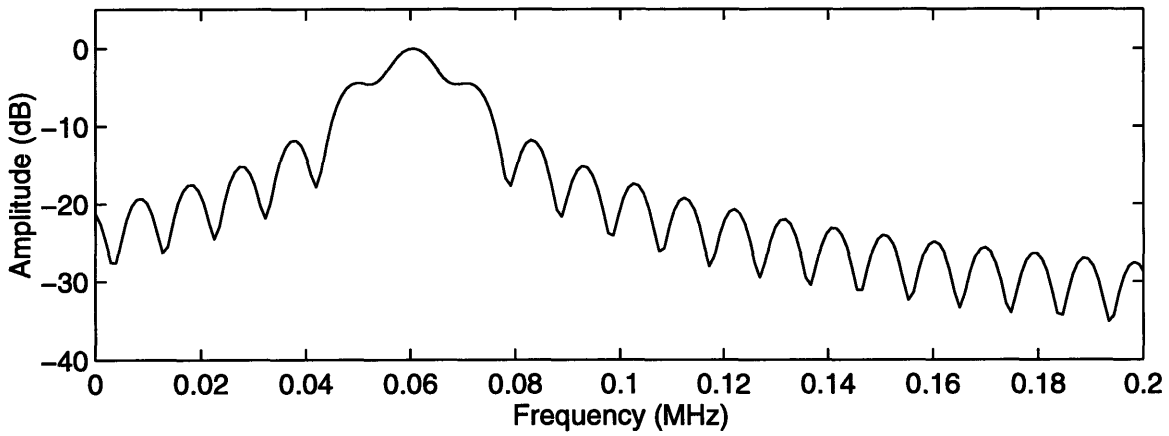

Figure 3-5: Frequency Spectrum of Compressed Pulse of CW Pulse Train Violating Nyquist Criterion.

It is evident in the plot of the frequency spectrum of the compressed pulse that it contains ripples. The level of the ripple is large enough such that the compressed pulse is severely distorted. It is intuitive that in violating the Nyquist criterion, the frequencies in the frequency train are too far apart to approximate a single wideband waveform, thus causing the ripples.

The case when the Nyquist criterion for the frequency step size is satisfied is shown in the following figures. Figure 3-6 is a plot of the frequency characteristic of a frequency train consisting of 20 pulses, each with a linearly increasing frequency. There is an initial frequency offset of 1 MHz, a frequency step size of 50 kHz, and a total bandwidth of 1 MHz. Each pulse is transmitted, and upon reception, processed coherently. The condition for processing is simulated using `simuspt2.m`. The procedure simulates the process of transmission, phase shift due to range, as well as pulse compression and pulse summation based on the equation for $q(x,t)$ for an ideal CW pulse train, a non-uniform CW pulse train, a gapped CW pulse train, as well as a CW pulse train with range walk distortions. Each

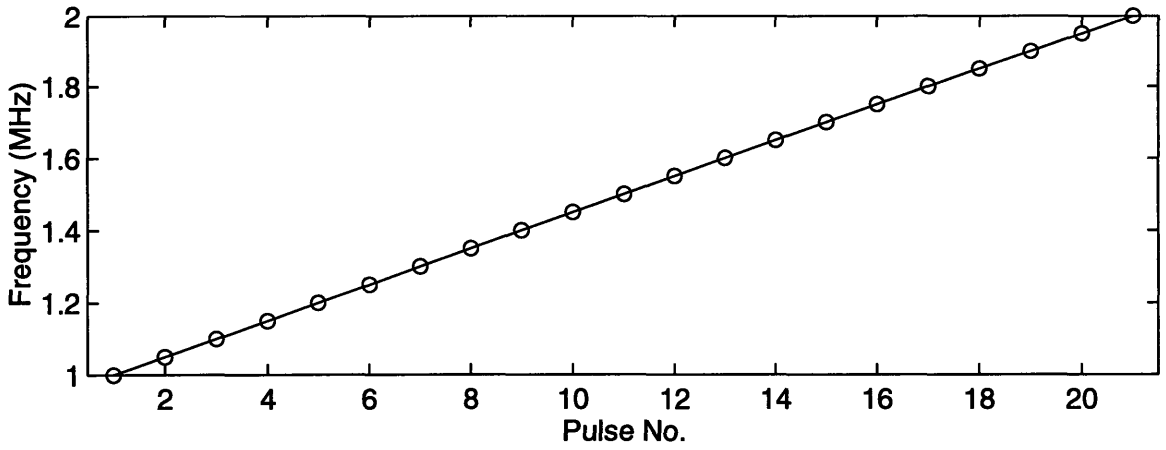

Figure 3-6: Plot of Frequency Characteristic of Ideal CW Pulse Train ($\Delta f = 50$ kHz, $\Delta = 1$ MHz).

pulse is again weighted by the Chebychev filter at -40 dB. The results are given in Figure 3-7 and Figure 3-8. The procedure used to generate the plots is `spt1_1.m`.

It is obvious from Figure 3-7 that the compressed pulse of a CW pulse train that does not violate the Nyquist criterion is similar to the compressed pulse of a chirp signal given in Figure 2-4. The transmitted pulse duration is 20μs, and the width of the compressed pulse, measured from -3dB below the peak, is about 2μs, which corresponds to a pulse width reduction factor of 10, which is approximately $T\Delta$. The time bandwidth product $T\Delta$ is equal to 20 in this case, which is less than $T\Delta$ in the chirp signal ($T\Delta = 100$). It can be increased if more pulses are transmitted or if the transmitted pulses are of longer duration.

The sidelobes of the compressed pulse are at approximately -40 dB, which are sufficiently low for range resolution. It is also clear from the frequency spectrum of the compressed pulse in Figure 3-8 that the compressed pulse does have the wideband characteristic of a chirp signal.

3.2.2 CW Pulse Train with Non-Uniform Step Sizes

In the actual implementation of the waveform, some frequencies in the frequency band may not be possible for the reasons given in Chapter 2. As a result, the difference between

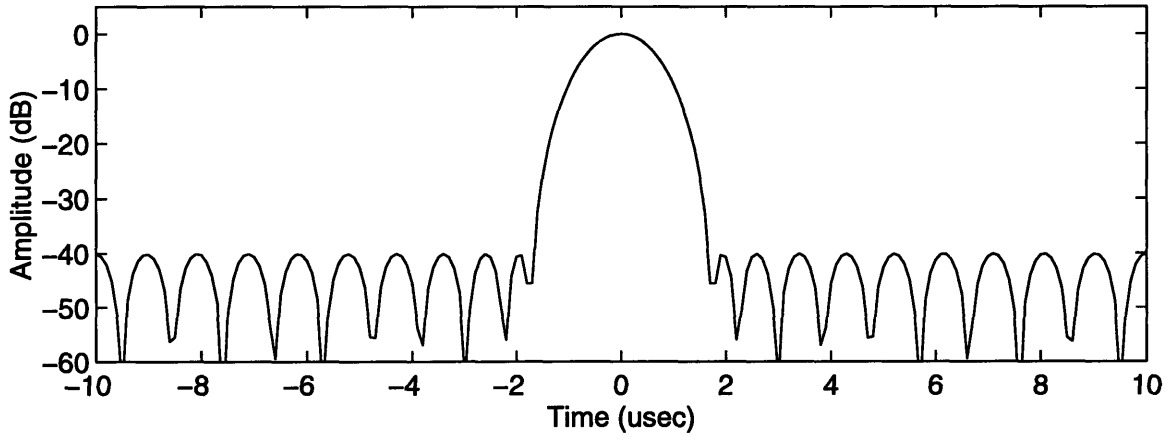

Figure 3-7: Plot of Compressed Pulse of Ideal CW Pulse Train.

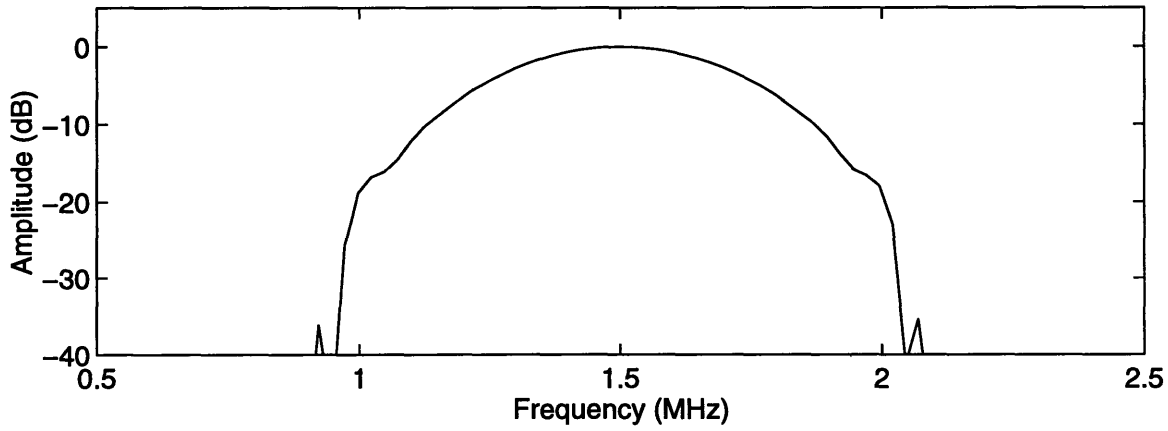

Figure 3-8: Frequency Spectrum of Compressed Pulse of Ideal CW Pulse Train.

consecutive frequency steps will be non-uniform. Non-uniformities in frequencies are usually due to hardware errors. This phenomenon is simulated by generating a frequency train with a uniformly distributed random step size error of $\pm\frac{\Delta f}{2}$, where Δf is again the frequency step size. The frequency characteristic of a CW pulse train with the random step size error is show in Figure 3-9. It is effectively the same pulse train as the one used for the ideal simulations. It is governed by the same set of parameters but with random step size error introduced.

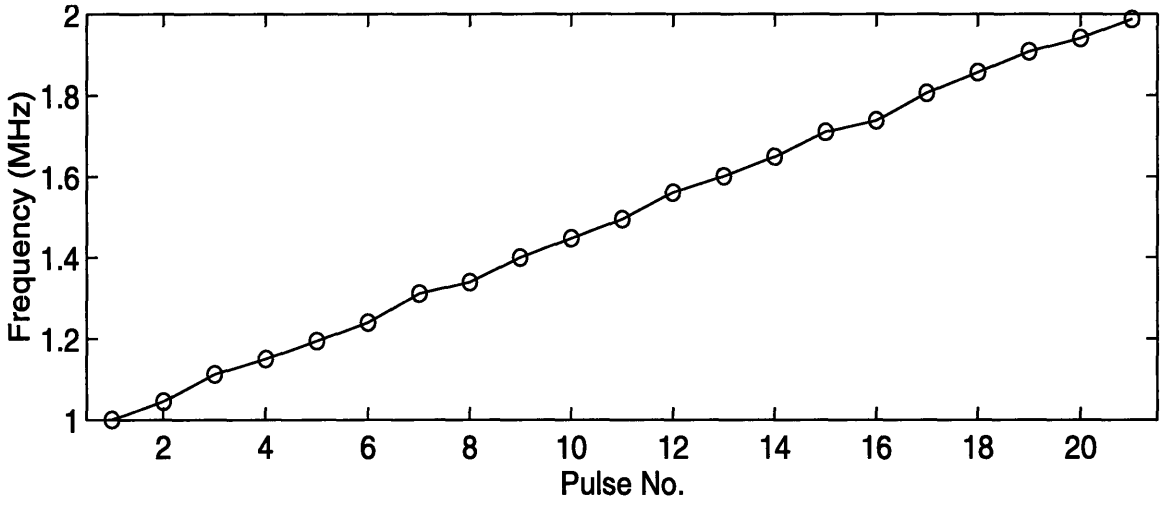

Figure 3-9: Plot of Frequency Characteristic of Non-Uniform CW Pulse Train ($\Delta f = 50$ kHz, $\Delta = 1$ MHz).

The weighted compressed pulse and the frequency spectrum of the compressed pulse of a non-uniform CW pulse train are plotted as the solid line in Figure 3-10 and Figure 3-11, respectively. The compressed pulse and the frequency spectrum of the compressed pulse for the case of the ideal CW pulse train is given in dashed line for comparison. The code for the simulation is also given in `spt1_1.m`.

It is apparent that the compressed pulse in the time domain for the case when there is non-uniform step size in the frequency train has higher range sidelobes compared to the ideal CW pulse train, and that there are ripples in the frequency spectrum of the compressed pulse. The effect of non-uniformity simulated in this case does not result in significant distortions in the compressed pulse because it is the far sidelobes that have

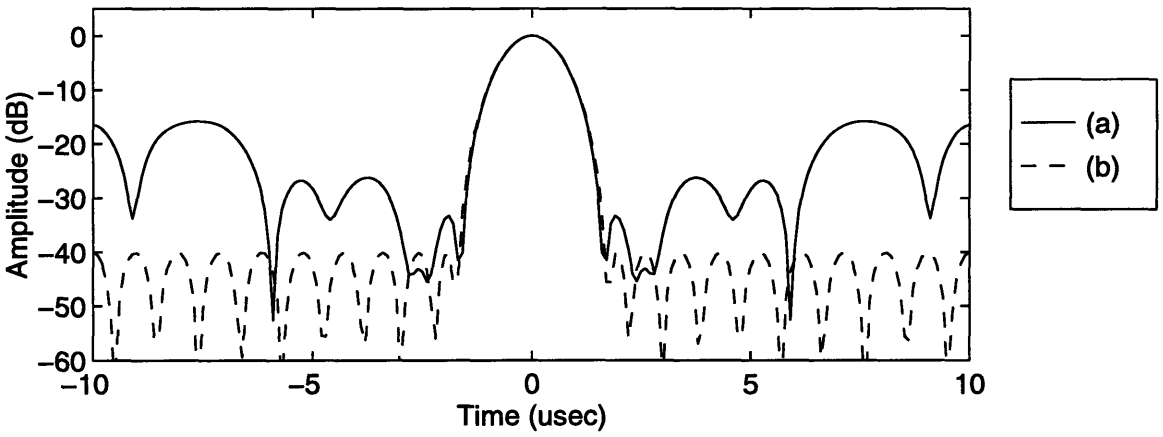

Figure 3-10: Plot of (a) Compressed Pulse of Non-Uniform CW Pulse Train and (b) Compressed Pulse of Ideal CW Pulse Train.

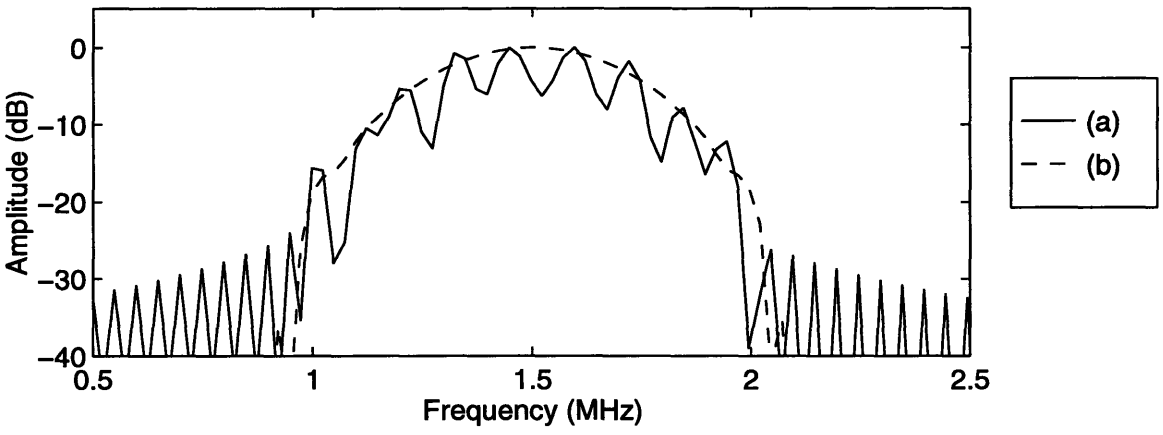

Figure 3-11: (a) Frequency Spectrum of Compressed Pulse of Non-Uniform CW Pulse Train (b) Frequency Spectrum of Compressed Pulse of Ideal CW Pulse Train.

increased significantly, while the near-in sidelobes did not increase by much. The sidelobes are now at approximately -18 dB, which would still be acceptable for range resolution.

3.2.3 CW Pulse Train with Gaps in Frequency Steps

As pointed out in Chapter 2, there are often significant gaps in the frequency transmission band. The cases when there are gaps in the frequency band is simulated using `spt1_2.m`, and the results are shown in Figure 3-12, Figure 3-13, and Figure 3-14.

Figure 3-12 shows a frequency train with missing steps between two sets of pulses, which models one gap in the transmission frequency band. The frequency steps within each set of pulses are uniform and has the same set of characteristics as the ideal CW pulse train.

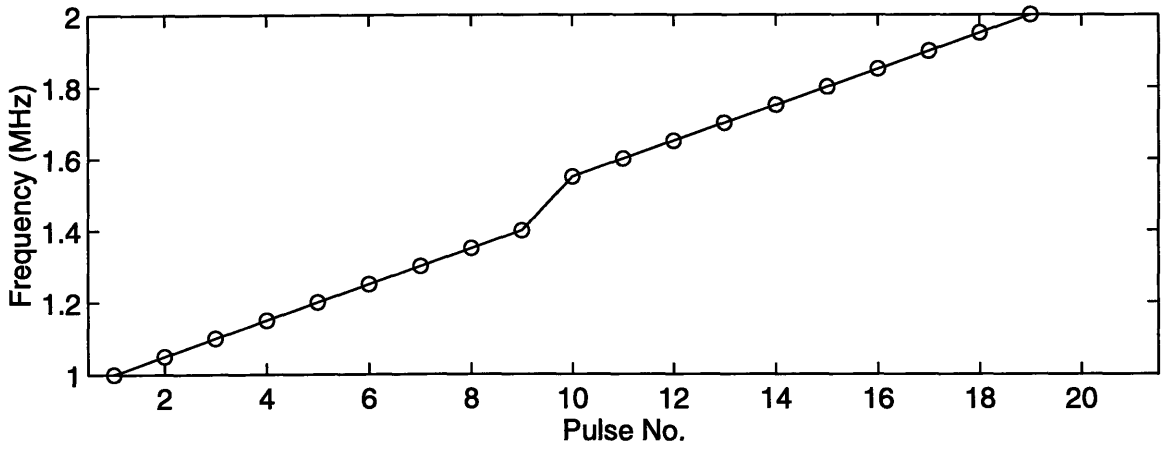

Figure 3-12: Plot of Frequency Characteristic of CW Pulse Train with Gaps in Frequency Steps ($\Delta f = 50$ kHz).

The effect of a gap in the frequency train on the compressed pulse and the frequency spectrum of the compressed pulse can be seen in Figure 3-13 and Figure 3-14, respectively. The compressed pulse for the frequency train with missing steps, shown as the solid line, has higher far sidelobes as well as higher near-in sidelobes than the compressed pulse of an ideal frequency pulse train, shown as the dashed line. The increase in sidelobes is more severe than in the case of a non-uniform CW pulse train. The near-in sidelobes are now at approximately -12 dB, which could lead to potential range detection problems, especially

in the presence of noise and background clutter.

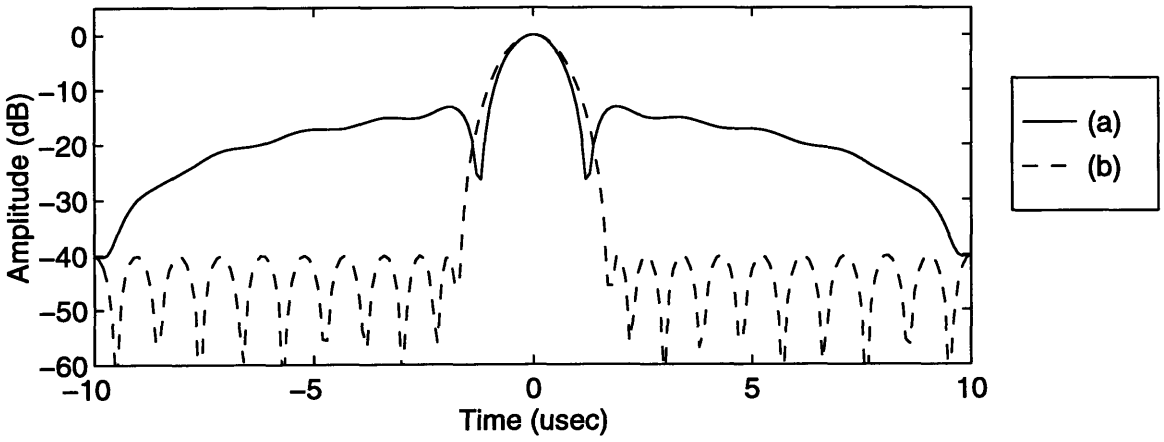

Figure 3-13: Plot of (a) Compressed Pulse of CW Pulse Train with Gaps in Frequency Steps and (b) Compressed Pulse of Ideal CW Pulse Train.

Due to the gap in the frequency train, the frequency spectrum of the compressed pulse for the frequency train with missing steps, again shown as the solid line, is no longer a continuous band but is composed of two discrete bands, which is similar to the likely frequency band shown in Figure 2-7. This characteristic would be expected, since the frequency components for those frequency bands are missing.

3.2.4 CW Pulse Train with Range Walk

Besides the frequency step issues addressed in previous sections, phase distortions due to target motion have to be considered. As explained in Chapter 2, when a target is moving with certain velocity, it will appear at different range bins between consecutive pulse transmissions due to the fact that there is delay between consecutive pulse transmissions. The effect on the compressed pulse has been simulated using the procedure `spt1_3.m` and is shown in Figure 3-15 and Figure 3-16.

The ideal CW frequency train from Figure 3-6 is used to construct the compressed pulse. A phase distortion of $0.5\mu s$ is introduced for each individual pulse. The distortion is used mainly for illustration and is somewhat high, but it would be applicable to the case when the target is moving very rapidly or when there is significant delay between consecutive

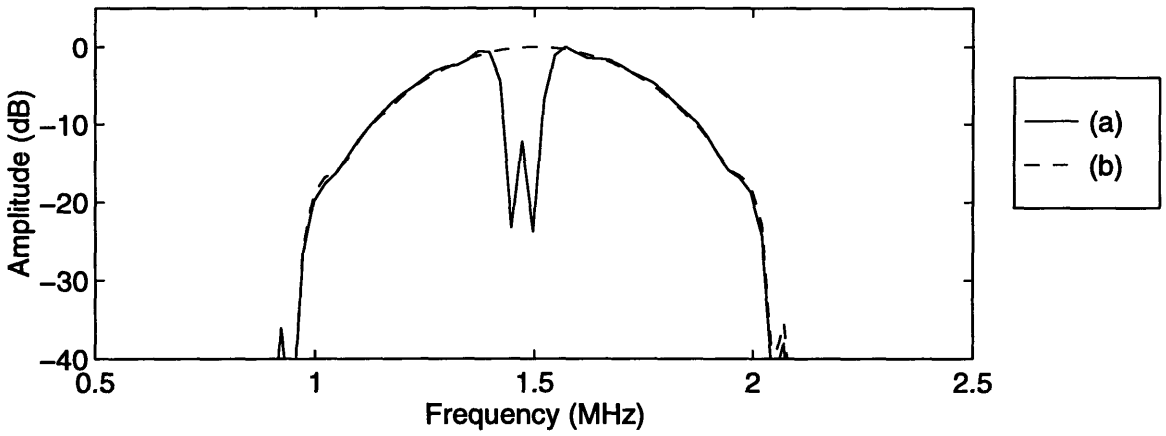

Figure 3-14: (a) Frequency Spectrum of Compressed Pulse of CW Pulse Train with Gaps in Frequency Steps and (b) Frequency Spectrum of Compressed Pulse of Ideal CW Pulse Train.

pulse transmissions.

Due to the nature of transmission, the phase distortion due to target motion increases with pulse transmission and is proportional to the sum of the pulse durations and the delays between consecutive pulses. It can be easily derived that the total phase distortion ϵ_n of pulse n from the first pulse, where the duration of each pulse is T and the delay between consecutive pulse transmission is δ for a target moving with constant velocity v, is:

$$\epsilon_n = \frac{2vn(T+\delta)}{c} \tag{3.6}$$

The compressed pulse and the frequency spectrum of the compressed pulse for the case of range walk due to targets moving with a constant velocity are shown in solid in Figure 3-15 and Figure 3-16, respectively. For comparison, the compressed pulse and the frequency spectrum of the compressed pulse for the ideal CW pulse train is again given as the dashed line. It is evident from Figure 3-15 that compared to the ideal case, shown as the dashed line, the compressed pulse has completely lost its compression in the time domain. The dot-dashed line shows the outline of the envelope of a single pulse. It is clear that the compressed pulse with range distortion is not much narrower than the original pulse envelope. It is evident from the frequency spectrum that there is amplitude distortion as

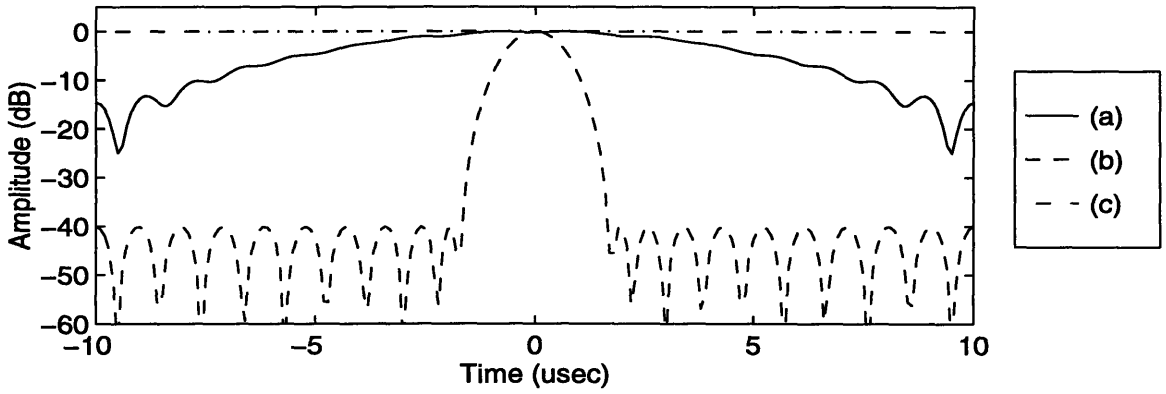

Figure 3-15: Plot of (a) Compressed Pulse of CW Pulse Train with Range Walk, (b) Compressed Pulse of Ideal CW Pulse Train, and (c) Envelope of a Single Pulse of the CW Pulse Train.

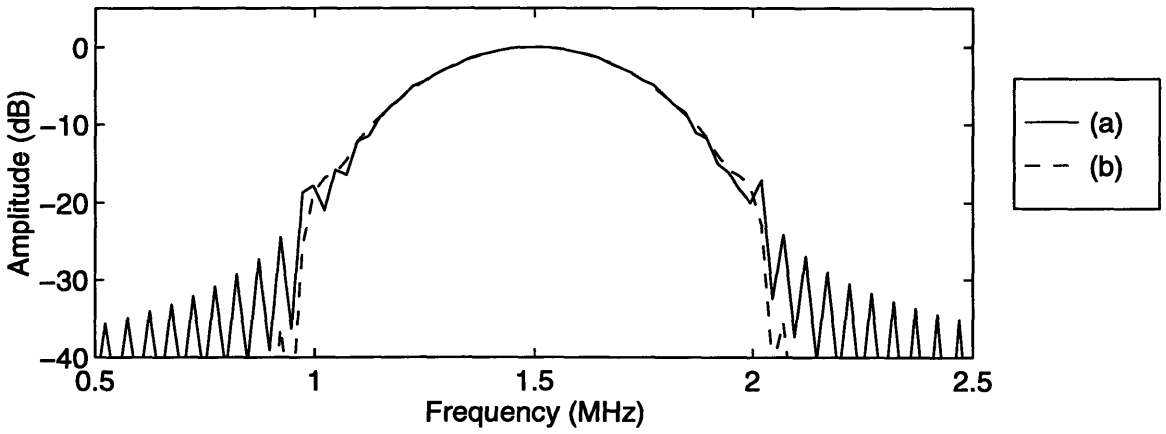

Figure 3-16: (a) Frequency Spectrum of Compressed Pulse of CW Pulse Train with Range Walk and (b) Frequency Spectrum of Compressed Pulse of Ideal CW Pulse Train.

a result of the phase distortion. The wideband characteristic of the compressed pulse is no longer preserved.

3.3 Summary

Due to hardware limitations in the present radar system, a CW pulse train is used to approximate a chirp signal. Given an ideal CW pulse train with uniform frequency step sizes, it is possible to approximate a chirp signal by phase weighting consecutive pulses by the appropriate frequencies provided that the Nyquist criterion for frequency step size given by Equation 3.5 is satisfied. The factor of reduction in the width of the compressed pulse from the width a single pulse is approximately $T\Delta$.

When there are non-uniformities in the form of uniform random step size errors of $\pm\frac{\Delta f}{2}$, there is an increase in the sidelobes of the compressed pulse and ripples in the frequency spectrum of the compressed pulse. The increase in the sidelobe level is not too severe, and mainly the far out sidelobes are affected, so range detection would still be possible. When there are gaps in the transmission frequency band, there is a more significant increase in the sidelobes of the compressed pulse, and the near-in sidelobes are the ones that are affected the most. The frequency spectrum of the compressed pulse has gaps that correspond to the missing frequencies. The increase in the level of sidelobes may be severe enough to interfere with range detection, especially in the presence of noise and background clutter.

Although both the non-uniformities in frequency step sizes and gaps in the frequency band result in distortions in the compressed pulse, the most severe distortion is by far due to range walk. Range walk results in loss of compression in the time domain and distortion of the frequency spectrum. The amount of distortion is proportional to the velocity of the target, the total number of pulses transmitted, as well as the pulse duration and the delay between consecutive pulse transmissions. When there is significant phase distortion due to target motion, the width of the compressed pulse is about the same as the width of the envelope of a single pulse, which defeats the purpose of utilizing the CW pulse train.

It is clear that a CW pulse train can approximate a chirp signal but is severely distorted when there are gaps in the frequency train and when there is phase distortion due to target

motion - range walk. An alternative approach will be considered that may lead to better performance given range walk, namely the LFM pulse train.

Chapter 4

LFM Pulse Train

4.1 Background

The use of a Linear Frequency Modulated (LFM) pulse train to approximate a chirp signal consists of transmitting a pulse train where each pulse within the pulse train is a small LFM pulse, as shown in Figure 4-1. In effect, the chirp signal is now approximated using a series of smaller chirp signals, and the frequency spectrum of each small chirp signal has a constant slope κ about a center frequency f_o.

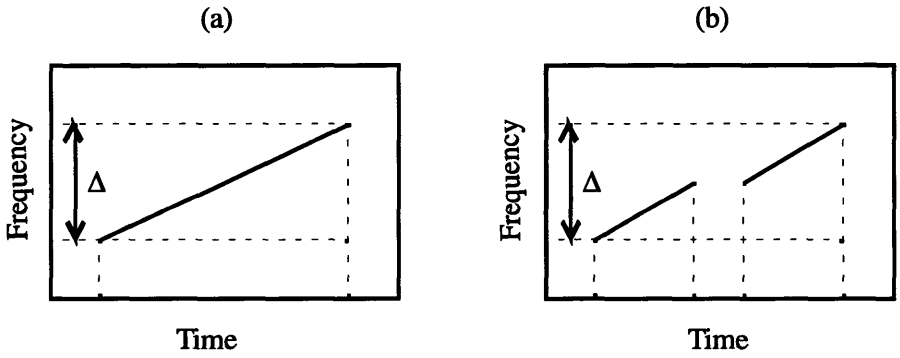

Figure 4-1: (a) Frequency Characteristic of Chirp Signal and (b) Frequency Characteristic of LFM Pulse Train Implementation.

The hardware implementation of the waveform is essentially the same as that given in

Figure 3-2. The only difference is instead of having the local oscillator transmit at a constant frequency f_k, the oscillator will now produce a linear frequency ramp as a function of time, with center frequency $\overline{f_k}$ and a constant slope κ. The same oscillator at that particular center frequency is then used to bring the received signal down to baseband in the mixer. The mathematical model of transmission and detection is essentially the same, except the signals are chirps instead of CW pulses. The mathematics now becomes vector analysis, where the transmitted frequency is a vector instead of a single number, and the results are essentially the same. The mathematics for the mixing operation and pulse compression routine is given for completeness as follows: the transmitted signal is given by $r(t)$, which is the product of the pulse envelope multiplied by an exponential with a frequency *vector* $\underline{f_k}$ with center frequency $\overline{f_k}$ for pulse k.

$$\begin{aligned} r(t) &= p(t) \cdot e^{2\pi i \underline{f_k} t} \\ \underline{f_k} &= \overline{f_k} + \frac{\kappa t}{2} \end{aligned} \tag{4.1}$$

The received signal is again the transmitted signal shifted by the phase offset x, and the calculations are carried out the same way for processing returns and filtering the signal, except the frequency is no longer a constant but a vector that is multiplied element by element with the time vector.

$$\begin{aligned} y(t) &= r(t-x) \\ &= p(t-x) \cdot e^{2\pi i \underline{f_k}(t-x)} \\ v(t) &= y(t) \cdot r^*(t) \\ &= p(t-x) \cdot e^{2\pi i \underline{f_k}(t-x)} \cdot e^{-2\pi i \underline{f_k} t} \\ &= p(t-x) \cdot e^{-2\pi i \underline{f_k} x} \end{aligned} \tag{4.2}$$

The result of the matched filtering operation is now a chirp signal about a center frequency instead of a single frequency. The processing of the pulses follows the same method, whereby

each pulse $V(\underline{f_k}, t)$ is shifted and combined to form the compressed pulse $q(x, t)$.

$$q(x,t) = \sum_{k=0}^{N-1} V(\underline{f_k}, t) \cdot e^{2\pi i \underline{f_k} x} \cdot \Delta f \tag{4.3}$$

Δf is the frequency spacing of the center frequency $\overline{f_k}$ between each pulse. The equation is about the same, and the frequency is replaced by a vector.

The Nyquist criterion for the frequency step size Δf is still applicable to the LFM pulse train. The LFM pulse train approximation of a chirp signal will be simulated in subsequent sections for the cases at the end of Chapter 2. A simulation code written in Matlab, `simufjb2.m` is used in the simulations and can be found in Appendix A. It models the transmission, reception, mixing, and summation for a series of -40 dB Chebychev weighted pulses for an ideal LFM pulse train, a non-uniform LFM pulse train, a LFM pulse train with gaps in frequency steps, and an LFM pulse train subject to phase distortion due to target motion.

4.2 Simulations

4.2.1 Ideal LFM Pulse Train

The case of an ideal LFM pulse train is simulated and shown. Figure 4-2 is a plot of the center frequency of a frequency train consisting of 15 pulses, which spans the entire frequency range of the 20 pulses of the CW pulse train presented in Chapter 3. There is an initial frequency offset of 1 MHz, a frequency step size of 75 kHz, an instantaneous bandwidth of 40 kHz, and an overall bandwidth of about 1 MHz. Each pulse is transmitted, and upon reception, processed coherently. The condition for processing is simulated, and the plots are generated using `spt2_1.m`. The results are plotted in Figure 4-3 and Figure 4-4. Figure 4-3 shows the compressed pulse in the time domain, and Figure 4-4 shows the spectrum of the compressed pulse in the frequency domain. The results are similar to that of the CW pulse train, which is expected since when the Nyquist criterion is obeyed, the CW pulse train should be no different from an LFM pulse train. The pulse width of the original pulses is the same as the CW case, and there is a pulse width reduction by a

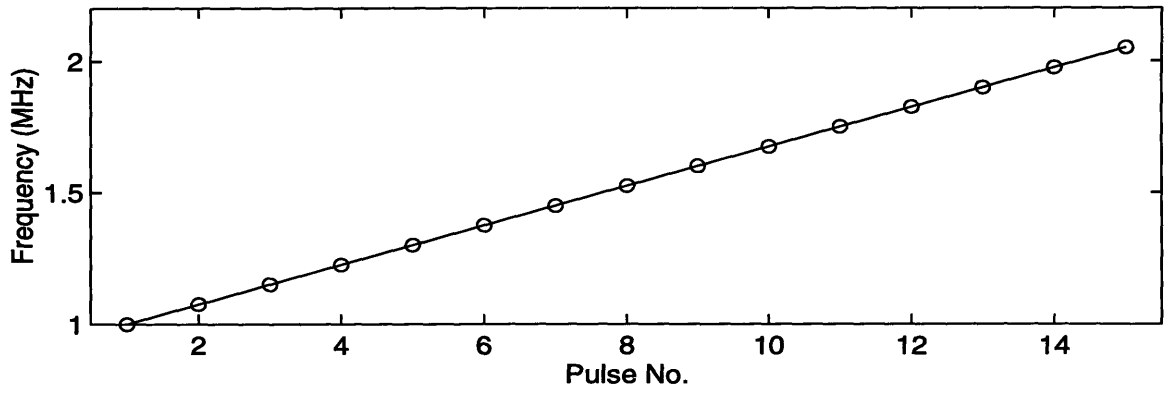

Figure 4-2: Plot of Frequency Characteristic Center Frequencies of Ideal LFM Pulse Train ($\Delta f = 75$ kHz, $\Delta \approx 1$ MHz).

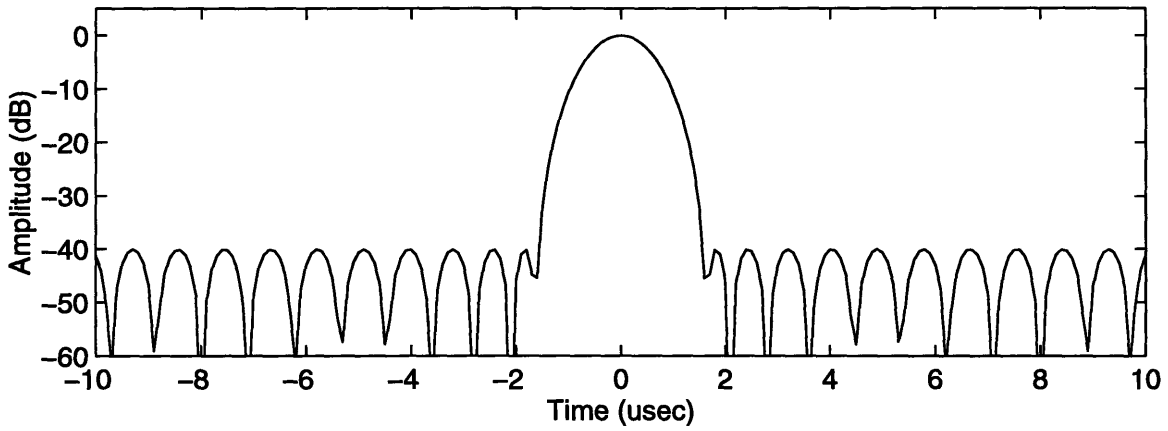

Figure 4-3: Plot of Compressed Pulse of Ideal LFM Pulse Train.

factor of approximately $T\Delta$ in the compressed pulse. The compressed pulse has a maximum sidelobe level of -40 dB below the peak, which is a result of the weighting function. The frequency spectrum shows a wide frequency band with very low sidelobes.

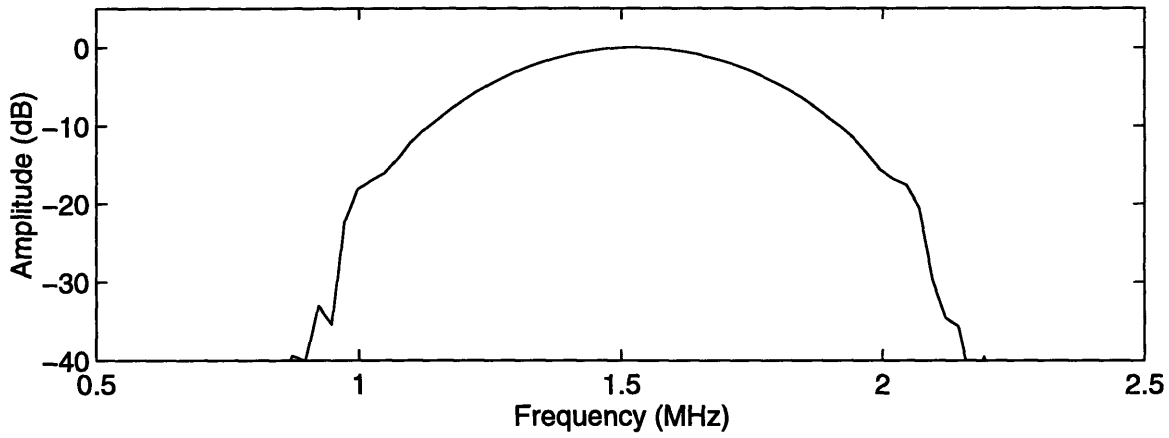

Figure 4-4: Frequency Spectrum of Compressed Pulse of Ideal LFM Pulse Train.

4.2.2 LFM Pulse Train with Non-Uniform Step Sizes

The case when there are non-uniformities in the frequency train is considered next. The non-uniformity investigated is that of the frequency step sizes between each pulse. The non-uniformity of the frequency steps within each pulse is fairly negligible compared to the frequency step size between each pulse because the magnitude of Δf is significantly greater than the magnitude of δf (δf is the frequency step between consecutive time samples within a single LFM pulse). For example, the frequency step size between consecutive pulses of the ideal LFM pulse train simulated is 75 kHz, while the frequency step size within each pulse of the pulse train is only 0.1 kHz.

The process of transmitting the LFM pulse train with non-uniformities in the frequency step sizes between pulses and uniform steps within each pulse is simulated using `spt2_1.m` and given in Figure 4-5, Figure 4-6, and Figure 4-7. Figure 4-5 presents the frequency characteristic of the center frequencies of the pulse train as a function of pulse number for a total of 15 pulses. There is a uniformly distributed random frequency step size error of $\pm\frac{\Delta f}{2}$ between consecutive pulse transmissions. The parameters of the frequency characteristic in

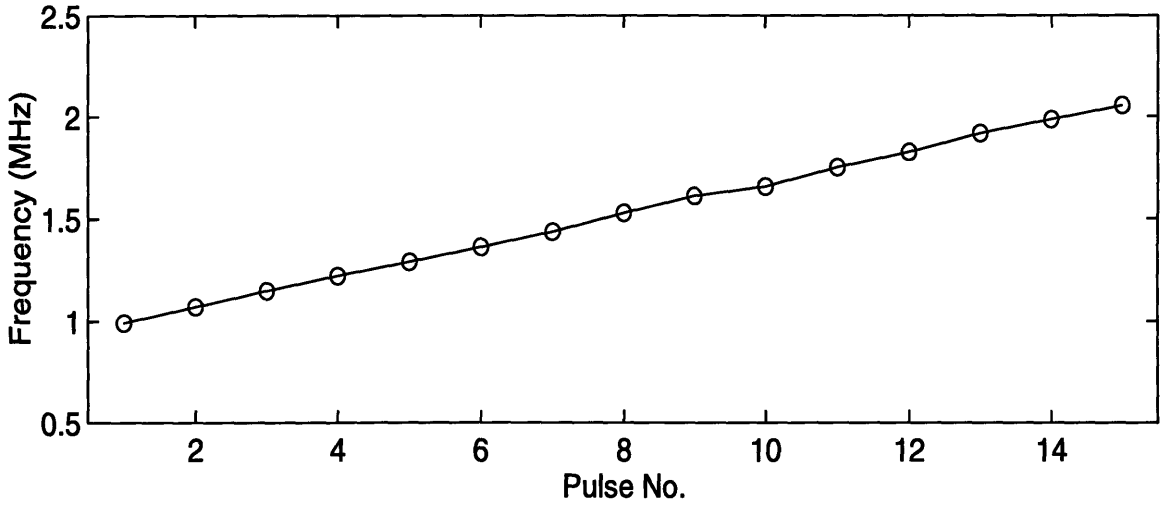

Figure 4-5: Plot of Frequency Characteristic of Center Frequencies of Non-Uniform LFM Pulse Train ($\Delta f = 75$ kHz, $\Delta \approx 1$ MHz).

this case is the same as that of the ideal LFM pulse train. There is a frequency step size of approximately 75 kHz (due to errors introduced), an instantaneous bandwidth of 40 kHz, and an overall bandwidth of about 1 MHz. Figure 4-6 shows the compressed pulse for the non-uniform LFM pulse train as the solid line and the compressed pulse for the ideal LFM pulse train as the dashed line for comparison. The frequency spectra for both the ideal case and the non-uniform case are shown in Figure 4-7. It is evident from the figures that when there are non-uniformities in the frequency step size, there is an increase in the sidelobes of the compressed pulse as well as ripples in the frequency spectrum of the compressed pulse, which is also the case for the CW pulse train. Again the far out sidelobes are affected more than the near-in sidelobes. The level of the sidelobes are now at about -10 dB below the peak, which is an 8 dB increase from the sidelobe level of the CW pulse train. This is due to the fact that the frequency step size, Δf is greater in this case than in the case of the CW pulse train in order for the LFM pulse train to span the same bandwidth with fewer pulses. The frequency step size of the CW pulse train is 50 kHz and is 75 kHz for the LFM pulse train. This shows that as the range of non-uniformities increase, there is an increase in the level of sidelobes. In the case where the span of non-uniformity is very large, it would

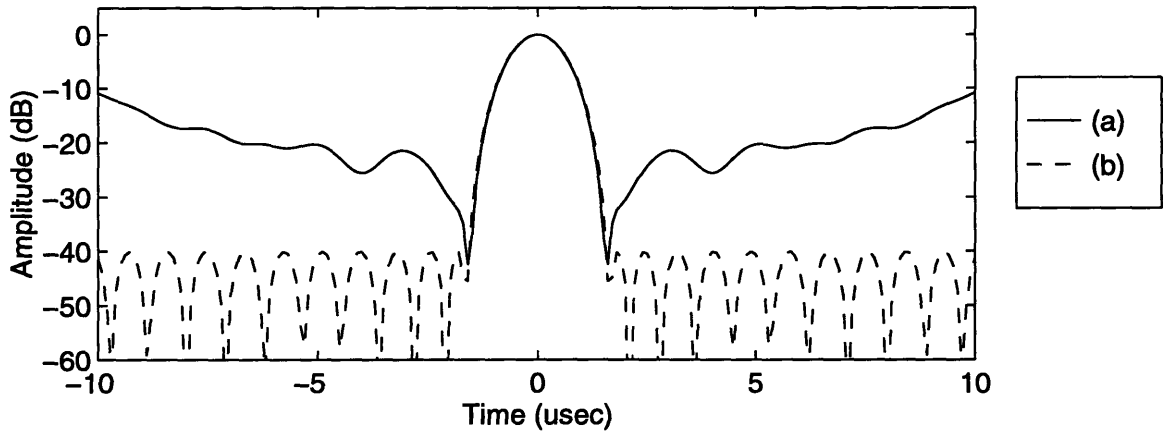

Figure 4-6: Plot of (a) Compressed Pulse of Non-Uniform LFM Pulse Train and (b) Compressed Pulse of Ideal LFM Pulse Train.

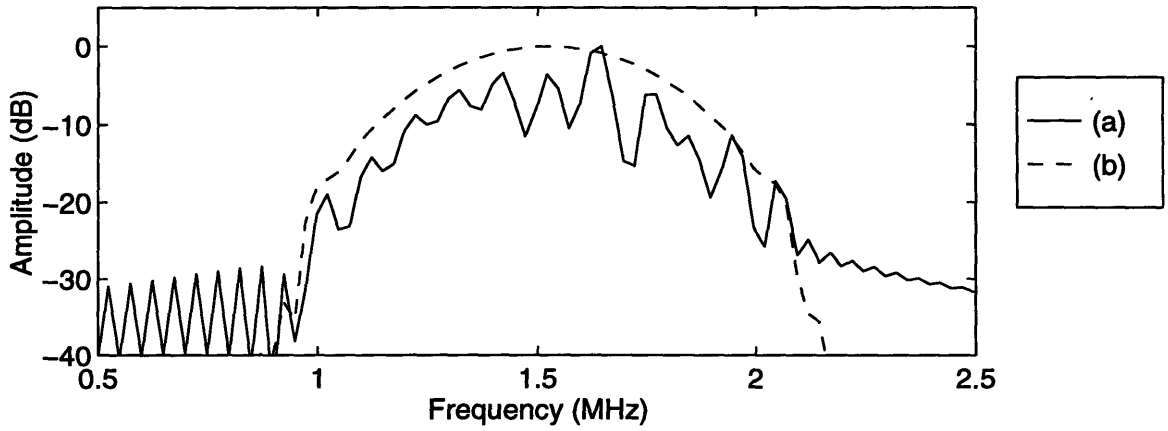

Figure 4-7: (a) Frequency Spectrum of Compressed Pulse of Non-Uniform LFM Pulse Train and (b) Frequency Spectrum of Compressed Pulse of Ideal LFM Pulse Train.

correspond to a band gap, which results in a very severe sidelobe increase, as seen earlier. Besides the increase in sidelobe level, there is also an increase in the level of ripples in the frequency spectrum of the compressed pulse as compared to the case of the non-uniform CW pulse train, which is again expected since there is an increase in frequency step sizes as well as the range of non-uniformities in the frequency step sizes.

4.2.3 LFM Pulse Train with Gaps in Frequency Steps

The case when there are gaps in the transmission frequency band is studied and simulated using `spt2_2.m`, and the results are presented in Figure 4-8, Figure 4-9, and Figure 4-10. Figure 4-8 presents the frequency characteristic of the center frequencies of the transmitted pulse train as a function of pulse number. There is a gap in the middle of the frequency train that may correspond to actual frequency spectrum conditions. The frequency steps outside the gap are uniform and are the same as the ideal LFM pulse train ($\Delta f = 75$ kHz). Figure

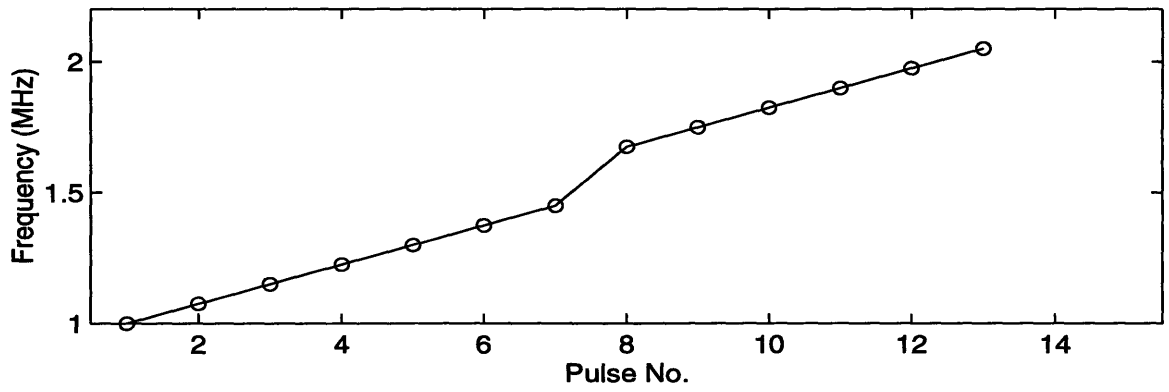

Figure 4-8: Plot of Frequency Characteristic of Center Frequencies of LFM Pulse Train with Gap in Frequency Steps ($\Delta f = 75$ kHz).

4-9 shows the compressed pulse of the gapped frequency train in solid and the compressed pulse of the ideal frequency train for comparison in dashed. The frequency spectra of the compressed pulses are shown in Figure 4-10. It is evident from the figures that gaps in the transmission frequency band will result in an increase in the sidelobes of the compressed

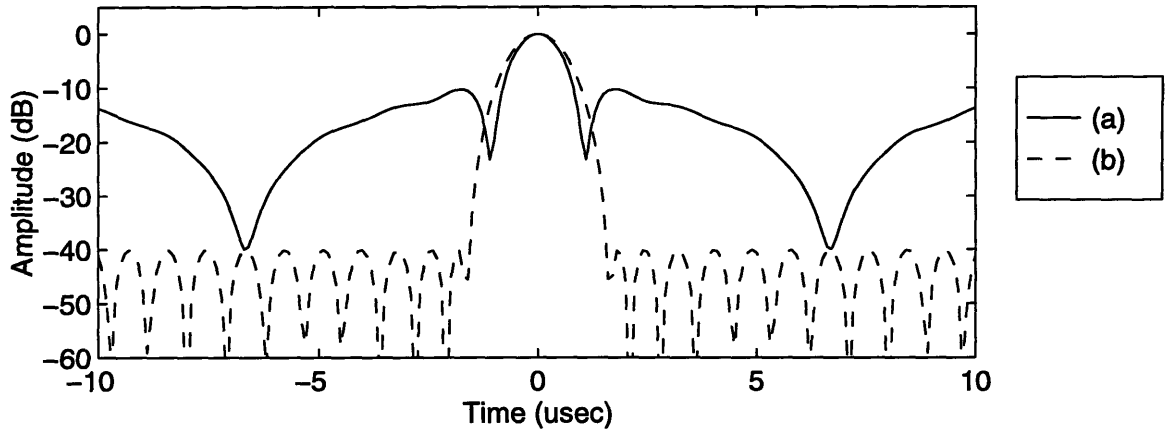

Figure 4-9: Plot of (a) Compressed Pulse of LFM Pulse Train with Gaps in Frequency Steps and (b) Compressed Pulse of Ideal LFM Pulse Train.

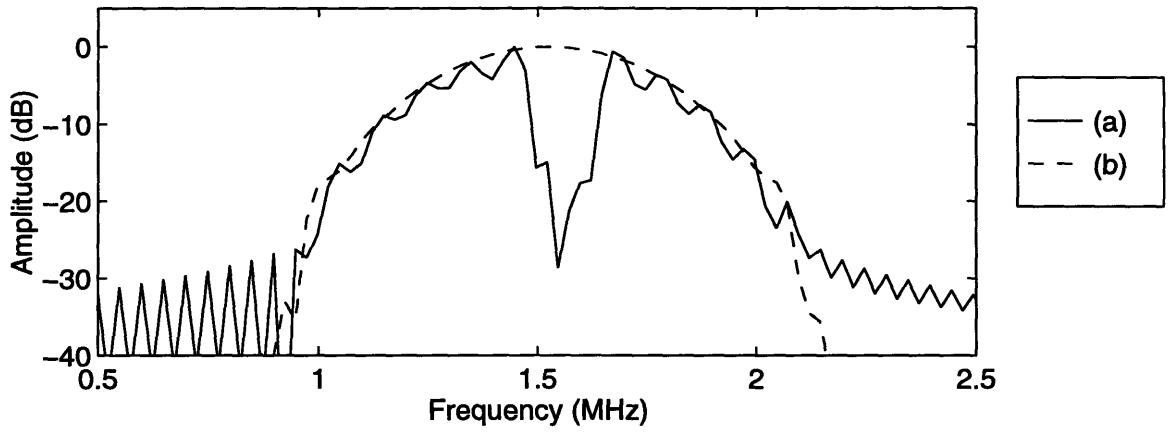

Figure 4-10: (a) Frequency Spectrum of Compressed Pulse of LFM Pulse Train with Gaps in Frequency Steps and (b) Frequency Spectrum of Compressed Pulse of Ideal LFM Pulse Train.

pulse (usually the near-in sidelobes) and corresponding gaps in the frequency spectrum of the compressed pulse. The sidelobes of the compressed pulse has increased to about -10 dB, which would cause problems in noise and background clutter.

4.2.4 LFM Pulse Train with Range Walk

The case when there is range walk between consecutive pulse transmissions is simulated using `spt2_3.m`, and the results are found as follows. The ideal LFM pulse train in Figure 4-3 is used, and a significant phase distortion due to target motion ($0.5\mu s$) is introduced between consecutive pulse transmissions. The phase distortion is again somewhat high for illustration purposes. This phase distortion also increases with consecutive pulse transmissions. Figure 4-11 shows the compressed pulse of the LFM pulse train with significant phase distortion due to target motion in solid and the compressed pulse when there is no range walk in dashed. For further comparison, the magnitude of the pulse envelope of a single pulse is shown in dot-dashed. It is apparent that range walk will lead to severe distortions in the

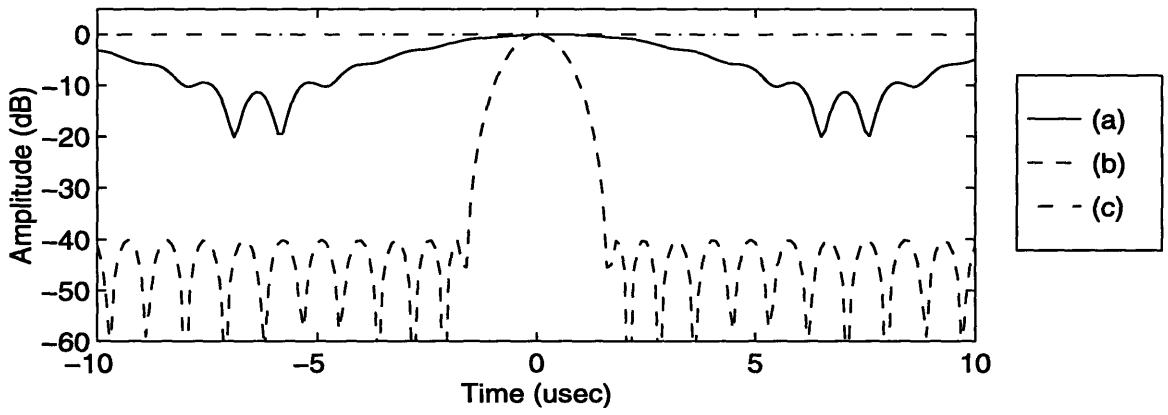

Figure 4-11: Plot of (a) Compressed Pulse of LFM Pulse Train with Range Walk ($0.5\mu s$), (b) Compressed Pulse of Ideal LFM Pulse Train, and (c) Envelope of Single Pulse of LFM Pulse Train.

compressed pulse. In this case, the distortion is slightly better than the case of range walk in the CW pulse train but is still very severe. There is not a total loss of compression, as in the case of the CW pulse train. There is an increase in the width of the envelope, and

the near-in sidelobes are about -10 dB below the peak, but the far sidelobes are about -3 dB from the peak, which would result in severe interference and loss of compression. The frequency spectra of the compressed pulses of an ideal LFM pulse train and a LFM pulse train with range walk are shown in Figure 4-12, and the distortion due to range walk is also evident.

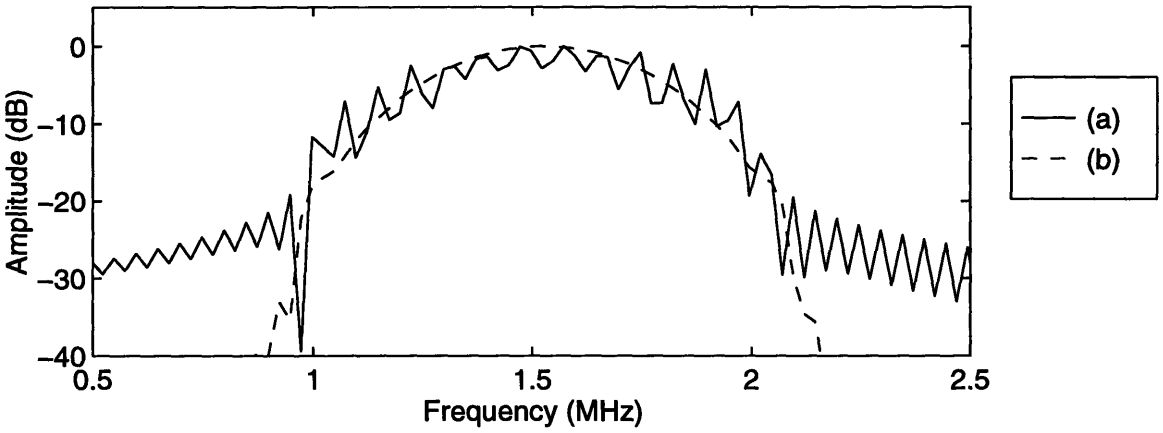

Figure 4-12: (a) Frequency Spectrum of Compressed Pulse of LFM Pulse Train with Range Walk (0.5μs) and (b) Frequency Spectrum of Compressed Pulse of Ideal LFM Pulse Train.

A more detailed comparison is made between the compressed pulse of an LFM pulse train with 15 pulses and the compressed pulse of a CW pulse train with 20 pulses covering the same bandwidth and subject to phase distortion due to target motion using `spt2_4.m`. The amount of range walk distortion introduced in this case is 0.03μs, which is more reasonable than that introduced in earlier simulations (0.5μs). Figure 4-13 shows the compressed pulse of an LFM pulse train with range walk as the solid line and the compressed pulse of a CW pulse train with range walk as the dashed line. It can be seen from the plot that the compressed pulse of the LFM pulse train has slightly less distortion than the compressed pulse of the CW pulse train in terms of the pulse width in the presence of range walk distortion, but not by much. The phase distortion due to target motion results in a range shift, and the range shift is slightly more severe in the compressed pulse of the CW pulse train than in the compressed pulse of the LFM pulse train.

By far the most severe distortion to the compressed pulse is due to range walk. It is

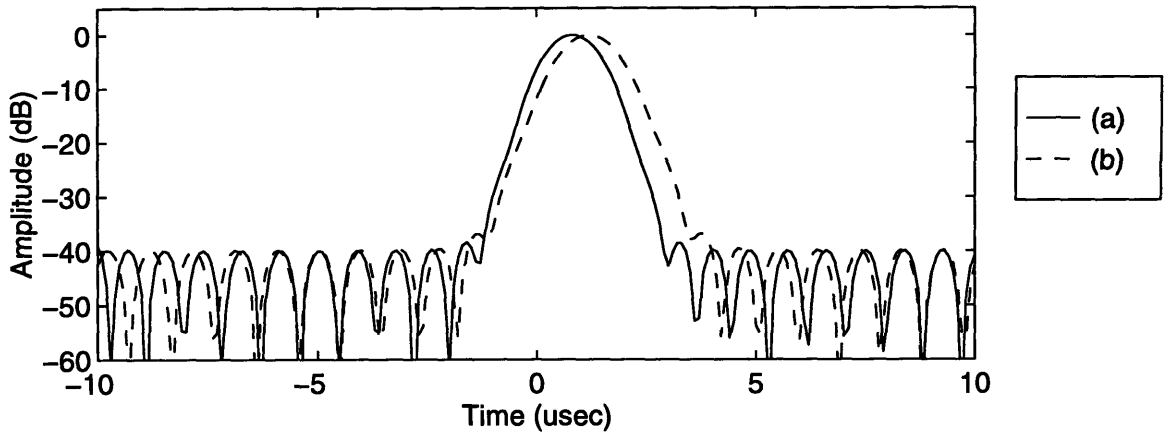

Figure 4-13: Plot of (a) Compressed Pulse of LFM Pulse Train with Range Walk (0.03μs) and (b) Compressed Pulse of CW Pulse Train with Range Walk (0.03μs).

very difficult to remove the phase distortion due to target motion from returns using only a range detection radar. Traditionally, the SPT waveform is transmitted in a rapid burst so there is very little range walk, or a separate velocity tracker is used that monitors the velocity of the target so the amount of phase distortion due to target motion from pulse to pulse can be estimated. This is not possible for the present radar system. Instead, an overlapping LFM pulse train can be used. The redundant frequency information in the overlapping region can be utilized to estimate and compensate for the phase distortion due to target motion.

4.3 Phase Compensation

An overlapping LFM pulse train approximation is given in Figure 4-14. The linear frequency characteristic of the chirp signal is approximated using a series of LFM pulses with a region of overlap in the transmitted frequency, shown by the shaded region. This region can be used to determine the phase shift due to range walk.

Pulse compressing an overlapping LFM pulse train follows the same steps as pulse compressing a non-overlapping LFM pulse train. Simulations for processing an overlapping LFM pulse train can be found in `simuolfjb.m` in Appendix A. The frequency characteristic

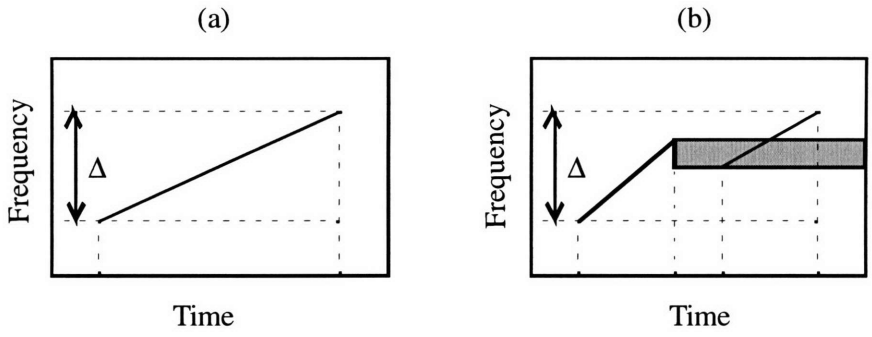

Figure 4-14: (a) Frequency Characteristic of Chirp Signal and (b) Frequency Characteristic of Overlapping (shown in shaded region) LFM Pulse Train Approximation.

of the center frequencies of the non-overlapping LFM pulse train in Figure 4-2 is used. The frequency step size is 75 kHz, and the overall bandwidth is about 1 MHz. The difference between the overlapping and the non-overlapping LFM pulse train simulations is the slope of the frequency within each pulse. There is an instantaneous bandwidth of 0.6 kHz in the pulse of an overlapping LFM pulse train (0.1 kHz in the pulse of a non-overlapping LFM pulse train), which results in a region of frequency overlap between consecutive pulses.

The processing is simulated, and the results are presented in Figure 4-15 and Figure 4-16. Figure 4-15 shows the compressed pulse of the overlapping LFM pulse train, and Figure 4-16 shows the frequency spectrum of the compressed pulse. The sidelobes of the compressed pulse is at -40 dB below the peak, which is expected since the Chebychev weighting function is used. There is a net pulse width reduction of about $T\Delta$ ($T = 20\ \mu s$, $\Delta = 1$ MHz). The frequency spectrum of the compressed pulse is again that of a wideband signal. This overlapping LFM pulse train can then be used to remove phase distortions due to target motion.

The processing of a frequency train consisting of two overlapping pulses to remove phase distortions due to target motion follows the flow chart given in Figure 4-17. An LFM pulse train with overlaps in frequency is transmitted, and the interval over which the frequencies overlap is noted. Prior to transmission, any additional phase as a result

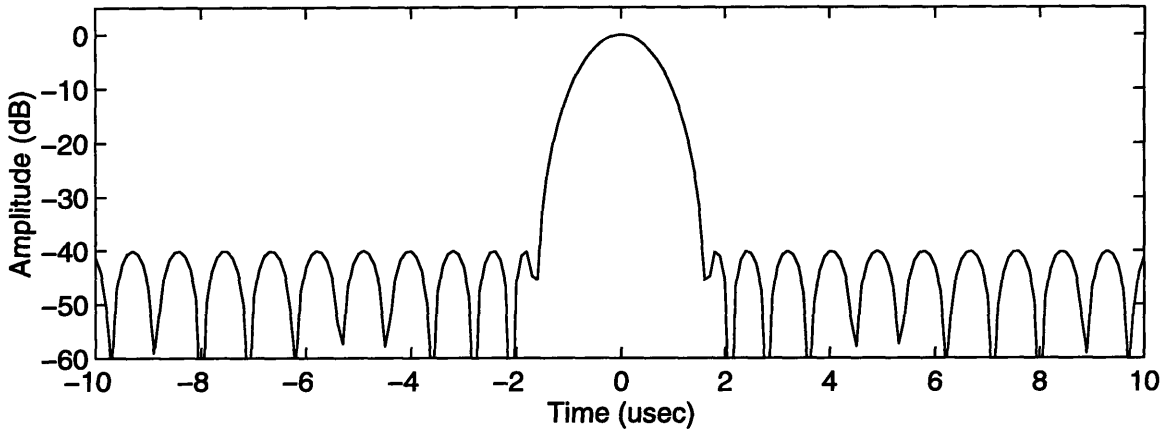

Figure 4-15: Plot of Compressed Pulse of Overlapping LFM Pulse Train.

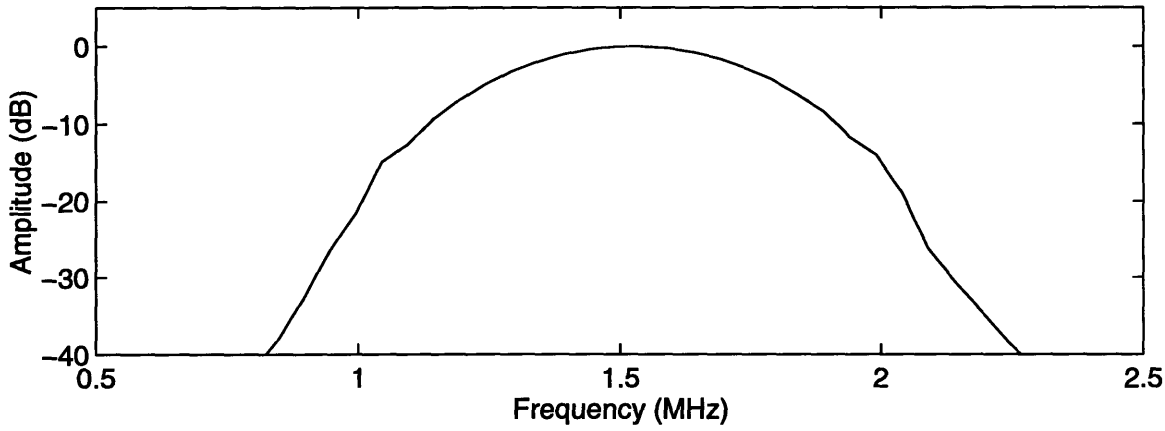

Figure 4-16: Frequency Spectrum of Compressed Pulse of Overlapping LFM Pulse Train.

of hardware differences for different frequencies in the local oscillator is recorded. Upon reception of the return signal, that phase difference is subtracted from the first pulse. It is not necessary to subtract or calibrate the phase difference for the second pulse because the phase difference due to hardware is indistinguishable from phase difference due to target motion and can be removed at the same time. The phase distortion due to target motion and any hardware difference is then given by the difference in phase in the region of frequency overlap, weighted by time offsets. An average phase offset can be found by averaging the phase offset over the entire overlapping interval to remove any noise effects. The phase of the second pulse is adjusted accordingly. The second pulse is then phase weighted by the appropriate frequency and added to the first pulse (according to the pulse compression equation given by Equation 3.4) for a compressed pulse. The second pulse can then be used to process the third pulse following the same procedure.

Following the algorithm, phase compensation in order to remove range walk is accomplished, as seen from the following simulations for an overlapping LFM pulse train consisting of 15 pulses with the frequency characteristic given in Figure 4-2. An increasing phase error, the same as in the case of the range walk simulations (0.5 μs) is introduced in the pulses. The algorithm outlined in the flow chart is used in the Matlab simulation given by `simuolfjb.m`. The phase offset is calculated using a single frequency overlap term and is removed from the pulses. Figure 4-18, Figure 4-19, and Figure 4-20 show the compressed pulse after phase compensation in solid, and the compressed pulse without phase compensation is shown in dashed line for a total compression of two, eight, and all fifteen pulses, respectively. It is evident from the figures that by using the phase compensation algorithm, the phase term due to range walk can be effectively estimated and removed, and the resulting compressed pulse is identical to that of the ideal case. Without phase compensation, the distortion of the compressed pulse increases as the number of pulses compressed increases.

This algorithm would be applicable only to targets moving with constant velocity because in the case of an accelerating target, there is a non-constant frequency offset in addition to a phase offset. As a result, the frequency of the overlapping region would no longer be equal between two consecutive pulses. The target velocity has to be known in order to remove phase distortions so the phase compensation algorithm would not work.

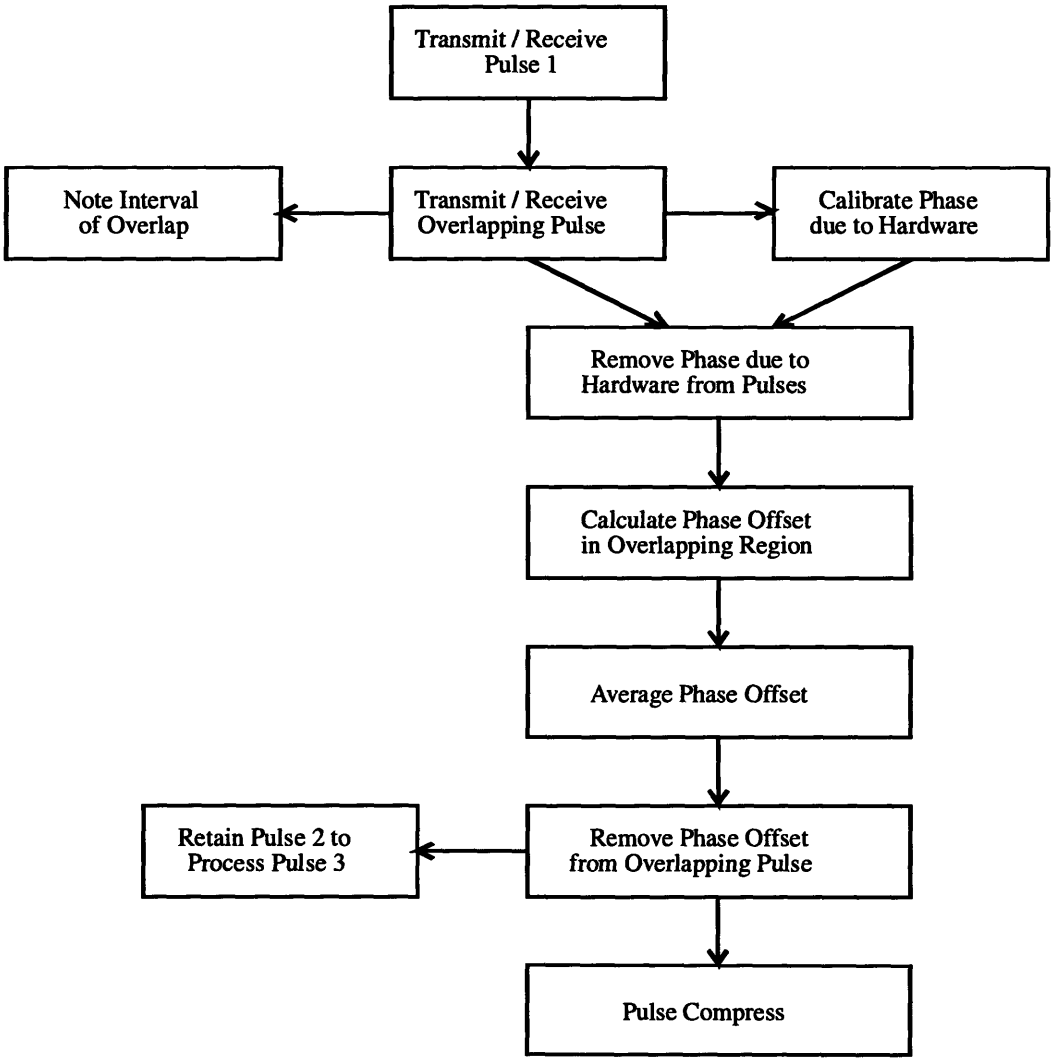

Figure 4-17: Flow Chart for Processing Overlapping LFM Pulse Train.

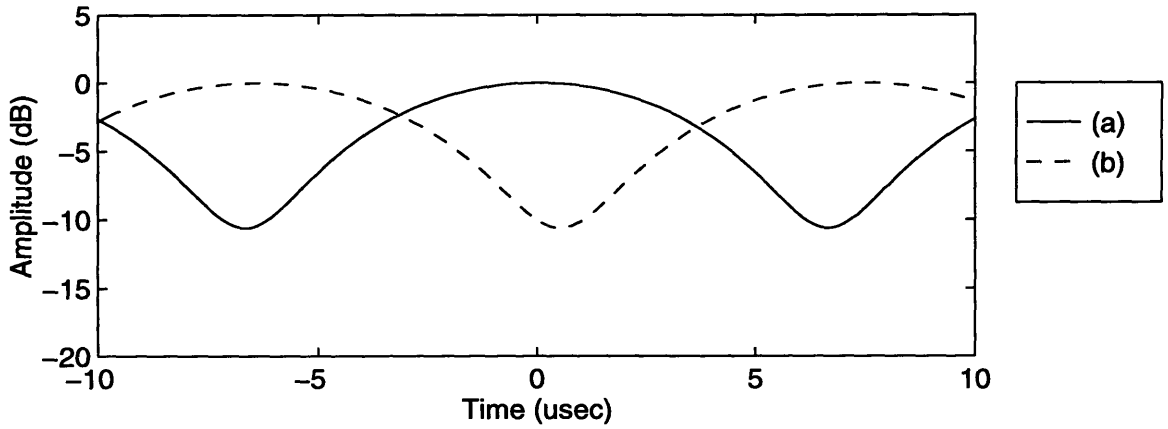

Figure 4-18: Plot of (a) Compressed Pulse of Overlapping LFM Pulse Train after Phase Compensation for 2 Pulses and (b) Compressed Pulse of LFM Pulse Train with Range Walk for 2 Pulses.

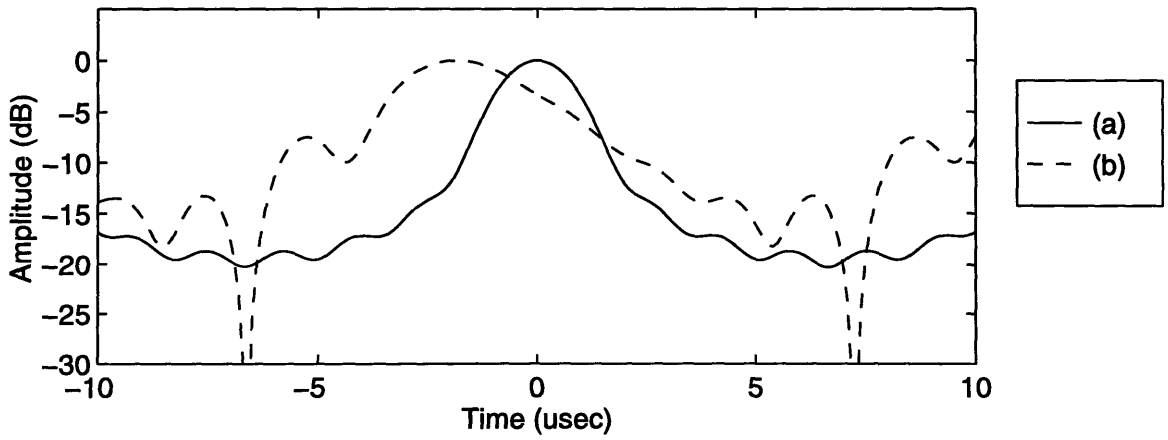

Figure 4-19: Plot of (a) Compressed Pulse of Overlapping LFM Pulse Train after Phase Compensation for 8 Pulses and (b) Compressed Pulse of LFM Pulse Train with Range Walk for 8 Pulses.

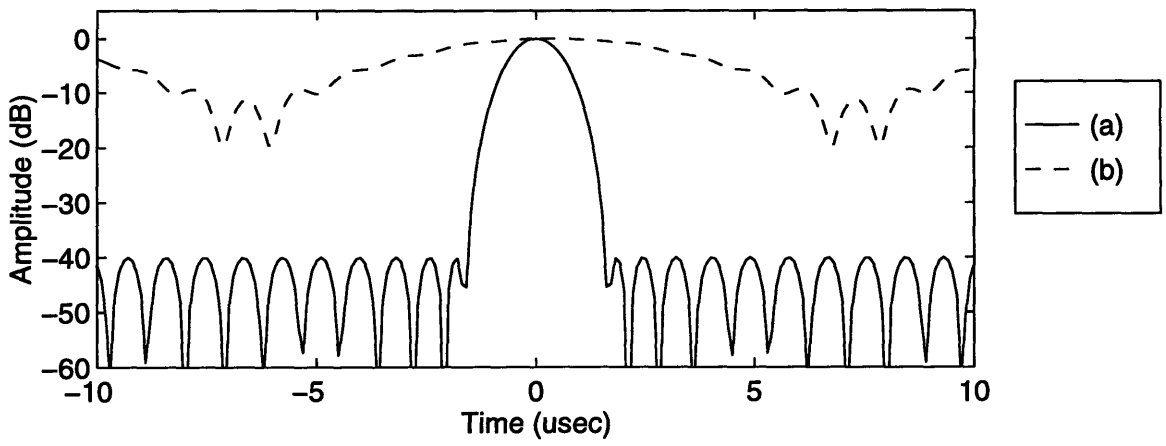

Figure 4-20: Plot of (a) Compressed Pulse of Overlapping LFM Pulse Train after Phase Compensation for 15 Pulses and (b) Compressed Pulse of LFM Pulse Train with Range Walk for 15 Pulses.

4.4 Summary

An LFM pulse train is able to approximate the chirp signal much in the same way as the CW pulse train. The achievable instantaneous bandwidth of each pulse is governed by hardware limitations of the radar system. The case of an ideal LFM pulse train is studied, and the frequency spectrum of the compressed pulse does indeed approximate the frequency spectrum of a chirp signal. There is a pulse width reduction of $T\Delta$. The case when there is a non-uniform frequency train with non-uniformities in the frequency step sizes between consecutive pulses is simulated, and the results show that there is an increase in the sidelobes of the compressed pulse as well as ripples in the frequency spectrum of the compressed pulse, much like in the case of non-uniformities in the CW pulse train. However, the amount of increase in sidelobes is higher in the case of the LFM pulse train because the frequency step size simulated is greater, so larger non-uniformities result in bigger ripples in the frequency spectrum, which in turn lead to higher sidelobes in the compressed pulse. The case when there is a gap in the transmission frequency band of the LFM pulse train is simulated, and the results are again similar to the results for the case when there are gaps in the frequency band for a CW pulse train. There is a severe increase in the sidelobes of the compressed pulse as well as corresponding gaps in the frequency spectrum of the

compressed pulse consistent with the missing frequency components.

In the case where range walk between consecutive pulse transmission is simulated, there is severe distortion to the compressed pulse. There is very little pulse compression evident, and the compressed pulse width is about the same as the pulse width of the original envelope of a single pulse. It is slightly better than in the case of the CW pulse train, which results in complete loss of compression. A comparison is made between the LFM pulse train with 15 pulses and a CW pulse train with 21 pulses subject to phase distortion due to target motion. In terms of the compressed pulse, LFM pulse train results in less distortion because there are fewer pulses in the LFM pulse train.

The issue of range walk is alleviated by using the overlapping LFM pulse train. The overlapping LFM pulse train is processed much in the same way as a non-overlapping LFM pulse train and achieves the same pulse width reduction of $T\Delta$. Furthermore, following the phase compensation algorithm, it is possible to use an overlapping LFM pulse train to compensate for range walk for targets moving with constant velocity.

Chapter 5

Multipath Height Finding

The background and theory of using target multipath for height finding has been explained in Chapter 1. It is possible to estimate the height of a target given the height of the radar and the multipath delay (thus the path length difference between the direct path and the multipath) for the given bandwidth of the radar system using the SPT waveform approximation. The radar system acquires data, and the data can be processed non-coherently by looking at the absolute value of radar returns for different frequencies of the SPT waveform approximation, or the data can be processed coherently using the phase weighting by appropriate frequencies and summing method given in Chapter 3 by Equation 3.4.

The data acquisition procedure and processing routines are explained briefly for different types of targets for the RSTER system. The non-coherent processing routine is introduced and applied to radar data for different targets, and the coherent processing routine is introduced. It is not carried out on actual data due to lack of time.

5.1 Data Acquisition

The RSTER system consists of 14 channels that transmit a six degree by eight degree wide beam at a specified azimuth and elevation. Before data collection missions take place, there are usually certain calibrations that have to be done. The purpose of the calibrations is to gauge the characteristics of the system hardware and the environment during a particular mission so as much distortion can be removed from the data as possible before the data is

processed. Included among the calibrations are the receiver and antenna frequency response for the radar system, as well as noise calibrations for the system hardware and background clutter at the beginning of a particular mission.

After the calibrations are complete, the system is prepared for transmission. According to the specifications of the mission, there are three possible types of targets and returns to record and process.

1. Internal MTS.
2. Niihau MTS.
3. Actual Targets.

The return from an internal Moving Target Simulator (MTS) is a type of return that does not require external Radio Frequency (RF) transmission. After the transmission signal is generated, specific phase offsets that correspond to a specified Doppler and range for a particular mission are programmed and generated internally. The phase offsets are then injected into the transmission signal and recorded as the return signal. This process takes place internally, so there is no actual radar transmission, and therefore it is possible to use all frequencies without concern for interference or range walk.

There is also an external MTS on Niihau, which is a neighboring island about 23 nmi from the cliff on which the radar is mounted. The Niihau MTS is designed to receive the transmitted signal and produce a return signal at a specific Doppler. It is mounted at a fixed location, so it will always appear at the same range between consecutive radar transmissions, in which case range walk would not be an issue.

The third type of return is actual planes that fly by during a recording session. For this thesis, commercial air traffic from the far east approaching Honolulu International Airport in Oahu, which is about 200 nmi east of the radar site, is observed. In many instances, when receiving returns from actual planes, the type of plane and its altitude are recorded by interrogating the aircrafts' transponder.

After the returns are recorded, they have to be converted to files that can be processed off-line. There have been numerous scripts written to convert the data to a format that can be processed. The data is usually converted into Matlab format, and the general shape

of a particular data set is given in Figure 5-1. The data consists of a string of Coherent

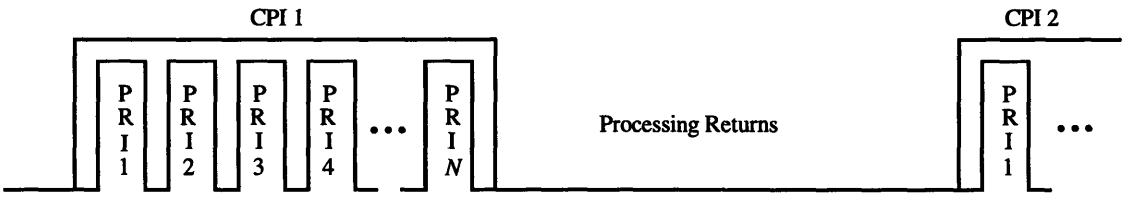

Figure 5-1: Picture Representation of Transmitted Data Set.

Processing Intervals (CPI's). Each CPI is at a specified frequency (a single frequency for a CW pulse train and a linear frequency range for the LFM pulse). Each CPI contains data across 14 channels for N identical pulses at a specified Pulse Repetition Interval (PRI). There is a total of N pulses in a single CPI rather than a single pulse in order to estimate the Doppler bin of the target. The Matlab data set is given in terms of CPI's, and the shape of a single CPI is in matrix form in Figure 5-2. The total number of columns of a CPI is equal to the total number of channels, which is equal to 14 for the RSTER system. This number is always constant from one mission to the next. The number of rows is the product of the total number of range gates, M per PRI, and N PRI's, which is equal to $M \times N$. The total number of range gates is different from mission to mission, as well as N. For the CW pulse train, $N = 16$, and for the LFM pulse train, $N = 8$.

After the data is converted to Matlab format, it is ready for analysis. There is a set of standard post-mission analysis routines for the RSTER system. The analysis includes:

- Data equalization - which consists of using calibration coefficients to remove any frequency distortions due to internal radar hardware and the environment.
- Beam-forming - which consists of applying weighting over the 14 channels and summing them accordingly to form a focused beam in a desired transmission direction.
- Pulse compression - which involves matched filtering the received pulses for better range resolution.

These analyses are not all needed to demonstrate that the CW pulse train or the LFM pulse train is capable of estimating the target height using the target multipath. The data

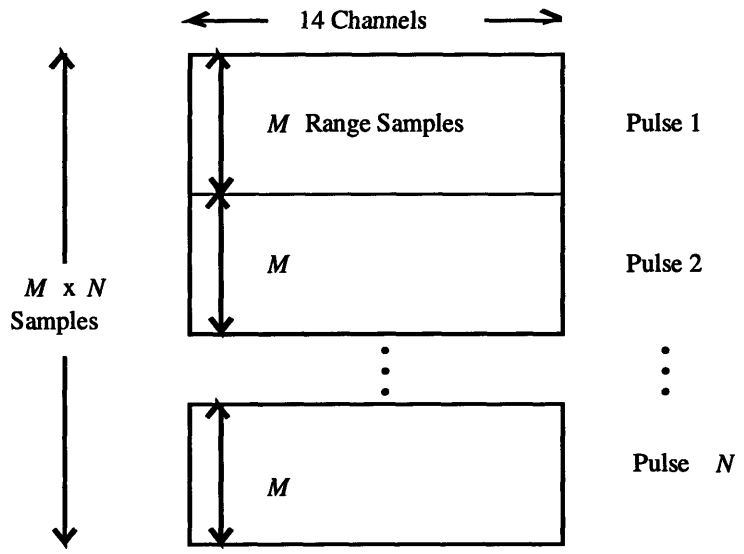

Figure 5-2: Matrix Structure of a Single CPI.

collected using the CW pulse train is processed non-coherently, and it is shown that the target height can be estimated. If the LFM pulse train data is processed coherently, it can also estimate the target height, and it can do it more accurately because the overlapping region can be used to compensate for target motion if the phase distortion due to target motion is significant.

5.2 Non-Coherent Processing of CW Pulse Train

The term non-coherent refers to the fact that the phase information in the return signals is not accounted for in processing the returns. The flow chart for processing the CPI's non-coherently is given in Figure 5-3.

The first step is to obtain a Doppler range map that indicates the Doppler and range bin of the target. The Doppler range map can be thought of as a Doppler plot for each sample across all range samples. The target is assumed to be at the same azimuth for different transmissions. Therefore, each range sample is obtained by summing the returns for each sample for a single pulse across all 14 channels. Then the return for the N pulses are weighted, and a 32-point FFT is taken of the range sample for the N pulses to form

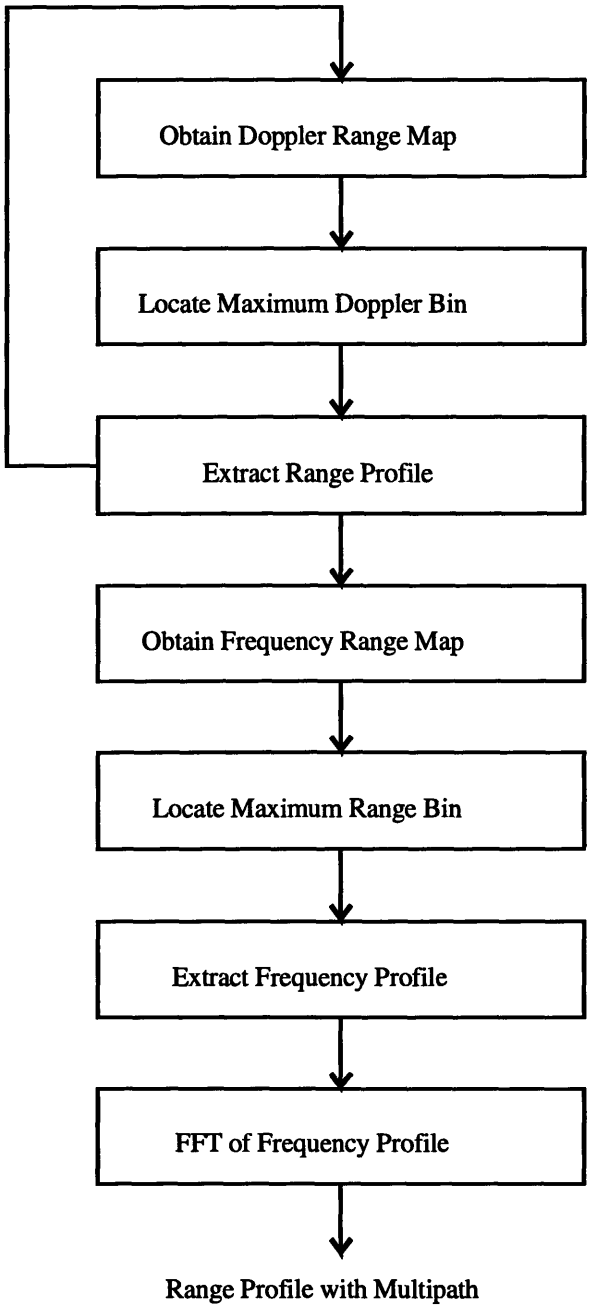

Figure 5-3: Flow Chart of Non-Coherent Processing of SPT Approximation Waveforms.

the 32-point Doppler plot for that particular range sample. After the Doppler range map is plotted, the Doppler and range bin of the target can then be identified. It usually occupies several range and Doppler bins, but the bin in which the maximum Doppler occurs is noted. The M-point range profile within that particular Doppler bin is extracted, and the frequency for that particular CPI is noted. There is a loop to process all the CPI's, and the range profile of the same Doppler bin is extracted for each CPI. The result is a frequency range map. The target then appears at a particular range bin across all frequencies, and the frequency profile is extracted for the maximum range bin, which is the bin the target is in. The FFT of the frequency profile will then give information about the height of the target. When taking the FFT of the frequency profile at a particular range bin, only the absolute value of the frequency profile is used, thus the processing is non-coherent.

5.2.1 Simulation

A simulation is performed which demonstrates that the FFT of the absolute value of the frequency profile does indeed give information about the altitude of the target when there is target multipath interference using `simuolfjb.m`. The simulation is done for a target at a height of 37 kft and a range of 60 nmi, and a radar at a height of 1.5 kft (which is the height of the cliff on which the RSTER is mounted). The frequency ranges from 420 MHz to 450 MHz, covering a bandwidth of 30 MHz.

When the signal is transmitted at a particular frequency and the return is received for a particular range, there is interference due to the target multipath. Given that the target is at height H_1 and range R, and the radar is height H_2, the range of the multipath, R_2 can be calculated using simple geometry [1].

$$R_2 = \sqrt{R^2 + 4H_1H_2} \tag{5.1}$$

The difference between R_2 and R_1 is the path difference ΔR that will be present in the range plot of the returns.

The plot of the actual interference is given in Figure 5-4. The figure shows the frequency characteristic of the target range bin when there is multipath interference. If there is no

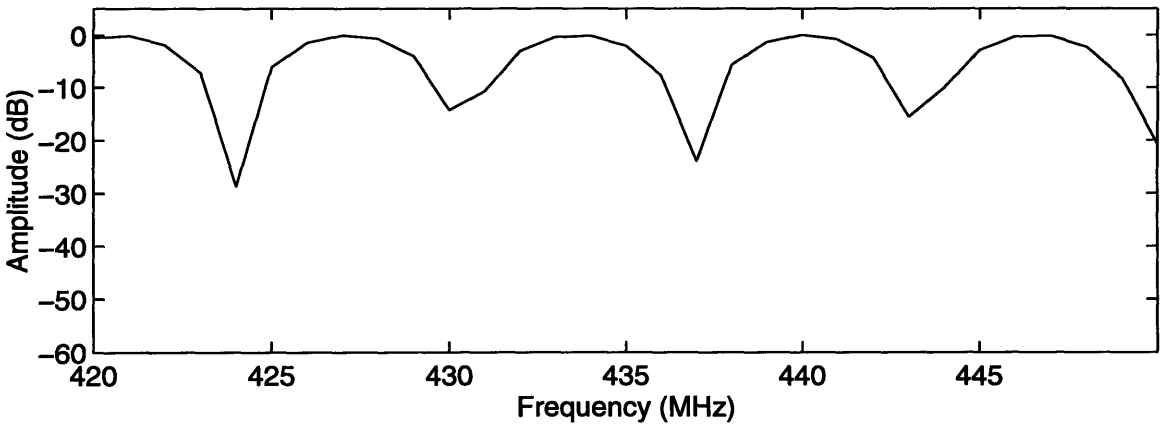

Figure 5-4: Frequency Plot of Target Range Bin with Target Multipath Interference ($R = 60$ nmi, $H_1 = 37$ kft, and $H_2 = 1.5$ kft).

multipath interference, the frequency characteristic of the target range bin would be a straight line. It is clear that there is periodicity in the frequency characteristic. The FFT of the magnitude of the frequency plot weighted by the -40 dB Chebychev weighting function is given in Figure 5-5. Since it is the FFT of a real signal, the target multipath interference

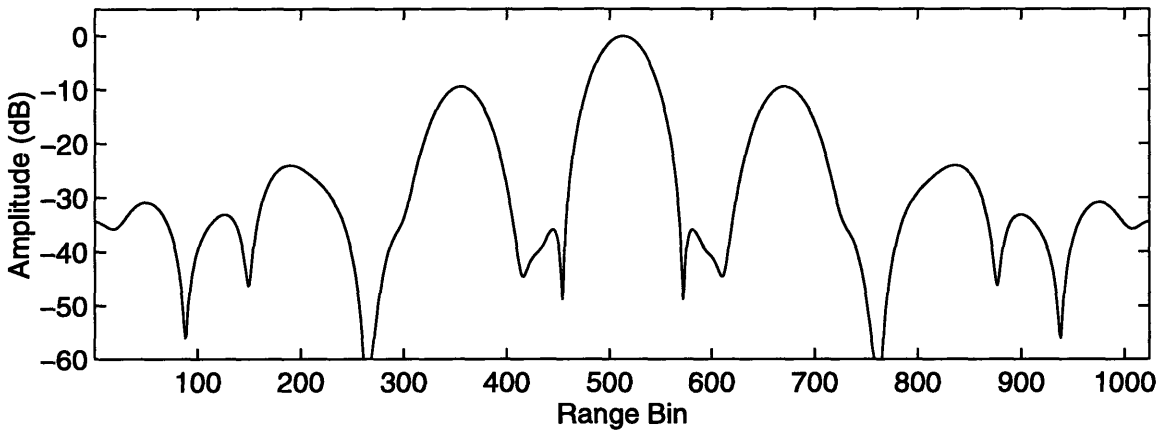

Figure 5-5: FFT of Frequency Plot of Target Range Bin with Target Multipath Interference ($R = 60$ nmi, $H_1 = 37$ kft, and $H_2 = 1.5$ kft).

appears at symmetrical positive and negative frequencies. The frequency spectrum is in essence a time plot since it is the FFT of a frequency plot, and the target multipath

information is given by the delay between the main lobe and the secondary sidelobes.

5.2.2 Internal MTS

The non-coherent processing of the CW pulse train is applied to data collected from the internal MTS. The CW pulse train consists of 101 CPI's, each containing 8 PRI's. The duration of the pulse is 5 μs, and the frequency of the CPI's starts at 420 MHz and increases at 0.2 MHz per CPI to 439.8 MHz for the last CPI, covering a total bandwidth of 19.8 MHz. Since the internal MTS transmits a delay that corresponds to a particular Doppler and range, there is no multipath effect. The results, as expected, are shown in the following figures.

Figure 5-6 is the Doppler range map for a particular CPI for mission number 9029 generated using `rdplot.m` found in Appendix B, along with other Matlab routines used for data analysis. The maximum Doppler bin is located using `multiplot.m`. The target is seen very clearly in the middle of the plot. The target is seen so clearly in this case because it is an internal MTS, so there is only internal hardware noise, which is negligible compared to background clutter of the environment. The frequency range map is generated using `multiplot.m` and plotted using `rdplot.m`, and it is given in Figure 5-7. There is an obvious target at range gate 51 across all frequencies.

The frequency plot for the range sample is generated using `ncprocw.m` and given in Figure 5-8. It is clear from the plot that there is slight oscillation and very little periodicity, which is expected since the internal MTS should not have any multipath images. The periodicity and oscillation are direct results of the hardware. The FFT of the frequency plots shows a single spike that corresponds to the programmed range. The secondary sidelobes at around -30 dB below the peak are also results of the hardware of the radar system. The internal MTS is used to show that the non-coherent processing technique is able to produce an accurate and expected range profile for a particular target. The multipath effect can be better seen when applied to an actual plane with multipath interference.

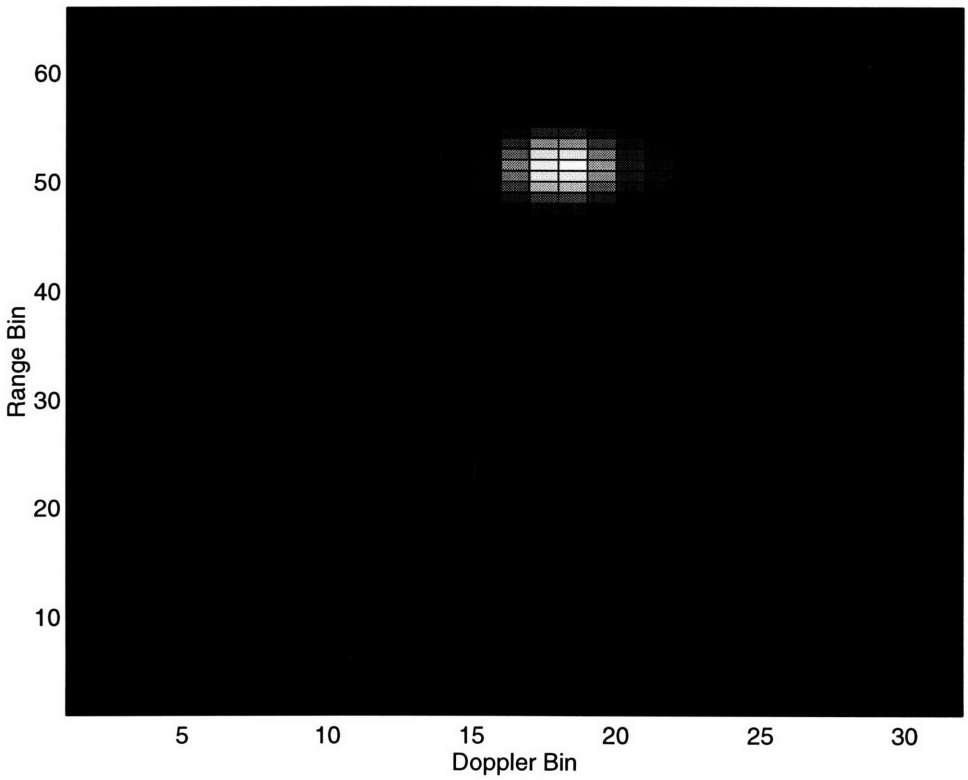

Figure 5-6: Doppler Range Map of Internal MTS.

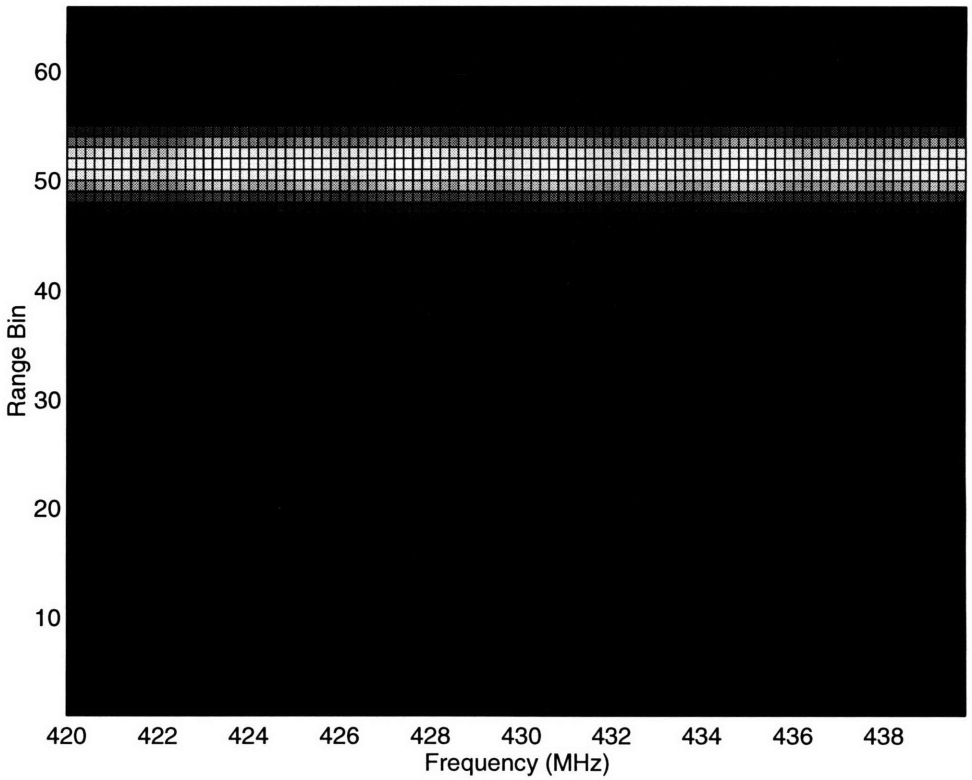

Figure 5-7: Frequency Range Map of Internal MTS.

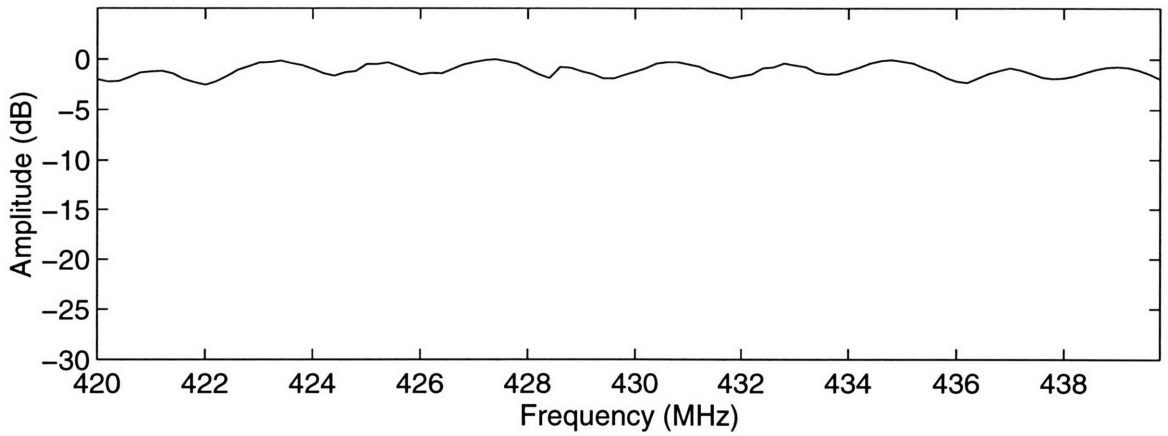

Figure 5-8: Frequency Plot for Target Range Bin for Internal MTS ($\Delta f = 0.2$ MHz and $\Delta = 19.8$ MHz).

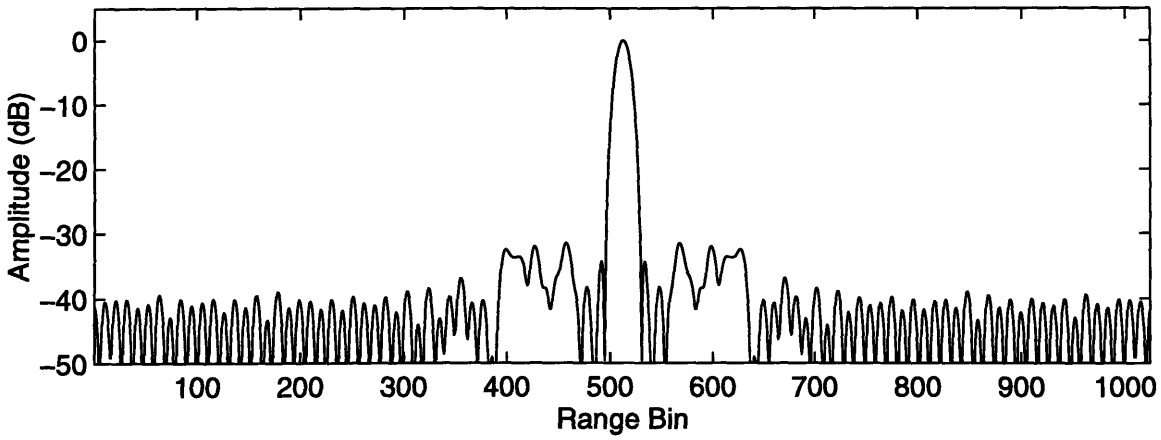

Figure 5-9: FFT of Frequency Plot of Target Range Bin for Internal MTS.

5.2.3 Actual Plane

The non-coherent processing technique is applied to an actual target flying over water at an altitude of 39 kft. The mission number for the collection is 9013, and the CW pulse train used on the internal MTS is also used to collect the data. The results demonstrate that the non-coherent processing technique is able to accurately determine the height of the target. The Doppler bin of the target is found using `multiplot.m`, and the Doppler range plot of the target is again generated using `rdplot.m` and given in Figure 5-10. The location of the target is not as evident in this map as it is in the Doppler range map of the internal MTS. There is considerably more noise, and the target is somewhat hidden. But upon closer inspection and with the aid of a color map, it is clear that the target is at the lower right hand corner of the map, at Doppler bin 31. The range profile for the bin is used to construct the frequency range map in Figure 5-11. It is clear in the plot that the target is at the bottom of the map, and that there is definite periodicity. Due to the fact that this is an actual transmission, there are frequencies for which the range plot is missing or highly corrupted, so only a subset of the frequency is used in the frequency range map as well as the frequency plot which is again generated using `ncprocw.m` and shown in Figure 5-12. It is clear that the frequency plot looks very much like the frequency plot of the simulation in Figure 5-4. The FFT of the frequency plot in Figure 5-13 shows a main lobe and the

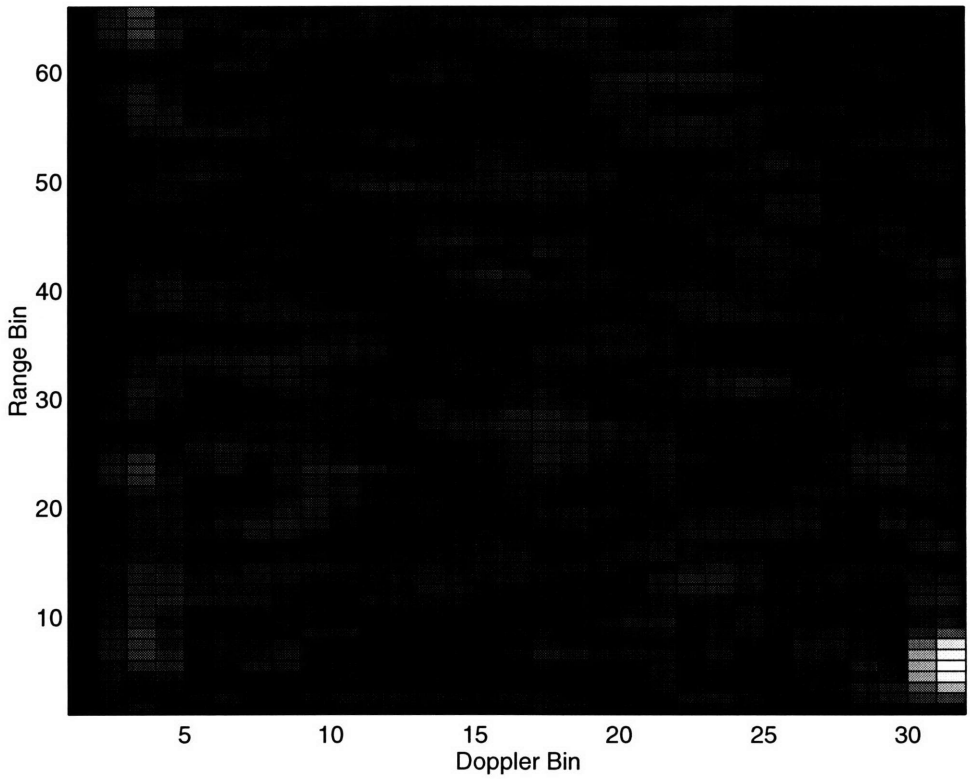

Figure 5-10: Doppler Range Map of Actual Plane.

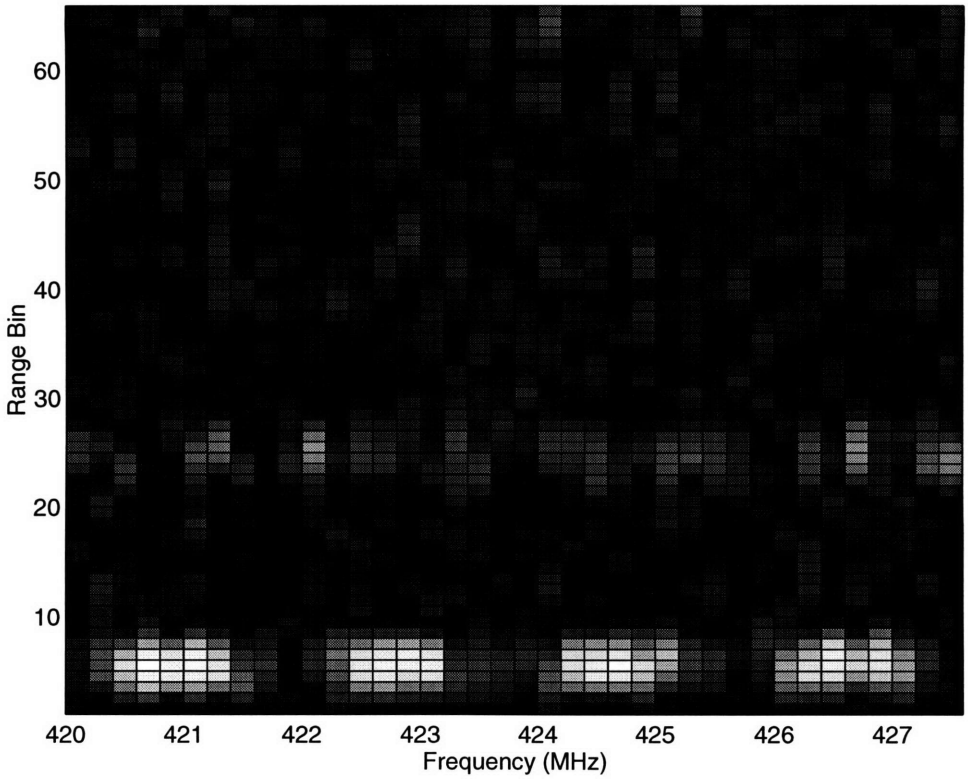

Figure 5-11: Frequency Range Map of Actual Plane.

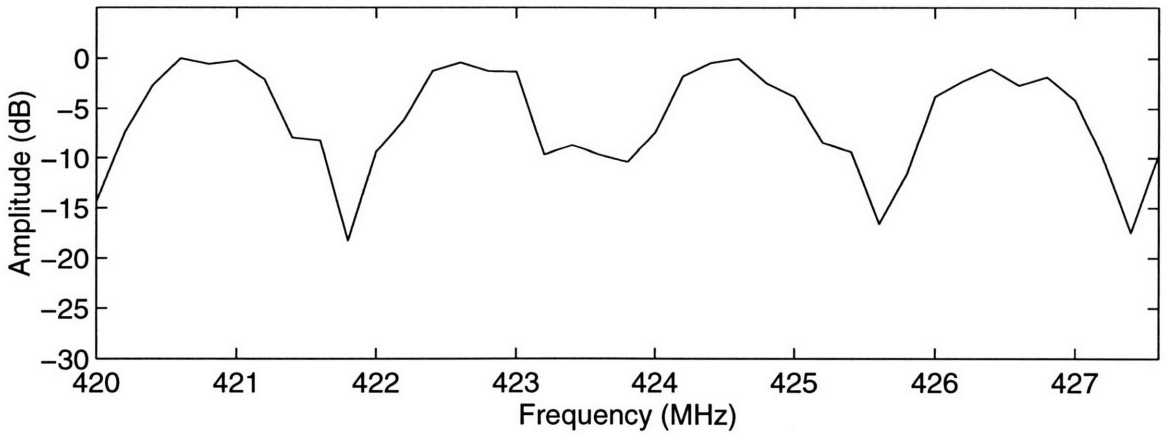

Figure 5-12: Frequency Plot of Target Range Bin for Actual Plane.

equidistant sidelobes corresponds to the multipath interference of the target.

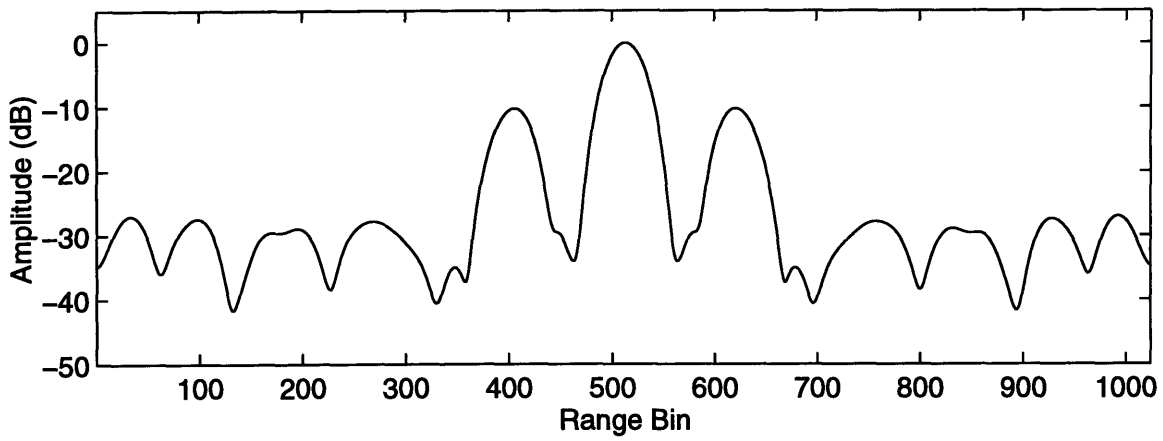

Figure 5-13: FFT of Frequency Plot of Target Range Bin for Actual Plane.

It is appropriate at this point to look at the entire frequency profile of the frequency range map. The frequency profile for the entire frequency train is given in Figure 5-14. There

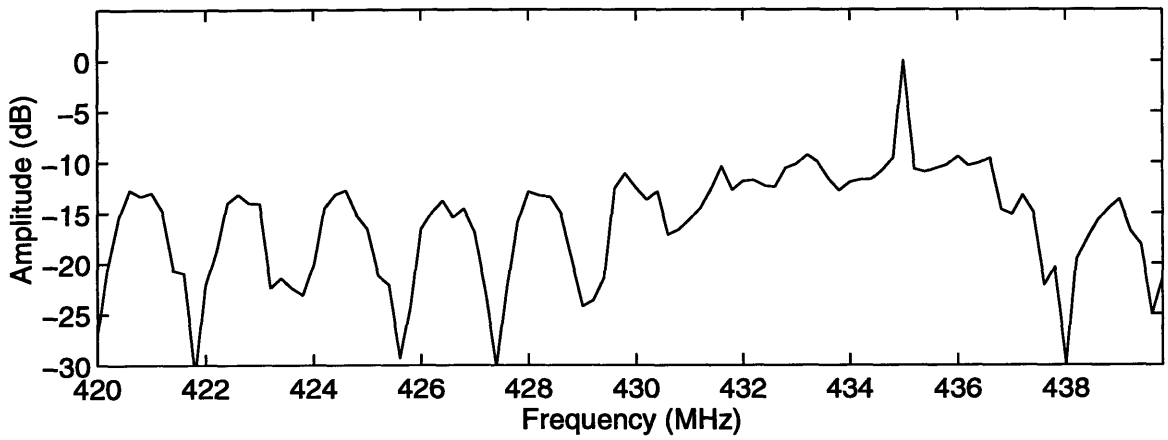

Figure 5-14: Frequency Plot of Target Range Bin with All Frequencies of Frequency Train Present.

is distortion in the frequency samples ranging from about 430 MHz to 438 MHz, which may be due to interference from other communication channels. It is not due to radar hardware differences because these frequencies are valid for the internal MTS. The FFT of the entire frequency profile is given in Figure 5-15 as the solid line, and for comparison, the FFT of

the frequency profile of a portion of the frequency train is given in dashed. There is more

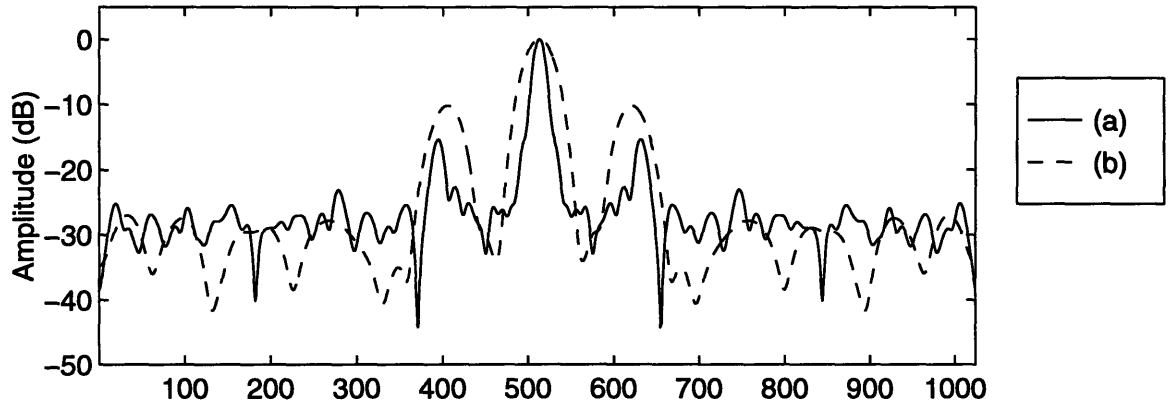

Figure 5-15: (a) FFT of Frequency Plot of Target Range Bin with Entire Frequency Train Present and (b) FFT of Frequency Plot of Target Range Bin for a Portion of the Frequency Train.

distortion although the pulse width is slightly narrower. The distorted frequencies can be zeroed out, and it would be a case of a pulse train with gaps in frequency steps simulated earlier. If the frequency profile for frequency ranging from 428 MHz to 438 MHz are zeroed out, the resulting frequency profile is shown in Figure 5-16. There is a gap in the frequency

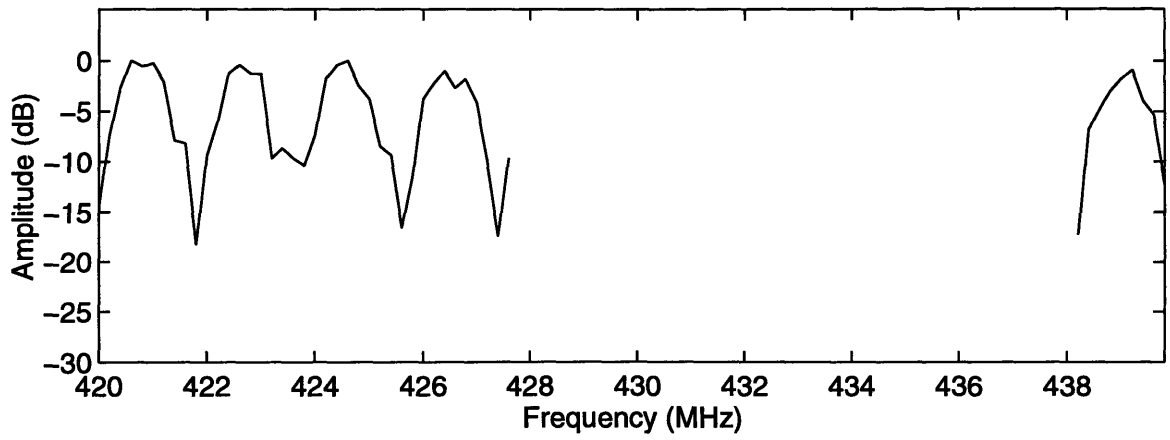

Figure 5-16: Frequency Plot of Target Range Bin for Frequency Train with Gaps in Frequency Steps.

profile, which is similar to the gap in the frequency spectrum of the compressed pulses for

the CW pulse train and the LFM pulse train simulated earlier. The FFT of the frequency profile is given in Figure 5-17 in solid, and the FFT of the frequency profile of only a portion of the frequency train is given in dashed for comparison. There is severe distortion in this

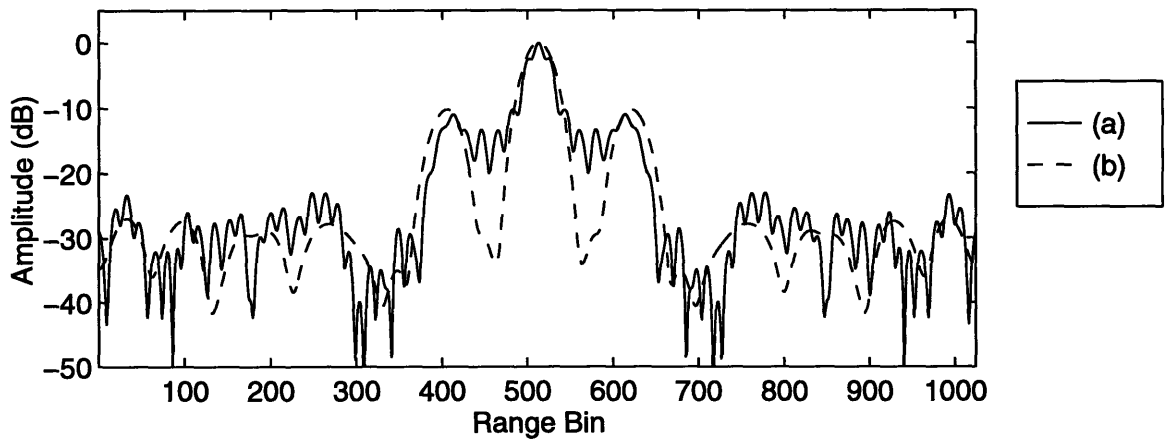

Figure 5-17: (a) FFT of Frequency Plot of Target Range Bin for Frequency Train with Gaps in Frequency Steps and (b) FFT of Frequency Plot of Target Range Bin for a Portion of the Frequency Train.

case, just as seen in earlier simulations. The sidelobes of the range profile is very high.

The data supports the fact that the non-coherent processing technique can determine the height of the target. However, the technique does not make use of the phase information, which can be used to better estimate the target height for more targets. There are many conditions under which the non-coherent method would not work as well. The non-coherent method extracts altitude information from the amplitude of the radar return only. The amplitude fluctuations are affected by the complex reflectivity of water and the complex reflectivity of the target at different aspect angles. These factors may greatly affect the non-coherent frequency spectrum, but have much less effect on a true multipath time delay estimate. Also, the target velocity may change so that it is in a different range bin, so there would be too few data points for the FFT. Therefore, the coherent processing technique needs to be investigated and incorporated for certain classes of targets.

5.3 Coherent Processing of Overlapping LFM Pulse Train

The flow chart for coherently processing the data is given in Figure 5-18. The top part of

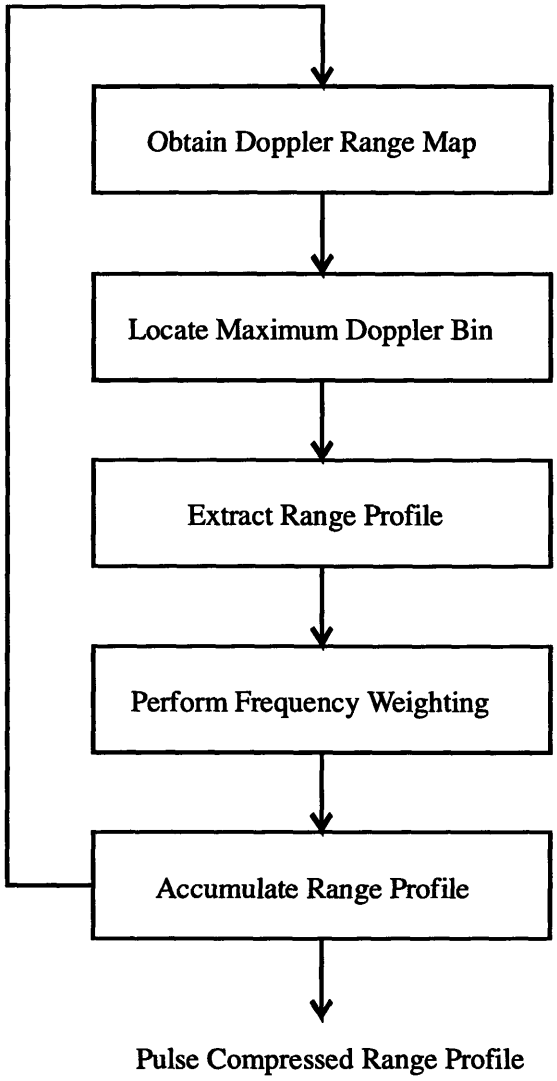

Figure 5-18: Flow Chart for Coherent Processing of SPT Approximation Waveforms.

the flow chart looks very much like the flow chart in Figure 5-3 for non-coherent processing. This is because the first part of the processing involves finding the exact location of the target and extracting the range profile from a specific Doppler bin. The coherent processing differs once the range profile for a single CPI is extracted. The range profile for the CPI is

processed according to the pulse compression equation given by Equation 3.4, and it will be the complex pulse envelope $V(f_k, t)$ in the equation. Although the complex envelope from Equation 3.4 applied to a single pulse before any Doppler processing, the coherent processing can be done after Doppler processing because it is a linear process, so the order which it is done is irrelevant. All N pulses in a single CPI are identical, so combining them would not have any effect on their phase, provided there is no phase distortion due to target motion within a CPI. Since coherent processing only requires that the detection be coherent, it can be done for the RSTER system since the detection is coherent, as explained in Chapter 3. The range profile is phase weighted by its frequency and then summed to produce the high range profile simulated in Chapter 3 and Chapter 4. The constant phase offsets due to hardware are embedded in the phase of the MTS, which can be used to remove phase offsets due to hardware from returns of actual planes. The coherent processing can then be carried out. Unfortunately, due to the lack of time, the simulations performed in Chapter 3 and Chapter 4 could not be verified against actual data.

Chapter 6

Conclusion

The purpose of this thesis has been to investigate methods of improving the bandwidth performance of Airborne Early Warning (AEW) radar systems. The RSTER system, which transmits in the UHF band, is an adaptive radar system built to emulate AEW radars and to study their performance under different conditions.

Chapter 1 investigates the applications of the AEW radar, which includes target length estimation and target height finding. Target length estimation requires a very high bandwidth for the classes of targets that are of interest, such as missiles. It is not practical to increase the bandwidth of the present radar system to the desired bandwidth in order to accomplish target length estimation, so the attention is turned toward estimating target height. Because the targets observed by AEW radars are usually flying over water, there is multipath interference between the direct transmission and the return bouncing off of the water surface. As a result, it may be possible to resolve the target height by looking at the range spacing between the target return and the return of the multipath. In order to accomplish this, the bandwidth of the radar system has to be increased.

Chapter 2 studies the chirp signal, which is the usual approach to achieving a wideband signal, resulting in a narrow pulse with high range resolution in the time domain. The chirp signal investigated is a signal whose carrier frequency increases linearly with time. Upon reception, the chirp signal is passed through a matched filter whose frequency versus delay characteristic is opposite to that of the transmitted signal, and the output is a compressed pulse in the time domain. For a signal with a pulse duration of T and spanning over a

bandwidth of Δ, the transmitted pulse will undergo an approximate pulse width reduction of $T\Delta$, as demonstrated by simulations in Chapter 2. In order to reduce range sidelobes, it is also shown that it is better to apply a weighting function to the signal, which in this case is a Chebychev weighting function with sidelobes at -40 dB below the peak. The weighted compressed pulse is slightly wider, but the increase in width is negligible in light of the decreased sidelobes. The same weighting function is applied to all simulations and data analyses.

Certain implementation issues involved in adopting the chirp signal are also presented in Chapter 2. Due to hardware limitations as well as restrictions imposed by the availability of the UHF band, approximations of the chirp signal, known as the Stepped-Frequency Pulse Train (SPT) approximations, are investigated. Two types of SPT approximations are studied, the Continuous Wave (CW) pulse train, and the Linear Frequency Modulated (LFM) pulse train. For each SPT approximation waveform, there is a total of four cases simulated.

1. The ideal case.
2. The case when there are uniformly distributed random step size errors of $\pm\frac{\Delta f}{2}$, where Δf is the frequency step size.
3. The case when there are gaps in frequency steps.
4. The case when there is phase distortion due to target motion.

Range walk distortion is more significant for the RSTER system than for other radar systems because many radar systems transmit the pulse trains as a rapid burst of pulses, so there is negligible delay between consecutive pulse transmission. The RSTER system, however, processes a pulse before the transmission of the next pulse, so there is significant delay between consecutive pulse transmissions. This makes it more sensitive to target motion between consecutive pulse transmissions.

Chapter 3 investigates the CW pulse train, which is a pulse train consisting of single frequency pulses, each at a higher frequency than the previous pulse. The pulses of the pulse train are processed according to the pulse compression equation given by Equation

3.4. The frequency step size of the CW pulse train has to obey the Nyquist criterion given by Equation 3.5, otherwise there may be distortions in the compressed pulse. When the CW pulse train does obey the Nyquist criterion, the compressed pulse approximates that of a compressed chirp signal, and the frequency spectrum of the compressed pulse is similar to that of a chirp signal. There is also a net pulse width reduction of $T\Delta$.

When there are non-uniformities in the CW pulse train, there is an increase in the level of sidelobes of the compressed pulse in the time domain, and there are ripples in the frequency spectrum of the compressed pulse. The distortions are not severe and should not have a tremendous impact on the resolution of the system. The distortions become more severe when there are gaps in the frequency steps of the pules train. The case when there is a single gap in the CW pulse train is simulated. It is found that there is a significant increase in the sidelobe level of the compressed pulse, and that there is a corresponding gap in the frequency spectrum of the compressed pulse. The level of the sidelobes may interfere with the resolution of the system in the presence of background noise and possible jammers. The most severe distortion, by far, is due to range walk between consecutive pulse transmissions. When range walk is introduced into the CW pulse train consisting of 21 pulses, there is a complete loss of compression. The width of the compressed pulse is the same as that of an envelope for a single pulse, so the pulse compression routine is no longer effective in that case.

The LFM pulse train approximation of the chirp signal is introduced in Chapter 4 in order to compensate for the range walk. A non-overlapping LFM pulse train approximates a chirp signal by breaking the chirp signal up into smaller chirp signals and transmitting them individually. These pulses are then received and processed much in the same way as the CW pulses, except there is no longer a single phase weighting factor at a single frequency but a set of frequencies in the phase weighting of the pulse compression equation. The case of an ideal LFM pulse train is simulated for a pulse train which consists of fewer pulses than the CW pulse train. It is found that the compressed pulse of the LFM pulse train also resembles that of a chirp signal with a pulse width reduction of $T\Delta$. The frequency spectrum of the compressed pulse is similar to that of the chirp signal and that of the compressed pulse of CW pulse train. When there are non-uniformities in the LFM pulse

train, the level of sidelobes is not only higher than the ideal case for the LFM pulse train but also higher than the non-uniform case for the CW pulse train due to the fact that the size of the frequency steps is greater in the LFM pulse train than in the CW pulse train. The ripples in the frequency spectrum of the compressed pulse is also bigger. The case when there is a gap in the frequency steps is simulated, and there is again a higher increase in the level of sidelobes of the compressed pulse than in the case of the CW pulse train with gaps in frequency steps. The level of sidelobe increase is fairly significant and would most likely interfere with target detection and target height finding.

Again, the most severe distortion is seen for the case of range walk introduced in the LFM pulse train. Unlike the non-uniform and gapped case, the distortion in the compressed pulse of the LFM pulse train as a result of range walk is slightly less than the distortion in the compressed pulse of the CW pulse train because fewer pulses are transmitted in the LFM pulse train. Therefore, there is a trade-off between the distortions due to non-uniformities and gaps in the frequency spectrum and phase distortions due to target motion when considering the total number of pulses to transmit in a pulse train and the frequency step size between each transmission. It would be beneficial to choose smaller steps and transmit more pulses if the targets are fairly slow moving and range walk would not be severe. In that case, there is less distortion due to non-uniformity. In the case of fast moving targets, it is better to transmit fewer pulses with bigger frequency steps.

It would be best to remove the distortion due to range so that smaller steps can be taken to reduce sidelobe levels when there are hardware limitations. The overlapping LFM pulse train is introduced for this purpose. It is an approximation that consists of a series of chirp signals with a region of frequency overlap between consecutive pulses. A phase compensation algorithm is developed that uses the redundant information in the overlapping frequency region to remove any phase distortion due to range walk for targets moving with constant velocity. If the target velocity changes, it results in a non-linear frequency shift in the transmitted pulses, so the overlapping region no longer has the same frequency between consecutive pulse transmissions and can no longer be used for phase compensation.

The case of the overlapping LFM pulse train is simulated, and it is found that the phase compensation can be used to remove any range walk due to target motion. The

phase compensation algorithm is iterative, so any errors would build up over time, and the phase estimate would deteriorate over too many pulses. There are limitations to the phase compensation algorithm, but it is still a tremendous improvement over not having any phase compensation.

Chapter 5 investigates some multipath height finding techniques for analyzing actual radar returns. The method of data collection, the data format, and some existing data processing routines are explained. There are two methods of processing the radar returns. The first method is the non-coherent processing method, which makes use of the amplitude and frequency characteristics of the pulse train, but not the phase information. The simulation for the non-coherent processing method shows that it is possible to resolve target multipath. The non-coherent processing method is applied to the internal Moving Target Simulator (MTS) as well as data from actual planes to show that it works. The range of the internal MTS is estimated correctly, and there is no multipath present, as is expected. The multipath effect is seen when analyzing the data from an actual plane. There is some frequency interference over the entire frequency span of the pulse train, so only a portion of the frequency profile is used for height finding. When the entire profile and the profile with zero padding in the region of frequency interference are used, there are distortions in the range profiles. The distortion due to zero-padding is more severe than the distortion to the compressed pulse when the entire frequency profile is used.

The second method is the coherent processing method, which makes use of the phase information between consecutive pulses. The method for processing is given, but due to the lack of time, it is not carried out for actual radar data.

6.1 Future Work

The SPT approximation waveforms show much promise and should be investigated further. First of all, the coherent processing method should be verified for an actual radar data set. After the coherent processing method is verified, the phase compensation algorithm can then be used to remove any range walk from data sets with range walk distortions, if there is any. If not, more data collection missions should be performed.

Since the phase compensation algorithm accumulates errors, more simulations should be carried out in order to better characterize the effect of hardware discrepancies, background clutter, and noise on the phase compensation algorithm as well as ways to average out any noise effects.

When there are non-uniformities in the frequency steps as well as gaps in the frequency steps, it results in an increase in sidelobes of the compressed pulse. Measures, such as frequency spectrum equalization, may be taken to remove the distortions. In the case when there are gaps in the frequency steps, it may be possible to patch the frequency spectrum by adjoining the separate frequency spectra to eliminate the gap so that there is a smaller bandwidth but lower sidelobes, and there would be better resolution overall. Instead of phase weighting the pulse envelope by a transmitted frequency, it may be possible to phase weight the pulse envelope by a lower frequency to make up for the gap.

There is a lot of promise in the SPT approximation waveforms. It not only applies to the case of the AEW radar and the RSTER radar system but the entire communications industry. The target multipath does not just pertain to the radar. Many land mobile communications applications encounter the same problem, and by better utilizing the frequency bands to understand the multipath, the knowledge may be applied to filter out any multipath interference. By understanding the SPT approximations and utilizing them effectively, the entire communications industry may see the benefits of those approximations in an age where bandwidth is such a precious commodity.

Bibliography

[1] Aumann, H.M.: Private conversations.

[2] Bhattacharya, T.K. and Mahapatra, P.R. *Powerful Range-Doppler Clutter Rejection Strategy for Navigational Radars.* Proc. of the IEEE 1989 National Aerospace and Electronics Conference. 22-26 May, 1989. Dayton, OH.

[3] Burrus, C.S, McClellan, J.H, Oppenheim, A.V, Parks, T.W, Schafer, R.W, and Schuessler, H.W. *Computer-Based Exercises for Signal Processing Using Matlab.* Englewood Cliffs, NJ: Prentice-Hall, 1994.

[4] Caputi, W.J. Jr. "Stretch: A Time-Transformation Technique." *IEEE Transactions on Aerospace and Electronic Systems.* AES-7 (March 1971): 269-78.

[5] Chin, J.E. and Cook, C.E. "The Mathematics of Pulse Compression – A Problem in Systems Analysis." *Sperry Engineering Review.* 12 (1959): 11-6.

[6] Cook, C.E. and Bernfeld, M. *Radar Signals – An Introduction to Theory and Application.* Norwood, MA: Artech House, 1993.

[7] Cook, C.E. *Pulse Compression - Key to More Efficient Radar Transmission.* Proc. of IRE. 48 (March 1960): 310-6.

[8] Cook, C.E. *Modification of Pulse Compression Waveforms.* National Electronics Conference Proceedings. 14 (October 1958): 1058-67.

[9] Klauder, J.R. et al. "The Theory and Design of Chirp Radars." *Bell System Technical Journal.* July 1960: 745-808.

[10] Klauder, J.R. "The Design of Radars Having Both High Range Resolution and High Velocity Resolution." *Bell System Technical Journal.* July, 1960: 809-20.

[11] Levanon, N. *Radar Principles.* NY: John Wiley & Sons, 1988.

[12] Mensa, D.L. *High Resolution Radar Cross-Section Imaging.* Norwood, MA: Artech House, 1991.

[13] Mersereau. R.M. and Seay, T.S. "Multiple Access Frequency Hopping Patterns with Low Ambiguity." *IEEE Transactions on Aerospace and Electronic Systems.* AES-17 (July 1981): 571-8.

[14] Morris, G.V. *Airborne Pulsed Doppler Radar.* Norwood, MA: Artech House, 1988.

[15] Nathanson, F.E, Reilly, J.P, and Cohen M.N. *Radar Design Principles – Signal Processing and the Environment.* 2nd. ed. NY: McGraw-Hill, 1991.

[16] Ohman, G.P. "Getting High Range Resolution with Pulse-Compression Radar." *Electronics.* October, 1960.

[17] Oligboh, C.N. and Ackroyd, M.H. *Linear Frequency Coded Sequences.* IEEE Proceedings Part G. 127 (August 1980):191-8.

[18] Oppenheim, A.V. and Schafer, R.W. *Discrete-Time Signal Processing.* Englewood Cliffs, NJ: Prentice-Hall, 1989.

[19] Oppenheim, A.V, Willsky, A.S, and Young, I.T. *Signals and Systems.* Englewood Cliffs, NJ: Prentice-Hall, 1983.

[20] Ramirez, R.W. *The FFT – Fundamentals and Concepts.* Englewood Cliffs, NJ: Tektronix, 1985.

[21] Ramp, H.O. and Wingrove. E.R. Jr. "Principles of Pulse Compression." *IRE Transactions on Military Electronics.* MIL-5 (1961): 109-16.

[22] Rihaczek, A.W. *Principles of High-Resolution Radar.* Los Altos, CA: Peninsula Publishing, 1985.

[23] Skolnik, M.I. *Introduction to Radar Systems.* 2nd. ed. NY: McGraw-Hill, 1980.

[24] Skolnik, M.I. *Radar Handbook.* 2nd. ed. NY: McGraw-Hill, 1990.

[25] Stimson, G.W. *Introduction to Airborne Radar.* El Segundo, CA: Hughes Aircraft Company, 1983.

[26] Titlebaum, E.L. "Time-Frequency Hop Signals Part I: Coding Based upon the Theory of Linear Congruences." *IEEE Transactions on Aerospace and Electronic Systems.* AES-17 (July 1981): 490-3.

[27] Titlebaum, E.L. and Sibul, L.H. "Time-Frequency Hop Signals Part II: Coding Based upon Quadratic Congruences." *IEEE Transactions on Aerospace and Electronic Systems.* AES-17 (July 1981): 494-500.

Appendix A

Matlab Simulation Routines

1. chirp.m
2. vncspt1.m
3. simuspt.m
4. simuspt2.m
5. spt1_1.m
6. spt1_2.m
7. spt1_3.m
8. simufjb2.m
9. spt2_1.m
10. spt2_2.m
11. spt2_3.m
12. spt2_4.m
13. simuolfjb.m
14. simumulti.m

chirp.m

```
%Simulates the generation of a chirp signal and the receiver
%characteristic to match filter the chirp signal.
%Signal generation.
fo=1e5;
k=1.6e9;
T=2.5e-4;
t=[0:2.5e-7:T];
e1=exp(j*2*pi*(fo*t+k*t.*t/2));
e1fft=fft(e1);
%Plotting the signal and the frequency spectrum of signal.
figure(1)
clg
subplot(211)
plot(t*1e6,imag(e1));
set(gca,'XLim',[0,100])
set(gca,'YLim',[-1.25,1.25])
xlabel('Time (usec)')
ylabel('Amplitude')
print -deps chirp
fh=[1:1001];
fh=(fh-1)*(1/2.5e-7)/1001;
figure(2)
clg
subplot(211)
plot(fh*1e-6,20*log10(abs(e1fft)/max(abs(e1fft))))
set(gca,'XLim',[0,0.8])
set(gca,'YLim',[-30,5])
xlabel('Frequency (MHz)')
ylabel('Amplitude (dB)')
print -deps chirpfft
%Generating the receiver characteristic.
f=[-2e6:4e6/1000:2e6];
Y=exp(j*pi*(f-fo).^2/k);
y=ifft(Y);
%Matched filtering of chirp signal by convolution.
ye1=conv(y,e1);
%Plotting the result of matched filtering.
th=[-T:2.5e-7:T];
figure(3)
clg
subplot(211)
plot(th*1e6,20*log10(abs(ye1)/max(abs(ye1))))
set(gca,'XLim',[th(970),th(1030)]*1e6);
set(gca,'YLim',[-30,5])
xlabel('Time (usec)')
ylabel('Amplitude (dB)')
print -deps mfchirp
%Creating the weighting function.
wf=chebwin(length(e1),40)';
e1w=e1.*wf;
figure(4)
subplot(211)
plot(t*1e6,imag(e1w));
set(gca,'XLim',[0,100])
set(gca,'YLim',[-1.25,1.25])
xlabel('Time (usec)')
ylabel('Amplitude')
print -deps wchirp
%Matched filtering of weighted chirp signal by convolution.
ye1w=conv(y,e1w);
%Plotting the result of matched filtering.
th=[-T:2.5e-7:T];
figure(5)
clg
subplot(211)
plot(th*1e6,20*log10(abs(ye1w)/max(abs(ye1w))))
hold on
plot(th*1e6,20*log10(abs(ye1)/max(abs(ye1))),'--')
legend('-','(a)','--','(b)',-1)
set(gca,'XLim',[th(970),th(1030)]*1e6);
set(gca,'YLim',[-50,5])
xlabel('Time (usec)')
ylabel('Amplitude (dB)')
print -deps mfwchirp
```

vncspt1.m

```
fo=1e5;
k=1.6e9;
T=104;
t=[0:0.5e-6:T*0.5e-6];
f=fo+k*t/2;
f1=f(18);
f2=f(53);
f3=f(88);
simuspt
%Values entered during the procedure call.
%[f1 f2 f3]
%t
%105
disp('Hit Any Key to Plot Results...')
pause
figure(1)
clg
subplot(211)
plot([1:3],f*1e-6)
hold on
plot([1:3],f*1e-6,'o')
set(gca,'XLim',[0.75,3.25])
set(gca,'XTick',[1,2,3])
xlabel('Pulse No.')
ylabel('Frequency (MHz)')
print -deps vncfreq
figure(2)
clg
subplot(211)
plot(t*1e6,20*log10(abs(q)/max(abs(q))));
hold on
plot(t*1e6,20*log10(abs(s)/max(abs(s))),'--');
legend('-','(a)','--','(b)',-1)
xlabel('Time (usec)')
ylabel('Amplitude (dB)')
set(gca,'XLim',[min(t),max(t)]*1e6);
set(gca,'YLim',[-40,5])
print -deps vnccp
figure(3)
clg
subplot(211)
qfft=abs(fft(q,1024));
fh=[0:1023]/1e-6/1024;
plot(fh*1e-6,20*log10(qfft/max(qfft)));
set(gca,'XLim',[0,0.2])
```

```
set(gca,'YLim',[-40,5])
xlabel('Frequency (MHz)')
ylabel('Amplitude (dB)')
print -deps vnccpfft
```

simuspt.m

```
f=input('Enter Frequency Vector -> ');
[a,N]=size(f);
disp(' ')
disp('Size of Frequency Train . . .')
disp(N)
fs=(f(N)-f(1))/(N-1);
disp('Size of Frequency Step . . .')
disp(fs)
t=input('Enter Time Vector -> ');
[b,T]=size(t);
disp('')
disp('Maximum Time . . .')
disp(t(T));
ts=(t(T)-t(1))/(T-1);
disp('Size of Time Step . . .')
disp(ts)
m=input('Enter No. of Bins of Envelope (Odd Number) -> ');
while floor(m/10) == ceil(m/10)
    disp('Even Number Entered, Please Reenter')
    m=input('Enter No. of Bins of Envelope (Odd Number) ->
');
end
pd=m*ts;
disp('Pulse Duration . . .')
disp(pd)
disp('Ratio of Frequency Step to Pulse Duration (<= 0.5) . . .')
disp(pd*fs);
s=[zeros(1,(T-m)/2),boxcar(m)',zeros(1,(T-m)/2)];
figure(3)
subplot(211)
stem(f*1e-6)
title('Frequency Train')
xlabel('Pulse No.')
ylabel('Frequency (MHz)')
subplot(212)
plot(t*1e6,s)
set(gca,'XLim',[t(1),t(T)]*1e6);
grid
title('Shape of Pulse Envelope')
xlabel('Time (usec)')
ylabel('Amplitude')
disp('Running . . . ')
w=chebwin(N,40);
W=w*ones(1,T);
S=ones(N,1)*s;
Z=S.*W.*exp(j*2*pi*f'*t)*fs;
q=sum(Z);
figure(4)
subplot(221)
plot(t*1e6,abs(q))
grid
title('Magnitude of High-Resolution Profile')
xlabel('Time (usec)')
ylabel('Amplitude')
subplot(222)
plot(t*1e6,20*log10(abs(q)/max(abs(q))));
grid
set(gca,'YLim',[-30,5])
title('Magnitude of High Resolution Profile')
xlabel('Time (usec)')
ylabel('Amplitude (dB)')
qfft=abs(fft(q));
qfft=qfft(1:(T-1)/2);
fh=[1:(T-1)/2];
fh=(fh-1)/(ts*T);
subplot(223)
plot(fh*1e-6,qfft);
grid
title('Frequency Spectrum of High Resolution Profile')
xlabel('Frequency (MHz)')
ylabel('Amplitude')
subplot(224)
plot(fh*1e-6,20*log10(qfft/max(qfft)));
grid
set(gca,'YLim',[-40,0])
title('Frequency Spectrum of High Resolution Profile')
xlabel('Frequency (MHz)')
ylabel('Amplitude (dB)')
disp('Pulse Compression Done')
```

simuspt2.m

```
%Simulates the conditon for pulse compressing the SPT I wave-
form
%approximation for the case of 21 pulses, with a specified initial
%frequency and the frequency step for a pulse of length 401.
fo=input('Enter Initial Frequency -> ');
fs=input('Enter Frequency Step -> ');
f1=[fo:fs:20*fs+fo];
t=input('Enter Time Vector -> ');
T=length(t);
c=menu('Simulations','Ideal Case','Non-Uniform Frequency
Train','Gapped Frequency Train','Range Walk');
if c==1
    disp('Ideal Case Used.')
    f2=f1;
elseif c==2
    disp('Non-Uniform Frequency Train Used.')
    noise=rand(1,21)-0.5;
    f2=f1+noise*0.5*fs;
elseif c==3
    disp('Frequency Train with Gaps Used.')
    f2=[f1(1:9),f1(12:21)];
elseif c==4
    disp('Range Walk Distortion Introduced.')
    dis=input('Enter Phase Shift Between Pulses (usec) -> ');
    f2=f1;
end
disp('Running . . .')
N1=21;
[a,N2]=size(f2);
disp('Size of Noisy Frequency Train . . .')
disp(N2)
if (c==4) & (dis ~= 0)
    x=[0:dis*1e-6:(N2-1)*dis*1e-6];
else
    x=zeros(1,N2);
```

```
end
ss=[zeros(1,100),boxcar(201)',zeros(1,100)];
w1=chebwin(N1,40);
W1=w1*ones(1,T);
disp('Calculating Ideal Case . . .')
SS1=ones(N1,1)*ss;
R1=exp(j*2*pi*f1'*t);
Y1=SS1.*exp(j*2*pi*f1'*t);
V1=conj(R1).*Y1.*W1;
Z1=V1.*exp(j*2*pi*f1'*t)*fs;
q1=sum(Z1);
disp('Calculating Noisy Case . . .')
w2=chebwin(N2,40);
W2=w2*ones(1,T);
SS2=ones(N2,1)*ss;
R2=exp(j*2*pi*f2'*t);
Y2=SS2.*exp(j*2*pi*(f2'*t-(f2.*x)'*ones(1,401)));
V2=conj(R2).*Y2.*W2;
Z2=V2.*exp(j*2*pi*f2'*t)*fs;
q2=sum(Z2);
q1fft=abs(fft(q1));
q1fft=q1fft(1:200);
q2fft=abs(fft(q2));
q2fft=q2fft(1:200);
fh=[1:401];
fh=(fh-1)*1e7/401;
fh=fh(1:200);
figure(1)
clg
subplot(211)
plot([1:N1],f1*1e-6);
set(gca,'XLim',[1,N1]);
grid
title('Ideal Frequency Train')
xlabel('Pulse No.')
ylabel('Frequency (MHz)')
subplot(212)
plot([1:N2],f2*1e-6)
set(gca,'XLim',[1,N2]);
grid
if c==2
    title('Non-Uniform Frequency Train')
elseif c==3
    title('Frequency Train with Gaps')
else
    title('Ideal Frequency Train')
end
xlabel('Pulse No.')
ylabel('Frequency (MHz)')
figure(2)
clg
subplot(211)
plot(t*1e6,20*log10(abs(q1)/max(abs(q1))));
grid
title('Magnitude of Ideal High Resolution Profile')
set(gca,'YLim',[-40,5]);
xlabel('Time (usec)')
ylabel('Amplitude (dB)')
subplot(212)
plot(t*1e6,20*log10(abs(q2)/max(abs(q2))));
grid
set(gca,'YLim',[-40,5]);
xlabel('Time (usec)')
ylabel('Amplitude (dB)')
figure(3)
clg
subplot(211)
plot(fh*1e-6,20*log10(q1fft/max(q1fft)))
set(gca,'XLim',[fh(10),fh(100)]*1e-6);
grid
title('Frequency Spectrum of Ideal High-Resolution Profile')
xlabel('Frequency (MHz)')
ylabel('Amplitude (dB)')
subplot(212)
plot(fh*1e-6,20*log10(q2fft/max(q2fft)))
set(gca,'XLim',[fh(10),fh(100)]*1e-6)
grid
xlabel('Frequency (MHz)')
ylabel('Amplitude (dB)')
if c==1
    title('Frequency Spectrum of Compressed Pulse (Ideal)')
    figure(2)
    title('Ideal Compressed Pulse')
elseif c==2
    title('Frequency Spectrum of Compressed Pulse (Non-Uni-
form)')
    figure(2)
    title('Compressed Pulse of Non-Uniform Pulse Train')
elseif c==3
    title('Frequency Spectrum of Compressed Pulse
(Gapped)')
    figure(2)
    title('Compressed Pulse of Gapped Frequency Train')
elseif c==4
    title('Frequency Spectrum of Compressed Pulse (Range
Walk)')
    figure(2)
    title('Compressed Pulse with Range Walk Distortion')
end
disp('Done with Pulse Compression')
```

spt1_1.m

```
clear all
simuspt2
%Values Entered:
%1e6
%50000
%[-2e-5:1e-7:2e-5]
%Choose Non-Uniform Case
disp('Hit Any Key to Plot Results . . .')
pause
figure(4)
clg
subplot(211)
plot([1:N1],f1*1e-6)
hold on
plot([1:N1],f1*1e-6,'o')
set(gca,'XLim',[0.5,21.5])
xlabel('Pulse No.')
ylabel('Frequency (MHz)')
print -deps cwifreq
figure(5)
clg
```

```
subplot(211)
plot(t*1e6,20*log10(abs(q1)/max(abs(q1))));
set(gca,'XLim',[-10,10])
set(gca,'YLim',[-60,5])
xlabel('Time (usec)')
ylabel('Amplitude (dB)')
print -deps cwicp
figure(6)
clg
subplot(211)
plot(fh*1e-6,20*log10(q1fft/max(q1fft)));
set(gca,'XLim',[0.5,2.5])
set(gca,'YLim',[-40,5])
xlabel('Frequency (MHz)')
ylabel('Amplitude (dB)')
print -deps cwicpfft
disp('Hit Any Key to Plot Noisy Case')
pause
figure(4)
clg
subplot(211)
plot([1:N2],f2*1e-6)
hold on
plot([1:N2],f2*1e-6,'o');
set(gca,'XLim',[0.5,21.5])
xlabel('Pulse No.')
ylabel('Frequency (MHz)')
print -deps cwnufreq
figure(5)
clg
subplot(211)
plot(t*1e6,20*log10(abs(q2)/max(abs(q2))));
hold on
plot(t*1e6,20*log10(abs(q1)/max(abs(q1))),'--');
legend('-','(a)','--','(b)',-1);
set(gca,'XLim',[-10,10])
set(gca,'YLim',[-60,5])
xlabel('Time (usec)')
ylabel('Amplitude (dB)')
print -deps cwnucp
figure(6)
clg
subplot(211)
plot(fh*1e-6,20*log10(q2fft/max(q2fft)));
hold on
plot(fh*1e-6,20*log10(q1fft/max(q1fft)),'--');
legend('-','(a)','--','(b)',-1);
set(gca,'XLim',[0.5,2.5])
set(gca,'YLim',[-40,5])
xlabel('Frequency (MHz)')
ylabel('Amplitude (dB)')
print -deps cwnucpfft
```

spt1_2.m

```
clear all
simuspt2
%Values Entered:
%1e6
%50000
%[-2e-5:1e-7:2e-5]
%Choose Gapped Case
disp('Hit Any Key to Plot Noisy Case')
pause
figure(4)
clg
subplot(211)
plot([1:N2],f2*1e-6)
hold on
plot([1:N2],f2*1e-6,'o')
set(gca,'XLim',[0.5,21.5])
xlabel('Pulse No.')
ylabel('Frequency (MHz)')
print -deps cwgfreq
figure(5)
clg
subplot(211)
plot(t*1e6,20*log10(abs(q2)/max(abs(q2))));
hold on
plot(t*1e6,20*log10(abs(q1)/max(abs(q1))),'--');
legend('-','(a)','--','(b)',-1);
set(gca,'XLim',[-10,10])
set(gca,'YLim',[-60,5])
xlabel('Time (usec)')
ylabel('Amplitude (dB)')
print -deps cwgcp
figure(6)
clg
subplot(211)
plot(fh*1e-6,20*log10(q2fft/max(q2fft)));
hold on
plot(fh*1e-6,20*log10(q1fft/max(q1fft)),'--');
legend('-','(a)','--','(b)',-1);
set(gca,'XLim',[0.5,2.5])
set(gca,'YLim',[-40,5])
xlabel('Frequency (MHz)')
ylabel('Amplitude (dB)')
print -deps cwgcpfft
```

spt1_3.m

```
clear all
simuspt2
%Values Entered:
%1e6
%50000
%[-2e-5:1e-7:2e-5]
%Choose Range Walk Case
%0.5
disp('Hit Any Key to Plot Noisy Case')
pause
ssfft=abs(fft(ss));
ssfft=ssfft(1:200);
figure(4)
clg
subplot(211)
plot(t*1e6,20*log10(abs(q2)/max(abs(q2))));
hold on
plot(t*1e6,20*log10(abs(q1)/max(abs(q1))),'--');
plot(t*1e6,20*log10(abs(ss)/max(ss)),'-.');
legend('-','(a)','--','(b)','-.','(c)',-1);
set(gca,'XLim',[-10,10])
set(gca,'YLim',[-60,5])
xlabel('Time (usec)')
```

```
ylabel('Amplitude (dB)')
print -deps cwrwcp
figure(5)
clg
subplot(211)
plot(fh*1e-6,20*log10(q2fft/max(q2fft)));
hold on
plot(fh*1e-6,20*log10(q1fft/max(q1fft)),'--');
legend('-','(a)','--','(b)',-1);
set(gca,'XLim',[0.5,2.5])
set(gca,'YLim',[-40,5])
xlabel('Frequency (MHz)')
ylabel('Amplitude (dB)')
print -deps cwrwcpfft
```

simufjb2.m

```
%Simulates the conditon for pulse compressing the SPT II
waveform
%approximation for the case of 11 pulses, with a specified initial
%frequency and the frequency step for a pulse of length 401.
fo=input('Enter Initial Frequency -> ');
fs=input('Enter Frequency Step -> ');
f1=[fo:fs:14*fs+fo];
t=input('Enter Time Vector -> ');
T=length(t);
k=input('Enter Slope for Frequency Modulation -> ');
c=menu('Simulations','Ideal Case','Non-Uniform Frequency
Train','Gapped Frequency Train','Range Walk');
if c==1
    disp('Ideal Case Used.')
    f2=f1;
elseif c==2
    disp('Non-Uniform Frequency Train Used.')
    noise=rand(1,15)-0.5;
    f2=f1+noise*0.5*fs;
elseif c==3
    disp('Frequency Train with Gaps Used.')
    f2=[f1(1:7),f1(10:15)];
elseif c==4
    disp('Range Walk Distortion Introduced.')
    dis=input('Enter Phase Shift Between Pulses (usec) -> ');
    f2=f1;
end
disp('Running . . .')
N1=15;
[a,N2]=size(f2);
disp('Size of Noisy Frequency Train . . .')
disp(N2)
if (c==4) & (dis ~= 0)
    x=[0:dis*1e-6:(N2-1)*dis*1e-6];
else
    x=zeros(1,N2);
end
ss=[zeros(1,100),boxcar(201)',zeros(1,100)];
disp('Calculating Ideal Case . . .')
w1=chebwin(N1,40);
W1=w1*ones(1,T);
TT1=ones(N1,1)*t;
A1=f1'*ones(1,401);
F1=A1+k*TT1;
SS1=ones(N1,1)*ss;
R1=exp(j*2*pi*F1.*TT1);
Y1=SS1.*exp(j*2*pi*F1.*TT1);
V1=conj(R1).*Y1.*W1;
Z1=V1.*exp(j*2*pi*F1.*TT1)*fs;
q1=sum(Z1);
disp('Calculating Noisy Case . . .')
w2=chebwin(N2,40);
W2=w2*ones(1,T);
TT2=ones(N2,1)*t;
A2=f2'*ones(1,401);
F2=A2+k*TT2;
SS2=ones(N2,1)*ss;
R2=exp(j*2*pi*F2.*TT2);
Y2=SS2.*exp(j*2*pi*F2.*(TT2-x'*ones(1,401)));
V2=conj(R2).*Y2.*W2;
Z2=V2.*exp(j*2*pi*F2.*TT2)*fs;
q2=sum(Z2);
q1fft=abs(fft(q1));
q1fft=q1fft(1:200);
q2fft=abs(fft(q2));
q2fft=q2fft(1:200);
fh=[1:401];
fh=(fh-1)*1e7/401;
fh=fh(1:200);
figure(1)
clg
subplot(211)
plot([1:N1],f1*1e-6);
set(gca,'XLim',[1,N1]);
grid
title('Ideal Frequency Train')
xlabel('Pulse No.')
ylabel('Frequency (MHz)')
subplot(212)
plot([1:N2],f2*1e-6)
set(gca,'XLim',[1,N2]);
grid
if c==2
    title('Non-Uniform Frequency Train')
elseif c==3
    title('Frequency Train with Gaps')
else
    title('Ideal Frequency Train')
end
xlabel('Pulse No.')
ylabel('Frequency (MHz)')
figure(2)
clg
subplot(211)
plot(t*1e6,20*log10(abs(q1)/max(abs(q1))));
grid
title('Magnitude of Ideal High Resolution Profile')
set(gca,'YLim',[-40,5]);
xlabel('Time (usec)')
ylabel('Amplitude (dB)')
subplot(212)
plot(t*1e6,20*log10(abs(q2)/max(abs(q2))));
grid
set(gca,'YLim',[-40,5]);
xlabel('Time (usec)')
ylabel('Amplitude (dB)')
figure(3)
```

```
clg
subplot(211)
plot(fh*1e-6,20*log10(q1fft/max(q1fft)))
set(gca,'XLim',[fh(10),fh(100)]*1e-6);
grid
title('Frequency Spectrum of Ideal High-Resolution Profile')
xlabel('Frequency (MHz)')
ylabel('Amplitude (dB)')
subplot(212)
plot(fh*1e-6,20*log10(q2fft/max(q2fft)))
set(gca,'XLim',[fh(10),fh(100)]*1e-6)
grid
xlabel('Frequency (MHz)')
ylabel('Amplitude (dB)')
if c==1
    title('Frequency Spectrum of Compressed Pulse (Ideal)')
    figure(2)
    title('Ideal Compressed Pulse')
elseif c==2
    title('Frequency Spectrum of Compressed Pulse (Non-Uni-
form)')
    figure(2)
    title('Compressed Pulse of Non-Uniform Pulse Train')
elseif c==3
    title('Frequency Spectrum of Compressed Pulse
(Gapped)')
    figure(2)
    title('Compressed Pulse of Gapped Frequency Train')
elseif c==4
    title('Frequency Spectrum of Compressed Pulse (Range
Walk)')
    figure(2)
    title('Compressed Pulse with Range Walk Distortion')
end
disp('Done with Pulse Compression')
```

spt2_1.m

```
clear all
simufjb2
%Values Entered:
%1e6
%75000
%[-2e-5:1e-7:2e-5]
%1e9
%Choose Non-Uniform Case
disp('Hit Any Key to Plot Results . . .')
pause
figure(4)
clg
subplot(211)
plot([1:N1],f1*1e-6)
hold on
plot([1:N1],f1*1e-6,'o')
set(gca,'XLim',[0.5,15.5])
xlabel('Pulse No.')
ylabel('Frequency (MHz)')
print -deps lfmifreq
figure(5)
clg
subplot(211)
plot(t*1e6,20*log10(abs(q1)/max(abs(q1))));
set(gca,'XLim',[-10,10])
set(gca,'YLim',[-60,5])
xlabel('Time (usec)')
ylabel('Amplitude (dB)')
print -deps lfmicp
figure(6)
clg
subplot(211)
plot(fh*1e-6,20*log10(q1fft/max(q1fft)));
set(gca,'XLim',[0.5,2.5])
set(gca,'YLim',[-40,5])
xlabel('Frequency (MHz)')
ylabel('Amplitude (dB)')
print -deps lfmicpfft
disp('Hit Any Key to Plot Noisy Case')
pause
figure(4)
clg
subplot(211)
plot([1:N2],f2*1e-6)
hold on
plot([1:N2],f2*1e-6,'o')
set(gca,'XLim',[0.5,15.5])
xlabel('Pulse No.')
ylabel('Frequency (MHz)')
print -deps lfmnufreq
figure(5)
clg
subplot(211)
plot(t*1e6,20*log10(abs(q2)/max(abs(q2))));
hold on
plot(t*1e6,20*log10(abs(q1)/max(abs(q1))),'--');
legend('-','(a)','--','(b)',-1);
set(gca,'XLim',[-10,10])
set(gca,'YLim',[-60,5])
xlabel('Time (usec)')
ylabel('Amplitude (dB)')
print -deps lfmnucp
figure(6)
clg
subplot(211)
plot(fh*1e-6,20*log10(q2fft/max(q2fft)));
hold on
plot(fh*1e-6,20*log10(q1fft/max(q1fft)),'--');
legend('-','(a)','--','(b)',-1);
set(gca,'XLim',[0.5,2.5])
set(gca,'YLim',[-40,5])
xlabel('Frequency (MHz)')
ylabel('Amplitude (dB)')
print -deps lfmnucpfft
```

spt2_2.m

```
clear all
simufjb2
%Values Entered:
%1e6
%75000
%[-2e-5:1e-7:2e-5]
%1e9
%Choose Gapped Case
disp('Hit Any Key to Plot Noisy Case')
```

```
pause
figure(4)
clg
subplot(211)
plot([1:N2],f2*1e-6)
hold on
plot([1:N2],f2*1e-6,'o')
set(gca,'XLim',[0.5,15.5])
xlabel('Pulse No.')
ylabel('Frequency (MHz)')
print -deps lfmgfreq
figure(5)
clg
subplot(211)
plot(t*1e6,20*log10(abs(q2)/max(abs(q2))));
hold on
plot(t*1e6,20*log10(abs(q1)/max(abs(q1))),'--');
legend('-','(a)','--','(b)',-1)
set(gca,'XLim',[-10,10])
set(gca,'YLim',[-60,5])
xlabel('Time (usec)')
ylabel('Amplitude (dB)')
print -deps lfmgcp
figure(6)
clg
subplot(211)
plot(fh*1e-6,20*log10(q2fft/max(q2fft)));
hold on
plot(fh*1e-6,20*log10(q1fft/max(q1fft)),'--');
legend('-','(a)','--','(b)',-1)
set(gca,'XLim',[0.5,2.5])
set(gca,'YLim',[-40,5])
xlabel('Frequency (MHz)')
ylabel('Amplitude (dB)')
print -deps lfmgcpfft
```

spt2_3.m

```
clear all
simufjb2
%Values Entered:
%1e6
%75000
%[-2e-5:1e-7:2e-5]
%1e9
%Choose Range Walk Case
%0.5
disp('Hit Any Key to Plot Noisy Case')
pause
ssfft=abs(fft(ss));
ssfft=ssfft(1:200);
figure(4)
clg
subplot(211)
plot(t*1e6,20*log10(abs(q2)/max(abs(q2))));
hold on
plot(t*1e6,20*log10(abs(q1)/max(abs(q1))),'--');
plot(t*1e6,20*log10(abs(ss)/max(ss)),'-.');
legend('-','(a)','--','(b)','-.','(c)',-1)
set(gca,'XLim',[-10,10])
set(gca,'YLim',[-60,5])
xlabel('Time (usec)')
ylabel('Amplitude (dB)')
print -deps lfmrwcp
figure(5)
clg
subplot(211)
plot(fh*1e-6,20*log10(q2fft/max(q2fft)));
hold on
plot(fh*1e-6,20*log10(q1fft/max(q1fft)),'--');
legend('-','(a)','--','(b)',-1)
set(gca,'XLim',[0.5,2.5])
set(gca,'YLim',[-40,5])
xlabel('Frequency (MHz)')
ylabel('Amplitude (dB)')
print -deps lfmrwcpfft
```

spt2_4.m

```
clear all
disp(' ')
disp(' ')
disp('CW Case . . .')
simuspt2
%Values Entered:
%1e6
%50000
%[-2e-5:1e-7:2e-5]
%Choose Range Walk Case
%0.03
cwq2=q2;
cwq2fft=q2fft;
disp(' ')
disp(' ')
disp('LFM Case . . .')
simufjb2
%Values Entered:
%1e6
%75000
%[-2e-5:1e-7:2e-5];
%1e9
%Choose Range Walk Case
%0.03
lfmq2=q2;
lfmq2fft=q2fft;
disp('Hit Any Key to Compare')
pause
figure(4)
clg
subplot(211)
plot(t*1e6,20*log10(abs(lfmq2)/max(abs(lfmq2))));
hold on
plot(t*1e6,20*log10(abs(cwq2)/max(abs(cwq2))),'--');
legend('-','(a)','--','(b)',-1)
set(gca,'XLim',[-10,10])
set(gca,'YLim',[-60,5])
xlabel('Time (usec)')
ylabel('Amplitude (dB)')
print -deps cwlfmcomp
```

simuolfjb.m

```
%Simulates the conditon for pulse compressing the SPT III
waveform
```

```
%approximation for the case of 11 pulses, with a specified initial
%frequency and the frequency step for a pulse of length 401, and
range
%walk distortion of 0.8 usec.
clear all
fo=1e6;
fs=75000;
f=[fo:fs:14*fs+fo];
t=[-1e-5:1e-7:1e-5];
T=length(t);
k=6e9;
disp('Range Walk Distortion Introduced.')
dis=0.5;
disp('Running . . .')
N=15;
x=[0:dis*1e-6:(N-1)*dis*1e-6];
ss=boxcar(201)';
disp('Calculating Ideal Case . . .')
TT=ones(N,1)*t;
A=f'*ones(1,201);
F=A+k*TT;
SS=ones(N,1)*ss;
R=exp(j*2*pi*F.*TT);
w=chebwin(N,40);
W=w*ones(1,T);
Y1=SS.*exp(j*2*pi*F.*TT);
V1=conj(R).*Y1.*W;
Z1=V1.*exp(j*2*pi*F.*TT)*fs;
q1=sum(Z1);
disp('Calculating Distortion Case . . .')
Y2=SS.*exp(j*2*pi*F.*(TT-x'*ones(1,201)));
V2=conj(R).*Y2.*W;
Z2=V2.*exp(j*2*pi*F.*TT)*fs;
q2=sum(Z2);
q1fft=abs(fft(q1));
q1fft=q1fft(1:200);
q2fft=abs(fft(q2));
q2fft=q2fft(1:200);
fh=[1:201];
fh=(fh-1)*1e7/201;
fh=fh(1:200);
figure(1)
clg
subplot(211)
plot([1:N],f*1e-6);
set(gca,'XLim',[1,N]);
grid
title('Ideal Frequency Train')
xlabel('Pulse No.')
ylabel('Frequency (MHz)')
figure(2)
clg
subplot(211)
plot(t*1e6,20*log10(abs(q1)/max(abs(q1))));
grid
title('Magnitude of Ideal High Resolution Profile')
set(gca,'YLim',[-60,5]);
xlabel('Time (usec)')
ylabel('Amplitude (dB)')
subplot(212)
plot(t*1e6,20*log10(abs(q2)/max(abs(q2))));
grid
set(gca,'YLim',[-60,5]);
xlabel('Time (usec)')
ylabel('Amplitude (dB)')
title('Compressed Pulse with Range Walk Distortion')
figure(3)
clg
subplot(211)
plot(fh*1e-6,20*log10(q1fft/max(q1fft)))
set(gca,'XLim',[fh(10),fh(100)]*1e-6);
grid
title('Frequency Spectrum of Ideal High-Resolution Profile')
xlabel('Frequency (MHz)')
ylabel('Amplitude (dB)')
subplot(212)
plot(fh*1e-6,20*log10(q2fft/max(q2fft)))
set(gca,'XLim',[fh(10),fh(100)]*1e-6)
grid
xlabel('Frequency (MHz)')
ylabel('Amplitude (dB)')
title('Frequency Spectrum of Compressed Pulse (Range Walk)')
disp('Done with Pulse Compression')
disp('Compensating . . .')
Z2P=unwrap(angle(Z2));
clear Z3
Z3(1,:)=Z2(1,:);
phoffv(1)=0;
for count=2:15;
    Z3P=unwrap(angle(Z3));
    phoff=Z2P(count,1)-Z3P((count-1),126).*TT(count)./
TT((count-1),126);
    disp(phoff);
    phoffv(count)=phoff;
    Z3(count,:)=Z2(count,:)*exp(-1*j*phoff);
    q3=sum(Z3);
%   figure(4)
%   clg
%   plot(20*log10(abs(q3)))
%   pause
end
disp('Hit Any Key for Ideal Plots . . .')
pause
figure(4)
clg
subplot(211)
plot([1:N],f*1e-6)
hold on
plot([1:N],f*1e-6,'o')
set(gca,'XLim',[0.5,15.5])
xlabel('Pulse No.')
ylabel('Frequency (MHz)')
print -deps olfmifreq
figure(5)
clg
subplot(211)
plot(t*1e6,20*log10(abs(q1)/max(abs(q1))));
set(gca,'XLim',[-10,10])
set(gca,'YLim',[-60,5])
xlabel('Time (usec)')
ylabel('Amplitude (dB)')
print -deps olfmicp
figure(6)
clg
```

```
subplot(211)
plot(fh*1e-6,20*log10(q1fft/max(q1fft)));
set(gca,'XLim',[0.5,2.5])
set(gca,'YLim',[-40,5])
xlabel('Frequency (MHz)')
ylabel('Amplitude (dB)')
print -deps olfmicpfft
disp('Hit Any Key for Compensating Values . . .')
pause
q1=sum(Z1(1:2,:));
q2=sum(Z2(1:2,:));
q3=sum(Z3(1:2,:));
figure(4)
clg
subplot(211)
plot(t*1e6,20*log10(abs(q1)/max(abs(q1))));
hold on
plot(t*1e6,20*log10(abs(q2)/max(abs(q2))),'--')
legend('-','(a)','--','(b)',-1)
set(gca,'XLim',[-10,10])
set(gca,'YLim',[-20,5]);
xlabel('Time (usec)')
ylabel('Amplitude (dB)')
print -deps olfmc2cp
q1=sum(Z1(1:8,:));
q2=sum(Z2(1:8,:));
q3=sum(Z3(1:8,:));
figure(5)
clg
subplot(211)
plot(t*1e6,20*log10(abs(q1)/max(abs(q1))));
hold on
plot(t*1e6,20*log10(abs(q2)/max(abs(q2))),'--')
legend('-','(a)','--','(b)',-1)
set(gca,'XLim',[-10,10])
set(gca,'YLim',[-30,5]);
xlabel('Time (usec)')
ylabel('Amplitude (dB)')
print -deps olfmc8cp
q1=sum(Z1(1:15,:));
q2=sum(Z2(1:15,:));
q3=sum(Z3(1:15,:));
figure(6)
clg
subplot(211)
plot(t*1e6,20*log10(abs(q1)/max(abs(q1))));
hold on
plot(t*1e6,20*log10(abs(q2)/max(abs(q2))),'--')
legend('-','(a)','--','(b)',-1)
set(gca,'XLim',[-10,10])
set(gca,'YLim',[-60,5]);
xlabel('Time (usec)')
ylabel('Amplitude (dB)')
print -deps olfmc15cp
```

simumulti.m

```
% Simulation of target transmission and multipath for typical set
of
% numbers for airborne radar over the frequency range of typical
pulse
% trains. The reflectivity of water is assumed to be 0.99.
clear all
r1=60*6080;
h1=1500;
h2=37000;
r2=sqrt(r1^2+4*h1*h2);
dfrq=.001;
frq0=.420;
frq=frq0:dfrq:30*dfrq+frq0;
for n=1:31;
wvl=0.98425/frq(n);
dtht=(r1-r2)*pi/wvl;
sg(n)=1+0.99*exp(-j*dtht);
end
figure(1)
clg
subplot(211)
plot(frq*1e3,20*log10(abs(sg)/max(abs(sg))));
set(gca,'XLim',[min(frq),max(frq)]*1e3)
set(gca,'YLim',[-60,5])
xlabel('Frequency (MHz)')
ylabel('Amplitude (dB)')
print -deps multifreq
wgt=chebwin(31,40);
y1=fftshift(fft(wgt'.*abs(sg),1024));
figure(2)
clg
subplot(211)
plot(20*log10(abs(y1)/max(abs(y1))))
set(gca,'XLim',[1,1024])
set(gca,'YLim',[-60,5])
xlabel('Range Bin')
ylabel('Amplitude (dB)')
print -deps multitime
```

Appendix B

Data Analysis Routines

1. `multifind.m`
2. `multiplot.m`
3. `rdplot,m`
4. `dataplot.m`
5. `ncprocw.m`
6. `ncprocg.m`

multifind.m

```
k=input('1 - Load File -> ');
if k == 1
      clear all
      datafname = r90input('Filename (no .mat) ');
      eval(['load',' ',datafname]);
end
[ncpi n]=size(azxmit);
for icpi=1:ncpi
freq(icpi)=fxmit(icpi)*1e-6;
clear cpi0;
cpi0=eval(['cpi',int2str(icpi)]);
wgt=chebwgt(npulses(icpi),40)';
n=0;
for rng0=1:1:wrecord;
idx30=rng0:wrecord:length(cpi0);
yf=sum(cpi0(idx30,:)');
r30=yf.*wgt;
r30m=mean(r30);
r30=r30-r30m;
yf=fft(r30,32);
n=n+1;
x(n)=n;
ply(n,:)=yf;
end
[a b]=max(max(abs(ply)));
DopMaxBin(icpi)=b;
scrdis=[icpi,b];
disp(scrdis)
figure(3)
colormap jet
clg
pcolor(abs(ply))
shading interp
pause
end
```

multiplot.m

```
k=input('1 - Load File -> ');
if k == 1
      clear all
      datafname = r90input('Filename (no .mat) ');
      eval(['load',' ',datafname]);
end
maxdopbin=input('Enter maximum Doppler bin -> ');
[ncpi n]=size(azxmit);
for icpi=1:ncpi
freq(icpi)=fxmit(icpi)*1e-6;
clear cpi0;
cpi0=eval(['cpi',int2str(icpi)]);
wgt=chebwgt(npulses(icpi),40)';
n=0;
for rng0=1:1:wrecord
idx30=rng0:wrecord:length(cpi0);
yf=sum(cpi0(idx30,:)');
r30=yf.*wgt;
r30m=mean(r30);
r30=r30-r30m;
yf=fft(r30,32);
n=n+1;
x(n)=n;
ply(n,:)=yf;
end
[a b]=max(max(abs(ply)));
DopMaxBin(icpi)=b;
scrdis=[icpi,b];
disp(scrdis)
colormap jet
tmp(:,icpi)=ply(:,maxdopbin);
end
[y,yi]=sort(freq);
[n npts]=size(freq);
m=0;
for n=1:npts;
m=m+1;
fr(m)=freq(yi(n));
tmp1(:,m)=tmp(:,yi(n));
if n>1
if fr(m-1) == fr(m)
m=m-1;
end
end
end
figure(1)
clg
pcolor(fr,x',abs(tmp1));
shading interp
xlabel('FREQUENCY (MHz)')
ylabel('RANGE SAMPLE')

[c d]=max(max(abs(tmp1')));
disp(d)
figure(2)
clg
subplot(211)
plot(fr,20*log10(abs(tmp1(d,:))))
[e f]=size(tmp1(d,:));
title('MAXIMUM RANGE CUT')
xlabel('FREQUENCY (MHz)')
ylabel('AMPLITUDE (dB)')
subplot(212)
plot(20*log10(abs(fft(tmp1(d,:)))/max(abs(fft(tmp1(d,:))))))
set(gca,'YLim',[-30,0])
set(gca,'XLim',[1,f])
title('FREQUENCY SPECTRUM OF MAXIMUM RANGE
CUT')
xlabel('INDEX')
ylabel('AMPLITUDE (dB)')
```

rdplot.m

```
k=input('1 - Load File -> ');
if k == 1
      clear all
      datafname = r90input('Filename (no .mat) ');
      eval(['load',' ',datafname]);
end
ncpi=input('Enter No. of CPI to Process -> ');
clear cpi0;
cpi0=eval(['cpi',int2str(ncpi)]);
wgt=chebwgt(npulses(ncpi),40)';
n=0;
```

```
for rng0=1:1:wrecord;
idx30=rng0:wrecord:length(cpi0);
yf=sum(cpi0(idx30,:)');
r30=yf.*wgt;
r30m=mean(r30);
r30=r30-r30m;
yf=fft(r30,32);
n=n+1;
x(n)=n;
ply(n,:)=yf;
end
[a b]=max(max(abs(ply)));
scrdis=[ncpi,b];
disp(scrdis)
figure(3)
colormap hot
clg
pcolor(abs(ply))
```

dataplot.m

```
clear all
load wdop9029
cpi0=cpi4;
wgt=chebwin(npulses(4),40)';
n=0;
for rng0=1:1:wrecord;
idx30=rng0:wrecord:length(cpi0);
yf=sum(cpi0(idx30,:)');
r30=[yf,zeros(1,1)].*wgt;
r30m=mean(r30);
r30=r30-r30m;
yf=fft(r30,32);
n=n+1;
x(n)=n;
ply(n,:)=yf;
end
[a b]=max(max(abs(ply)));
scrdis=[4,b];
disp(scrdis)
figure(1)
clg
colormap hot
clg
pcolor(1:32,x',abs(ply))
ylabel('Range Bin')
xlabel('Doppler Bin')
%title('Doppler Range Map of Internal MTS (CPI4)')
print -deps fdrm29004
figure(2)
clg
colormap hot
clg
pcolor(fr,x',abs(tmp1))
ylabel('Range Bin')
xlabel('Frequency (MHz)')
%title('Frequency Range Map of Internal MTS')
print -deps ffrm29
clear all
load wdop9013
cpi0=cpi12;
wgt=chebwin(npulses(12),40)';
n=0;
for rng0=1:1:wrecord;
idx30=rng0:wrecord:length(cpi0);
yf=sum(cpi0(idx30,:)');
r30=[yf,zeros(1,1)].*wgt;
r30m=mean(r30);
r30=r30-r30m;
yf=fft(r30,32);
n=n+1;
x(n)=n;
ply(n,:)=yf;
end
[a b]=max(max(abs(ply)));
scrdis=[12,b];
disp(scrdis)
figure(3)
clg
colormap hot
clg
pcolor(1:32,x',abs(ply))
ylabel('Range Bin')
xlabel('Doppler Bin')
%title('Doppler Range Map of Actual Plane (CPI12)')
print -deps fdrm13012
figure(4)
clg
colormap hot
clg
pcolor(fr(1:39),x',abs(tmp1(:,1:39)))
ylabel('Range Bin')
xlabel('Frequency (MHz)')
%title('Partial Frequency Range Map of Actual Plane')
print -deps ffrm13
```

ncprocw.m

```
clear all
load wdop9029
%figure(1)
%clg
%colormap hot
%pcolor(fr,x',abs(tmp1))
%shading interp
%disp('Hit any key to process ...')
%pause
disp('Maximum Range Bin . . .')
[a b]=max(max(abs(tmp1')));
disp(b)
prof1=abs(tmp1(b,:));
figure(1)
clg
subplot(211)
plot(fr,20*log10(prof1/max(prof1)))
%title('Frequency Profile of Internal MTS')
set(gca,'XLim',[min(fr),max(fr)])
set(gca,'YLim',[-30,5])
xlabel('Frequency (MHz)')
ylabel('Amplitude (dB)')
print -deps o29frprof
q=fftshift(fft(prof1(1:99).*chebwin(99,40)',1024));
figure(2)
clg
```

```
subplot(211)
plot(1:length(q),20*log10(abs(q)/max(abs(q))))
%title('FFT of Weighted Frequency Profile of Internal MTS')
set(gca,'XLim',[1,length(q)])
set(gca,'YLim',[-50,5])
xlabel('Range Bin')
ylabel('Amplitude (dB)')
print -deps o29rngprof
load wdop9013
%figure(3)
%clg
%colormap hot
%pcolor(fr,x',abs(tmp1))
%shading interp
%disp('Hit any key to process ...')
%pause
disp('Maximum Range Bin . . .')
[a b]=max(max(abs(tmp1')));
disp(b)
prof2=abs(tmp1(b,1:39));
figure(3)
clg
subplot(211)
fr=fr(1:39);
plot(fr,20*log10(prof2/max(prof2)))
%title('Frequency Profile of Actual Plane')
set(gca,'XLim',[min(fr),max(fr)])
set(gca,'YLim',[-30,5])
xlabel('Frequency (MHz)')
ylabel('Amplitude (dB)')
print -deps o13frprof
q=fftshift(fft(prof2.*chebwin(length(prof2),40)',1024));
figure(4)
clg
subplot(211)
plot(1:length(q),20*log10(abs(q)/max(abs(q))))
%title('FFT of Weighted Frequency Profile of Actual Plane')
set(gca,'XLim',[1,length(q)])
set(gca,'YLim',[-50,5])
xlabel('Range Bin')
ylabel('Amplitude (dB)')
print -deps o13rngprof
%100 range bins apart from the peak to the sidelobe.
```

ncprocg.m

```
clear all
load wdop9013
%figure(1)
%clg
%colormap hot
%pcolor(fr,x',abs(tmp1))
%shading interp
%disp('Hit any key for processing ...')
%pause
disp('Maximum Range Bin . . .')
[a b]=max(max(abs(tmp1')));
disp(b)
prof=abs(tmp1(b,:));
q=fftshift(fft(prof.*chebwin(length(prof),40)',1024));
frp=fr(1:39);
profp=abs(tmp1(b,[1:39]));
qp=fftshift(fft(profp.*chebwin(length(profp),40)',1024));
profg=abs(tmp1(b,[1:39,91:100]));
profg=[profg(1:39),zeros(1,52),profg(40:49)];
qg=fftshift(fft(profg.*chebwin(length(profg),40)',1024));
figure(1)
clg
subplot(211)
plot(fr,20*log10(prof/max(prof)))
%title('Entire Frequency Profile of Actual Plane')
set(gca,'XLim',[min(fr),max(fr)])
set(gca,'YLim',[-30,5])
xlabel('Frequency (MHz)')
ylabel('Amplitude (dB)')
print -deps o13frprofa
figure(2)
clg
subplot(211)
plot(1:length(q),20*log10(abs(q)/max(abs(q))))
hold on
plot(1:length(qp),20*log10(abs(qp)/max(abs(qp))),'--')
%title('FFT of Entire Weighted Frequency Profile of Actual
Plane')
set(gca,'XLim',[1,length(q)])
set(gca,'YLim',[-50,5])
legend('-','(a)','--','(b)',-1)
ylabel('Amplitude (dB)')
print -deps o13rngprofa
figure(3)
clg
subplot(211)
plot(fr,20*log10(profg/max(profg)))
%title('Gapped Frequency Profile of Actual Plane')
set(gca,'XLim',[min(fr),max(fr)])
set(gca,'YLim',[-30,5])
xlabel('Frequency (MHz)')
ylabel('Amplitude (dB)')
print -deps o13frprofg
figure(4)
clg
subplot(211)
plot(1:length(qg),20*log10(abs(qg)/max(abs(qg))))
hold on
plot(1:length(qp),20*log10(abs(qp)/max(abs(qp))),'--')
%title('FFT of Gapped Weighted Frequency Profile of Actual
Plane')
set(gca,'XLim',[1,length(qg)])
set(gca,'YLim',[-50,5])
legend('-','(a)','--','(b)',-1)
xlabel('Range Bin')
ylabel('Amplitude (dB)')
print -deps o13rngprofg
```